Habib Fathallah

OPTICAL FAST FREQUENCY HOPPING CDMA:

PRINCIPLE, SIMULATION AND EXPERIMENT

Thèse présentée
à la Faculté des études supérieures
de l'Université Laval
pour l'obtention
du grade de Philosophiæ Doctor (Ph.D.)

Département de Génie Électrique et Génie Informatique
FACULTÉ DES SCIENCES ET DE GÉNIE
UNIVERSITÉ LAVAL

JANVIER 2002

Habib Fathallah

OPTICAL FAST FREQUENCY HOPPING CDMA:

PRINCIPLE, SIMULATION AND EXPERIMENT

Thèse présentée
à la Faculté des études supérieures
de l'Université Laval
pour l'obtention
du grade de Philosophiæ Doctor (Ph.D.)

Département de Génie Électrique et Génie Informatique
FACULTÉ DES SCIENCES ET DE GÉNIE
UNIVERSITÉ LAVAL

JANVIER 2002

Résumé

Dans cette thèse, nous étudions une nouvelle méthode d'accès multiple par répartition de code (AMRC) par fibre optique que nous avons inventé et nommé AMRC- par saut rapide de fréquence optique (-SRFO). Nous avons défini et introduit les principes fondamentaux de la technique AMRC-SRFO (ou OFFH-CDMA). Nous avons également décrit différentes solutions d'implantation pratiques de cette technique, et démontré que les réseaux de Bragg permettent une implantation particulièrement élégante. Des analyses théoriques, numériques et expérimentales nous ont permis de démontrer l'efficacité du principe de codage. Nous avons également proposé une version du système spécialement appropriée pour des milieux de communications hostiles, où le contrôle de l'environnement s'avère difficile ou coûteux. En plus, nous avons monté un banc d'essai expérimental pour le système AMRC-SRFO incluant seize codeurs et un décodeur programmable et démontré une opération réussie de codage décodage pour différentes configurations et scénarios de communications.

Prof. Leslie Ann Rusch
Directrice de recherche

--
Prof. Sophie LaRochelle
Co-directrice de recherche

--
Habib Fathallah
Étudiant au doctorat

Abstract

In this dissertation, we address a new method of optical code division multiple access (CDMA) communications we invented and referred to as optical fast frequency hopping- (OFFH-) CDMA. We define the fundamental principles of the OFFH-CDMA and propose a set of implementation solutions. We have found, that multiple Bragg gratings (MBG) offer the most elegant method to implement the OFFH-CDMA encoding/decoding functions. Theoretical and computer simulation analysis have verified and demonstrated the effectiveness of the new principle. In addition, we propose new encoding/decoding architectures that enable a network to accommodate subscribers with different data rates and performance levels. We also propose and investigate a version of the system especially appropriate for communications in hostile temperature and stability conditions. Finally, we build an OFFH-CDMA experimental setup that includes sixteen encoders and four programmable decoders and demonstrate successful encoding/decoding operation in various communications scenarios.

Prof. Leslie Ann Rusch
Research Advisor

--
Prof. Sophie LaRochelle
Research Co-Advisor

--
Habib Fathallah
Doctoral Candidate

I dedicate this work to my

Mother

Remerciements

Depuis mon idée éclair et rudimentaire du 20 juin 1996, pendant que j'assistais au séminaire pré-doctoral de Dr Antoine Bellemare, et alors que je finissais la rédaction de mon mémoire de maîtrise, quelle longue période et quel mémorable trajet! Cette thèse est loin d'être le travail d'une seule personne, elle est réellement le résultat de contributions et d'influences d'un grand nombre de personnes et d'intervenants.

Je tiens à exprimer ma reconnaissance et ma gratitude au Dr Leslie Ann Rusch, ma directrice de recherche, qui a su orienter mes énergies et catalyser le milieu propice pour la créativité et l'innovation. Le OFFH-CDMA n'aurait pas été possible sans la confiance et la liberté qu'elle m'a laissées pour modifier la direction de mes recherches à la guise de mes intuitions.

J'aimerais aussi témoigner ma gratitude particulièrement au Dr Sophie LaRochelle. Sans ses conseils, ses idées et ses réflexions, ce travail n'aurait jamais atteint autant d'objectifs et achevé autant de succès. L'expertise aussi bien que la patience de Dr Pierre Yves Cortès ont grandement travaillé la cause du OFFH-CDMA et contribué à son succès.

Je remercie spécialement le Dr Jawad Salehi, professeur à Sharif University of Technology, Tehran, Iran, et le Dr Antonio J. Mendez, de El Segundo en Californie, d'avoir accepté d'être membres du jury de ma thèse. Ces deux hommes sont des pionniers du domaine du CDMA optique et ont eu un impact important sur ma formation en CDMA optique à travers ses contributions dans le domaine.

Je remercie également le Dr Michel Lecours, professeur au département de génie électrique et génie informatique à l'Université Laval, d'avoir accepté d'être membre du jury de ma thèse. En tant qu'étudiant étranger, et ex-étudiant de Dr Lecours, je ne peux oublier sa bonne humeur constante et ses qualités humaines.

De plus, mes remerciements s'adressent à toutes et tous mes collègues étudiantes et étudiants, particulièrement à ceux qui ont aimé le OFFH-CDMA et ont accepté d'y contribuer à travers leurs thèses, mémoires ou projets. Je nomme particulièrement, Louis-Patrick Boulianne, Kèrim Fouli, Hafedh Ben Jaafar, Elie Inaty, Mourad Menif, Lionel Pujol, Carl Bélanger, Hichem Farah et Jean-Pierre Bouchard. Je souligne spécialement le support et l'encouragement de Adel Baccouche.

La patience de Jihen, mon épouse, son support moral et son amour étaient irremplaçables pour le succès de ce travail. Qu'elle trouve en ceci la meilleure expression d'amour! Ma petite Hiba, elle aussi, a supporté, pendant qu'elle était fœtus de 4 mois, mes nuits blanches de rédaction de cette thèse.

Elhajja Douja, ma mère, ainsi que mes sœurs Zohra, Assia et Sihem, mes frères Mohamed, Mekki, Nejib et Azeiez, mes belles-sœurs et beaux-frères, mes nièces et mes neveux, ma grande famille et mes ami(e)s, ne pourraient être assez récompensés pour leur amour et leur soutien.

Une mention particulière à mon beau-père Elhaj Zoubeir, ma belle-mère Wahida et mon beau-frère Ahmed pour leur confiance soutenue et leur support.

Je souhaite noter la contribution financière et matérielle indispensable du COPL, du Conseil de recherches en sciences naturelles et en génie (CRSNG) du Canada, de l'agence spatiale canadienne (ASC), de Québec-Téléphone, du ministère de l'enseignement et de la recherche scientifique de la Tunisie et de l'agence canadienne de développement international (ACDI).

Table of contents

List of Figures

Chapter 1

Chapter 2

Chapter 3

Chapter 4

Chapter 5

Chapter 6

Chapter 7

Introduction

CDMA has enjoyed enormous success in radio frequency (RF) communications due to several advantages *vis-à-vis* other multiplexing strategies [1-12]. Technical differences between the radio and optical communications media are significant, and no simple relationship exists between solutions in each media. Therefore, optical implementations of CDMA have only benefited to a limited extent from research into RF implementations. Interest in OCDMA is at an all time high, in no small measure due to the tremendous demand for Internet services, including emerging bandwidth-hungry services like electronic commerce, virtual-reality, HDTV, Tele-medicine, video-on-demand, Tele-working, etc. Only optics can deliver the bandwidth required, and no clear solution yet exists for managing the complex multiple access problems associated with highly interconnected networks. While discussion is already underway for ten Gigabit-Ethernet, the current tendency towards frame- and packet-switched architectures in networks favors CDMA technology, as it better supports bursty traffic.

Code division multiple access can be considered the general case for time/frequency domain coding, with the special examples of frequency division multiple access (FDMA) that only codes in frequency, and time division multiple access (TDMA) that only codes in the time domain [6-8]. The space (or fiber) can also be used as an encoding dimension and this is called space division multiple access (SDMA) [6-8]. In most systems, allocation of frequency bands in FDMA, or time-intervals in TDMA, is made in a static manner, *i.e.*, the resource is allocated to users whether they are transmitting or not. This is especially inappropriate for public resources such as access networks, where the objective is to serve large communities. In fact, CDMA is a popular choice for urban and suburban wireless telephony due to the high number of subscribers that can be accommodated in addition to its tolerance to multipath fading. Despite a static allocation of codes, CDMA allows simultaneous active users to take advantage of all the available time and

frequency resources, while causing only tolerable interference, thus improving the quality and flexibility of their data transmission [11].

In CDMA, each user is identified by a different code or address. A CDMA user inserts its code (or address) in each data bit and asynchronously initiates transmission. In fiber-optic CDMA, the field of the optical signal carrying the data exhibits a set of signal processing operations, (the code). Hence, this modifies its time and/or frequency appearance, in a way recognizable only by the intended receiver who knows the code. Otherwise, only noise-like bursts are observed. The advantages of CDMA include the flexibility in the allocation of channels, the ability to operate asynchronously, enhanced privacy, and increased capacity in bursty-nature networks [14-17].

We begin in Chapter 1 with an overview of the optical code division multiple access (CDMA) encoding/decoding methods. In addition, we briefly review the two popular spread spectrum (SS) techniques, direct-sequence (DS) and frequency hopping (FH). In Chapter 2, we introduce the new principle of generating an optical fast frequency hopping (OFFH) signal. We propose some all-optical implementation solutions capable of fulfilling the requirements of OFFH-signal generation. We discuss the merits of the multiple Bragg grating (MBG) based solution.

In Chapter 3, we theoretically analyze the MBG based OFFH-CDMA system. Numerical simulation and performance results are presented in Chapter 4. In Chapter 5, we propose the OFFH-CDMA system as a robust communication technique in severe, non-controllable environments. We give a theoretical and numerical analysis for the system, we refer to the technique, for such applications, as Robust OFFH-CDMA.

In Chapter 6, an experimental demonstration of the OFFH-CDMA system is described. We discuss the design parameters of the experimental setup as well as the measured results. Auto-and cross-correlation functions are reported. Results for an OFFH-CDMA setup including eight encoders and one programmable decoder are also reported. A second generation of the setup including sixteen encoders and four tunable decoders is also shown with series of measurements, and observations.

In Chapter 7, we explore and discuss the potential of the Bragg grating structure to implement almost ideal OCDMA systems in the future. We introduce a new idea of a coherent OFFH-CDMA system, where the phase plays a key role in the encoding scheme. The new proposal is realistic although it requires more stringent and expensive optical devices. This idea is inspired from the all-optical coherent DS-CDMA schemes [18-28]. The chapter introduces also some potential applications and enhancements of the proposed scheme in order to allow multirate transmission, multiple quality of service and frequency encoded over frequency hopping-CDMA transmission.

Chapter

1

Optical CDMA Communications

Introduction and Overview

It is certainly difficult to compile an overview of optical CDMA that covers all techniques and systems. While most were never implemented in real systems, optical CDMA includes tens of different techniques that are difficult to categorize or classify [15-17]. In this chapter, we present a synthesis of the most well known optical CDMA techniques, emphasizing their encoding/decoding principles and their main objectives. The encoding/decoding principle is the essential feature of every optical CDMA technique, as it determines the system's flexibility, reliability, overall capacity, and performance.

Optical CDMA was born somewhat *premature*ly almost two decades ago [18-20, 27]. The first proposals appeared almost immediately following or concurrently with those in wireless communications. The motivation was the promise to accommodate a high number of low-bit-rate clients to communicate simultaneously through the fiber. Nevertheless, CDMA, in wireless and in optics, has observed completely different evolution speeds, and eventually different targets. If compared to current wireless technology, CDMA in optics is still a nascent technology.

In Section 1.1, through a historical analysis, we try to identify the factors leading to the difficulty in implementing optical CDMA into practical systems. Due to these difficulties, research in optical CDMA has unceasingly developed newer encoding methods in order to achieve the CDMA objectives. This has fortunately enriched the optical CDMA field. Indeed, various encoding methods have appeared in optics with no parallel in wireless; and they represent a turning point in the history of the optical CDMA [55-86]. Some of the most well known techniques will be reviewed in this chapter.

Furthermore, the optic-to-electronic and electronic-to-optic conversions have often imposed a limitation on the transmission rate and increased the overall system cost. It is hence preferable that encoding and decoding operations occur in the optical domain. This avoidance of ultra-fast electronics is a particularly attractive feature of so-called all-optical CDMA techniques [18,20]. Indeed, when optical encoding is performed, the required electronic speed is on the order of the data rate rather than the chip rate. Nevertheless, some all-optical CDMA systems may still require fast electronics for integration, threshold comparison, etc [29-31].

Sections 1.2 and 1.3 introduce two aspects of CDMA with largely different natures that we refer to as protocol and technical aspects. In these sections, the description may be more inspired from a wireless application context; however, it is applicable to the optical one as well.

The emergence of the all-optical CDMA techniques is introduced and discussed in Section 1.4. We especially show that the use of the phase of the optical field as a part (or a parameter) in the encoding scheme adds a substantial flexibility in the allocation of codes; *i.e.*, increases the number of subscribers. Unfortunately, this can be performed only at the cost of high complexity in the implementation of the system, generally requiring less-mature and/or expensive technology. Here we define three sets (or categories) of optical CDMA systems. The first regroups those that use the phase in their signaling waveforms; we refer to them as coherent techniques (Section 1.5). The second includes those that manipulate positive waveforms only, even in time and/or in frequency. Finally, we present the techniques that exploit space (fiber) as an encoding resource. They naturally differ from the former in their technologies and applications. Only a limited number of contributions will be reported in this last category.

1.1 Historical Analysis

For the first implementations of optical CDMA, people tried to imitate, in optics, CDMA techniques already established in wireless. They met serious difficulties in the practical implementation, and they developed techniques never displayed comparable success to that in wireless [10-12,15-16]. This is mainly due to the fundamental difference between the radio frequency and optical fiber communication environments. For instance, the optical source cannot be controlled as easily as the electrical one, optical fiber effects are unlike those in a RF channel, and optical detection instruments differ substantially from their RF counterparts.

a) Fundamental Difference Between RF and Optical Domains:

Firstly, the output characteristics of an optical source, such as phase, polarization, etc., are not as controllable as those of a microwave source. Secondly, the optical fiber exhibits

phenomena that are either not present or insignificant in the RF channel. Finally, the photodetector detects incident power only; the phase, polarization, etc. cannot be easily detected. In order to control and detect such parameters, a complex architecture is required, and it is still inappropriate for access communication systems [32].

One straightforward example is the high complexity that coherent optical CDMA requires to use bipolar {1, -1} bits and/or chips that are commonplace in microwave systems. This will be introduced in Section 1.4. The unipolar codes, despite their notably less interesting properties, are nonetheless easier to use in optics because they require only power detection [32]. Note that optical phase modulation devices are widely available however the capability to track and detect the phase in the reception side seriously limits the deployment of OPSK (optical phase shift keying) as a modulation scheme in TDM. OPSK can increase the power budget of a link by about 3dB pushing increasing the propagation distance by 15 km in a single mode fiber at the 1550 nm band.

b) Prior Established Systems

In wireless communications, the need for CDMA appeared after the traditional resource division techniques (FDMA and TDMA) were well established. CDMA was introduced as a solution to the overcrowded frequency spectrum that overcame the weakness of those traditional techniques and their inability to meet the demand of the growing number of subscribers in wireless networks in addition to its multipath resistance. In fiber optic communications, however, neither WDM nor TDM is mature, and their capacity is not exhausted. Hence, the need to develop a third technique to enhance throughput, increase the channel count, and resource allowance flexibility is just beginning to be a requirement, especially in access networks.

c) Customer-to-fiber Accessibility

Fiber is used throughout the long-haul global telecommunications infrastructure, yet there is a limited amount of fiber in the access level enabling direct connection of the end customers. In wireless, by contrast clients have direct access (*i.e.*, air interface) to the shared medium. In optics, however, the fiber is still a few tens of meters away from the client. The fast evolution of fiber-optic technology and the rapid decline in device cost will eventually link the fiber to the end user-in business, home and desk, etc. Finally, the microwave frequency domain is well engineered compared to the optical one. In the fiber optic, a significant work in the understanding, modeling and characterization of the fiber optic phenomena was achieved during the last decade driven by the tremendous growth of demand of WDM. A number of solutions and remedies already exist but still cannot be considered a commodity, even less for access areas. .

d) Bandwidth and Service Demand

Demand for Internet services is growing exponentially, and does/will include electronic commerce, virtual-reality, HDTV, Tele-medicine, video-on-demand, Tele-working, etc. End-users require higher and higher bandwidth. Traditional transmission systems are unable to fulfill this demand. The fast evolution of Ethernet from 10 Megabits/sec to one Gigabits/sec demonstrates the importance of high bandwidth to the end-users, yet is still far from satisfying projected throughput requirements

1.2 Protocol Aspects of CDMA

In this section, we introduce CDMA through its protocol aspects, *i.e.*, for resource management. Typically, time and frequency are considered the only sharable resources. This misreading is induced perhaps because time and frequency are most frequently exploited in the wireless domain. From the protocol viewpoint, the nature of the resource does not matter, *i.e.*, time, frequency, phase, polarization, space etc. In contrast, from the technical viewpoint, however,

the nature of the resource is primordial, as it brings its own constraints on system design and exhibits different phenomena.

1.2.1 Resource Management

The time and frequency resource management of a communications medium is a fundamental topic that has always preoccupied the communications community. Its principal goal consists of maximizing the information quantity transmitted through a given medium while ensuring a certain level of transmission quality (maximum probability of error), and minimizing cost (including energy) [2-4].

In order to improve the overall throughput of a communications medium, several tools are usually considered. Firstly, we usually seek to modulate the data bits using signaling waveforms occupying the minimum frequency bandwidth, thus minimizing the inter-symbol and inter-channel interference, and minimizing the energy per bit [2-4]. Secondly, information compression is considered as a potential tool to maximize the quantity of data transmitted through a channel.[1] Finally, the tool we are interested in here is the access protocol that users (or clients) exploit to access the available resources in a typical shared communications medium.

1.2.2 Multiple Access Protocols

The sharing policy of time and frequency resources is important for the overall throughput (or the capacity of use) of the channel. Frequency Division Multiple Access (FDMA) is the most widespread technique in current communications systems [1-11]. In FDMA (Figure 1.1), the available frequency band is sub-divided into disjoint intervals, each of which is dedicated to a particular user, even when it is not active. The number of users sharing the channel is equal to the number of frequency intervals.

[1] By the term channel we refer to the support (or the medium) of transmission including all the available resources. This term is sometimes used to refer to what we usually call a user.

In optical fiber communications, FDM or WDM[2] (wavelength division multiplexing) is well established in long-haul systems. Moreover, WDM has recently started to enter metropolitan level. The wavelength spacing between disjoint wavelengths is fixed to allow a 0.1-bit/s/Hz throughput. The ITU standard fixes a frequency spacing of 25, 50, 100, 200 and 400 GHz for bit rates 2.5, 5, 10, 20 and 40 Gb/sec respectively [206]. Industry and research efforts are continuously trying to increase this throughput.

As an alternative to the frequency domain partitioning strategy, there is TDMA: Time Division Multiple Access [1-11]. In TDMA (Figure 1.2), the time is divided into equal and successive periods, each of which is divided into an integer number of time-intervals. Each interval is allocated to a user to transmit its frame of bits. Once its dedicated time-interval has run out, a user should wait during the other time-intervals intended for other users. It resumes transmission when its interval in the following period starts. The allocation of time intervals is made in a permanent way to the users, although the user will not always need the time allocated. The number of users sharing the channel is equal to the number of time-intervals in a period.

In fiber optic transmission, the bit rate per wavelength channel is also rapidly growing. The 10 Gb/sec (OC 192) is commercial with tens of wavelengths per fiber. Data rate of 160 Gb/sec,

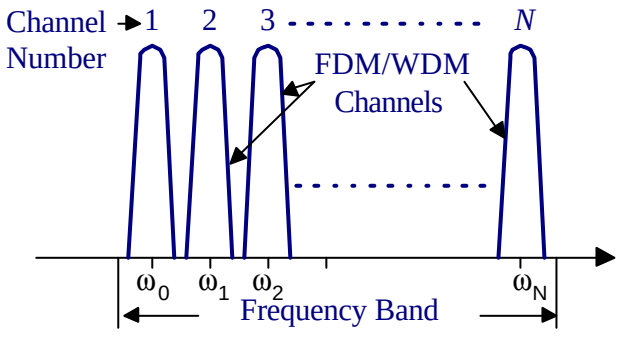

Figure 1.1: Resource Allowance in Typical FDMA/WDMA System.

[2] The FDM (or WDM) approach considers that every frequency (or wavelength) consists of a number of time division multiplexed (TDM) sub-channels, SONET over WDM example.

corresponding to the standard OC 3072 was demonstrated in some laboratories but it is not commercial yet. When the bit rate exceeds the 10 Gb/sec, the multiplexing is done using all optical components, mainly delay lines.

The allocation of frequency bands in FDMA, or time-intervals in TDMA, is made in a deterministic (or static) way, *i.e.*, the resource is allocated to users whether they are active or not. This effectively leads to undesirable situations, where certain intervals of frequency (resp. intervals of time) in FDMA (resp. TDMA) are not exploited whereas others are overloaded. This is always the case in typical access networks, where traffic is naturally bursty.

This problem has historically led the researchers to think about dynamic allocation of the resource, *i.e.*, the channel is given to the sub-set of users at the convenient time for them [11]. The first proposals required a centralized administration of the resource. This solution improved channel throughput at the price of additional complexity in the communications system. Indeed, this requires a complex supervisory system to arrange the users' requests, manage the queues lengths, and control the priority.

A multiple access protocol that can dynamically allocate resource without complex control overhead is extremely interesting. This explains the success of CDMA [7-9]. In CDMA, each user is identified by a different code, which represents, at the same time, its address. The CDMA user inserts its code (or address) in each data bit before transmission. Only the intended receivers,

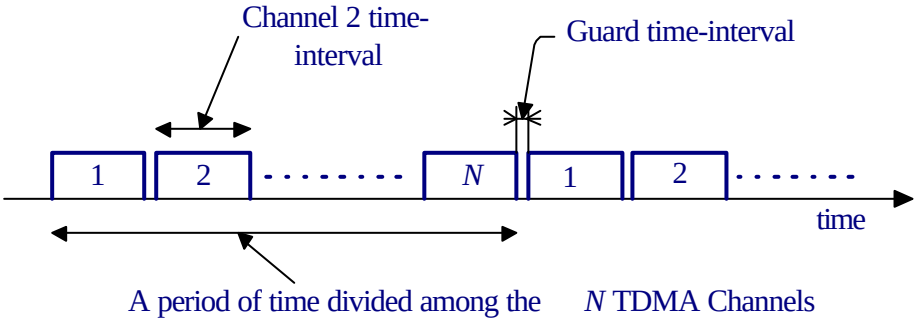

Figure 1.2: Resource Allowance in a TDMA System.

having the code used in transmission, are able to decode the message. Users other than the desired code are unable to pick up the data.

CDMA makes it possible for simultaneous active users to take advantage of all the available time and frequency resources, thus enormously improving the quality of their data transmission. CDMA users can embark or exit without supervision. When an additional user embarks, it slightly degrades the performance of all active users. Thanks to these significant properties, CDMA had much success in wireless and satellite communications. Moreover, CDMA is now classified among the most promising technologies for the next generation of fiber optic LANs (Local Area Networks) [14-17].

1.2.3 Random and Switched Access

Some random access strategies, especially CSMA/CD (Carrier Sense Multiple Access with Collision Detection) for Ethernet, have dominated local area networks for more than two decades [12]. Ethernet, the most implemented LAN worldwide, is now showing impressive evolution in bit rate and in architecture. From the conventional 10 Mb/sec rate, the standard has

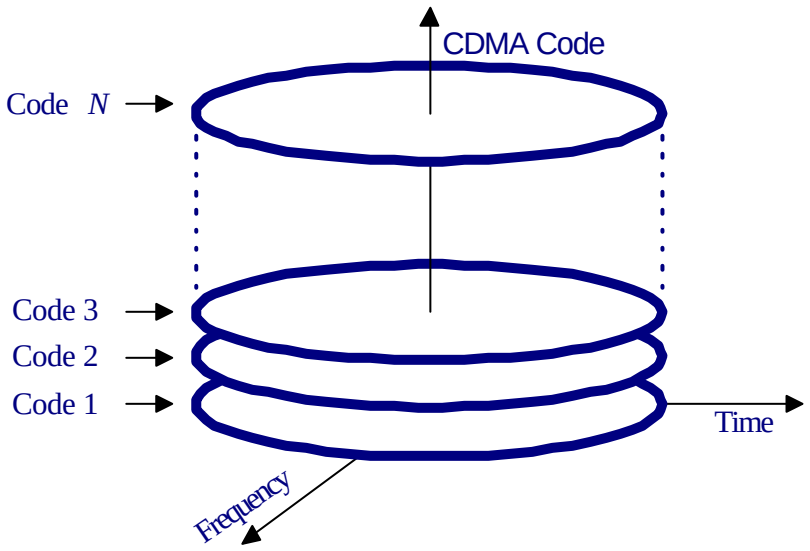

Figure 1.3: Resource Allowance in a Typical CDMA System

rapidly grown to 100Mb/sec (fast Ethernet) and finally 1 Gb/sec (Gigabit Ethernet). A few months ago, the IEEE 802.3ae started to study the future generation, operating at 10Gb/sec. The architecture of Ethernet also migrates from a common bus, with only one active user at a time, to a switched architecture in order to reduce the collision probability.

Switched architectures such as Figure 1.4, are more popular for ATM and IP standards [12]. There is no direct physical path between any pair of users; they are all connected to the input/output ports of the switch. The latter dynamically establishes the links between the client pairs, depending on their requests. In rising Ethernet networks, the switched architecture was adopted in order to reduce the collision probability between concurrent users. The switch allows more than one communication to be established simultaneously.

An optical CDMA based system can be seen as a non-centralized switch where the input/output ports are localized directly at the users' cites. A CDMA based system would alleviate the network from centralized, cumbersome, and costly switches.

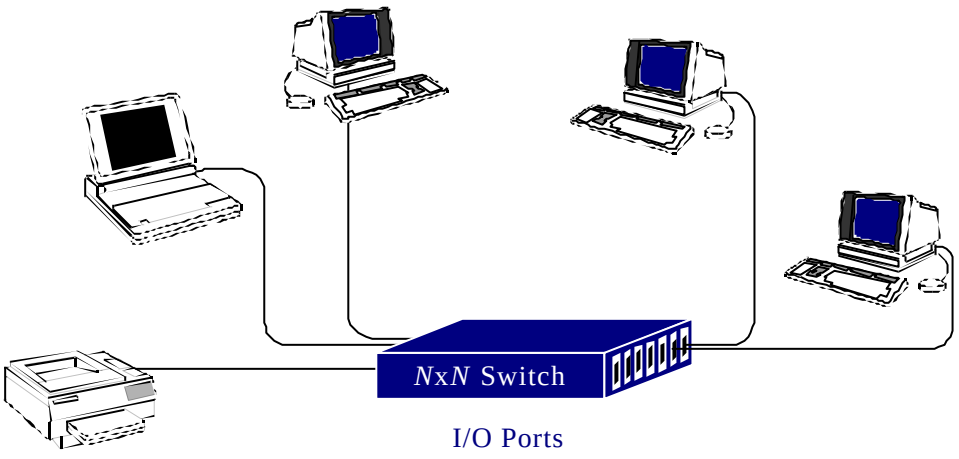

Figure 1.4: Typical Switch-based Network architecture

1.3 Technical Aspects of CDMA

In the previous section, we summarized the advantages of CDMA as a sharing technique. However, to reach its objective, CDMA usually makes use of traditional spread spectrum techniques. Spread spectrum signals can overlap in time and frequency if their spreading sequences are well selected so as to satisfy some pre-specified properties. Hence, CDMA benefits from substantial additional advantages, thanks to the important properties that are inherent to spread spectrum techniques. In this section, we introduce the principle of spread spectrum systems and highlight how CDMA takes advantage of that.

1.3.1 Spread Spectrum

Spread spectrum (SS) techniques are widely used in digital transmission systems. In these techniques, the transmitted signal occupies a bandwidth much wider than that of the original data. The spreading factor is defined as the ratio of the frequency bandwidth occupied by the SS signal over the original frequency bandwidth before spreading. It is usually much larger than one [1-11].

SS techniques are very popular in radio mobile and satellite communications. These fields are known for the severity of their communication environment. These channels are usually very

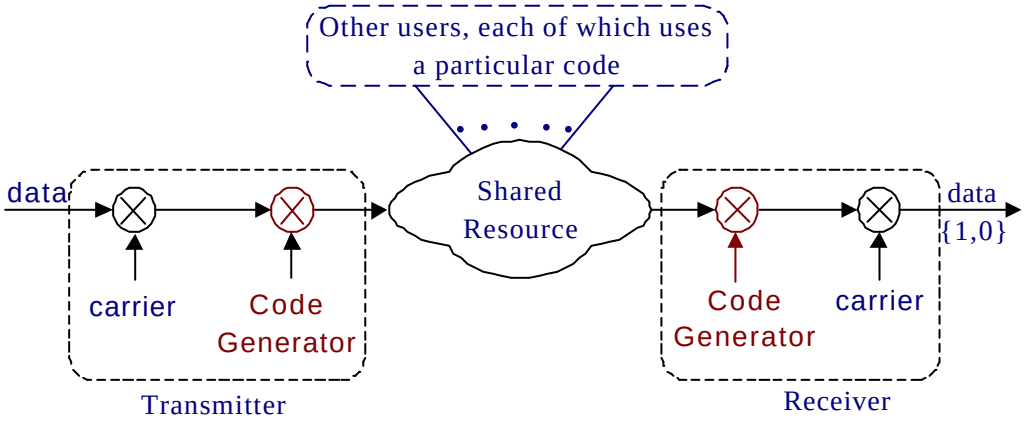

Figure 1.5: Spread Spectrum based CDMA System.

variable in time, selective in frequency, and have multi-path propagation problem, etc. In military systems, information can be successfully regenerated even though signals can undergo intentional narrow-band jamming signals. A military signal can also be susceptible of interception; coding fulfills the function of information camouflage. In addition, the power spectral density of the data signal, once encoded, is below the background noise level, avoiding interception.

It is well known that coding of the data, with the aim of creating a redundancy in the signal, results in a spreading of its spectrum. Therefore, coding was found as an excellent method to spread the spectrum of a signal. The redundancy is inherently achieved, when a signal's spectrum is spread. Given the important role of coding in information transmission, the spectral properties of the codes are of great importance. For example, the so-called pseudo-noise codes offer noise-like signal properties; hence, making it difficult for non-desirable receivers to intercept [10].

Depending on the coding technique, two categories of spread spectrum systems exist: direct sequence-spread spectrum (DS-SS), and frequency hopping-spread spectrum FH-SS [10]. The two next sections are devoted to introduce these systems. The latter, FH-SS, will take more attention throughout the document. Note that the introduction of spread spectrum here is inspired more from radio frequency area. This provides key insights on the fiber-optic application but cannot be considered fully applicable.

1.3.2 Direct Sequence-Spread Spectrum

In direct sequence spread spectrum (DS-SS) (Figure 1.5), each data bit is replaced by a sequence of symbols referred to as chips, multiplied by the binary value of the bit. In standard systems, the number of chips per sequence is an integer number that varies from a few to a few thousands chips; thus increasing considerably the bandwidth occupied by the signal.

In Figure 1.6, we show an example of DS-SS coding by using a sequence containing 7 chips. The bits and chips take bipolar values, *i.e.*, $\in \{+1, -1\}$. In radio frequency-CDMA, bipolar signals are more popular than unipolar ones. In optical communications, on the other hand, unipolar signals $\in \{1,0\}$ are more often used, *i.e.* the existence or not of light power. This is mainly

due to the optical detection component, the photodetector, which delivers a current proportional to the light power and not the phase.

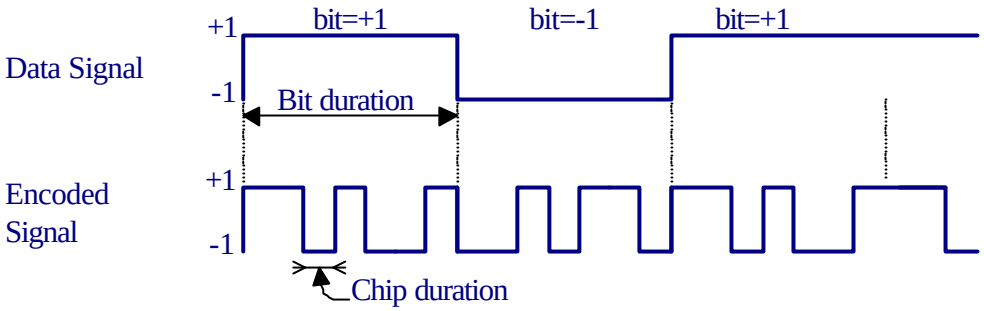

Figure 1.6: DS-SS Encoding Process.

Figure 1.7 shows the power spectral density (PSD) of the signal before and after the encoding operation. The power of the signal, the area under the PSD curve, does not change due to encoding. As shown in Figure 1.7, if other users' are simultaneously transmitting signals using judiciously selected codes, their respective spectra are also spread, and hence occupy the same frequency band.

When the DS-SS technique is used in a CDMA network, the system is called DS-CDMA where the SS acronym is omitted. In optical CDMA networks, unipolar chip and bit values are the most popular. These systems are usually referred to as positive and called incoherent DS-CDMA. Nevertheless, bipolar bit and chip values have been used in [21-31], and this is called coherent optical DS-CDMA. Moreover, a CDMA system where the chips have bipolar values and bits have unipolar ones was recently developed and demonstrated by Kitayama group [29-30]. This is called coherent pulsed optical CDMA.

When coding is achieved in the time domain, either unipolar or bipolar, systems are called DS-CDMA. The spectrum of the signal is spread in the same way, when the chips and the bits as well, have either bipolar or unipolar values. These waveform values only change the dc level of the signal. However, codes that operate well for bipolar coding based system are not suitable for

unipolar coding based one. Hence, the spreading operation in a positive system differs from that of a bipolar one.

Furthermore, when the chips are bipolar and the bits are unipolar [29-30], the spread spectrum should substantially change, since three levels exist in the transmitted signal. Up to now, in our knowledge, these questions are not yet well discussed, nor studied in the literature, at least in the context of optical CDMA system.

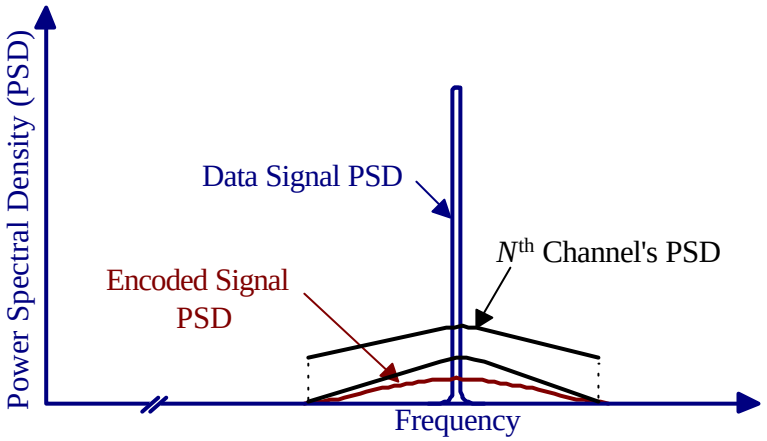

Figure 1.7: Spectrum spreading in DS-SS and users' PSDs superposition in typical DS-CDMA system.

1.3.3 Frequency Hopping-Spread Spectrum

Mainly two coding methods exist in Frequency Hopping-Spread Spectrum. The first consists of carrying out a frequency jump at each chip; this is called Fast Frequency Hopping-Spread Spectrum (FFH-SS). The second alternatively is Slow FH-SS (SFH-SS) where the frequency hops (or changes) at each data bit. In the literature, we also find very slow FH-SS where a frequency jump is performed every packet (or frame) of bits. Alternatively, we also meet the very fast FH-SS, in which the frequency hops many times at each chip [1-10].

In this context, we restrict our description to the FFH-SS system since it corresponds more to the focus of this thesis. Figure 1.8 describes a radio frequency FFH-SS transmitter

functionality using a block diagram [1-10]. The unipolar data bits {0,1} coming from the source first modulate the reference carrier. The code generator is usually made by shift-registers capable to generate the desired user code. The output of which drives the frequency synthesizer to generate successive frequency-shifts from the reference frequency as prescribed by the code.

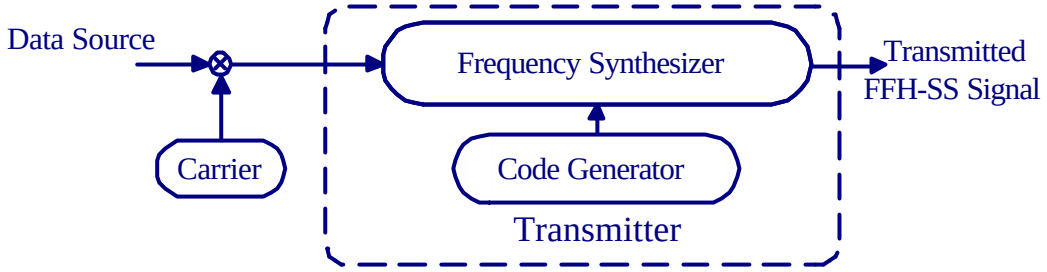

Figure 1.8: Radio-Frequency FFH-SS Transmitter Bloc Diagram.

Let's assume a code composed of a series of F frequencies. If the data bit is equal to one, the transmitted signal will be equal to a concatenation of F chips. Each of these is carried by different frequency in accordance with the selected code. If the data bit is equal to zero, nothing is transmitted.

Figure 1.9 explains through an example the time *vs*. frequency spaces occupied by the signal through the transmission chain. At the input, the data source delivers a baseband signal, which occupies a frequency band W_b and a time interval T_b. After modulation by ω_0, the signal occupies a time×frequency rectangle $T_b \times W_b$, centered at the frequency ω_0.

The modulation of this signal by the frequency synthesizer, gives rise to a signal that can be characterized by two factors:

1. The waveform (or data bit pulse) of duration T_b and bandwidth W_b is subdivided, in time into F pulses of chip duration $T_c=T_b/F$ while preserving the same bandwidth W_b.

2. Each of these F pulses is centered at a different frequency, according to the FFH-CDMA code.

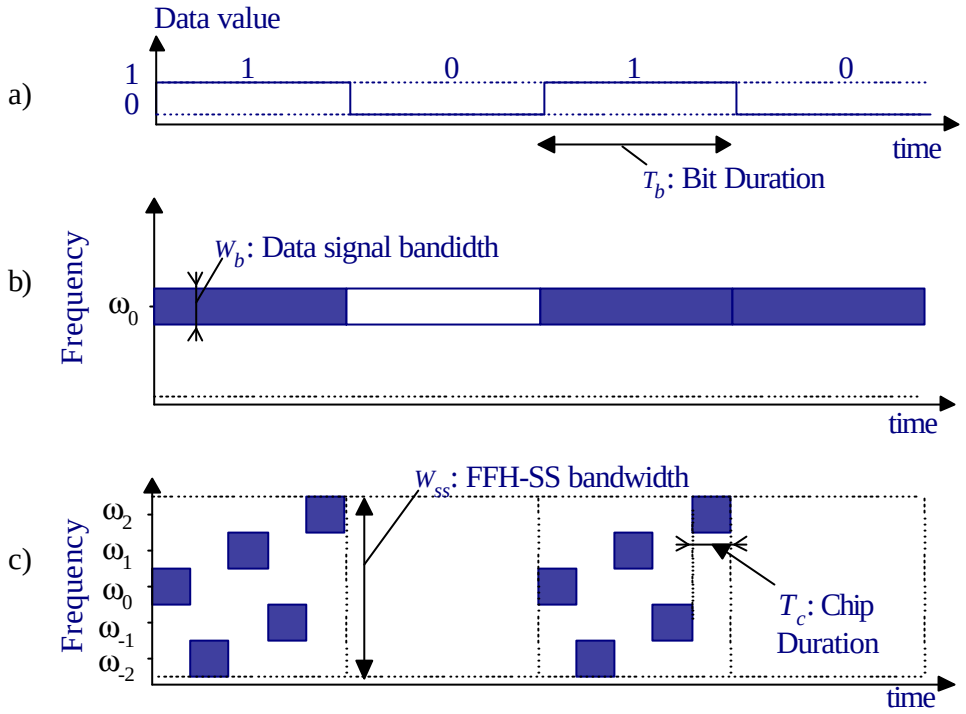

Figure 1.9: Radio-frequency FFH-SS Encoding Principle.

Figure 1.9 c), represents the frequency *vs*. time distribution of the encoded signal. The five pulses are centered at the frequencies ω_0, ω_{-2}, ω_1, ω_{-1} and ω_2. It is clear that the frequency synthesizer should be at least as fast as the flow of chips, therefore, *F* times faster than the data rate. This increases the system cost in satellite communications. Indeed, the faster the frequency synthesizer increases, the faster its cost increases.

At the receiver (Figure 1.10), the received signal is equal to the sum of the contributions of all the active transmitters. A frequency synthesizer is also necessary to generate a copy of the desired user code. The demodulation and decoding can be made in a combined or separate way depending on the application [10].

It is important to note the time-synchronization module in the receiver. A closed loop between the demodulated (or decoded) signal and the code generator is needed. Synchronization

consists in advancing or delaying the locally generated code in such way its period coincides exactly with the desired user signal period.

Under ideal conditions, at the demodulator output, the signal finds its initial time *vs.* frequency distribution. The F pulses are gathered in the same frequency band W_b, centered at ω_0 as in the transmitted data signal of Figure 1.9. Before decision, a pass-band filtering of W_b pass-band and integration over the period T_b are performed. According to the amount of detected energy, the received bit will be estimated to be 1 or 0.

We will see in Chapter 2 and 3 that in our optical FFH-CDMA system, these operations do not exist. They will be replaced by two steps: 1) an integration over a chip time, and 2) a filtering which is done over all the SS bandwidth. We will note that, in our system, we achieve the dual functions of that traditionally done in radio frequency FFH-CDMA. These fundamental differences will de highlighted in Section 2.4, and promises future exciting research.

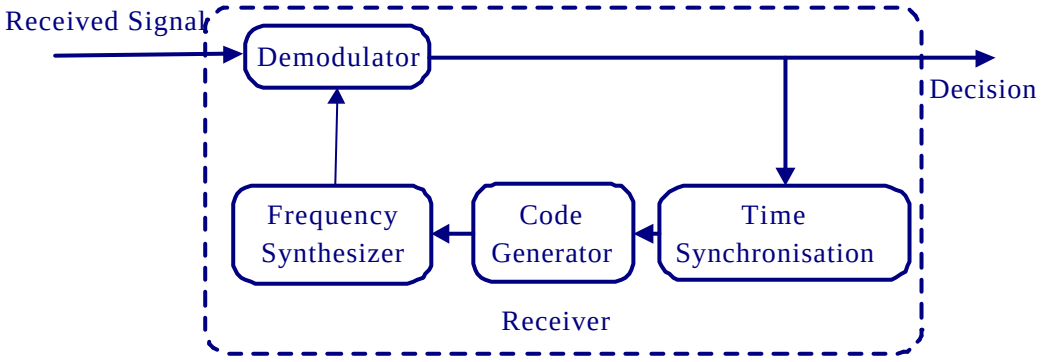

Figure 1.10: Block diagram of radio frequency FFH-CDMA receiver.

1.4 Emergence of All Optical CDMA

The difficulty and cost of implementing CDMA coding techniques from RF in optics has motivated all optical coding methods. Tens of variants of optical CDMA systems have appeared [14-17]. In Figure 1.11, we show a typical architecture of an all-optical CDMA system. At each transmitter, an optical source output is multiplied by the information data. Before transmission,

some parameters defining the data signal are manipulated by means of a set of optical devices referred to as the *encoder*. Each transmitter is assigned a specific set of operating parameters, which are defined as a specific code. All the transmitted encoded signals are then summed into the common optical transmission medium.

At each receiver, a copy of the aggregate optical signal is received and its optical field parameters are manipulated using a set of optical components referred to as a *decoder*. If the receiver knows the desired transmitter code, it will restore the optical data signal by nullifying the optical field transformations previously achieved by the desired user's encoder.

From a system viewpoint, hence, optical CDMA variants can be partitioned into two categories: 1) positive systems, where the phase is of no concern (Section 1.6); and 2) coherent systems where the phase counts in system design (Section 1.5).

The first category assumes only positive signaling waveforms (positive codes), in time and/or in frequency. Positive CDMA techniques based on power summation/splitting are in principle easier to implement, and use less-expensive and more-mature technology. Some of them already exist in the market. Coherent approaches, on the other hand, suffer from phase drifts and polarization dependency in the system components. They are consequently more expensive, less

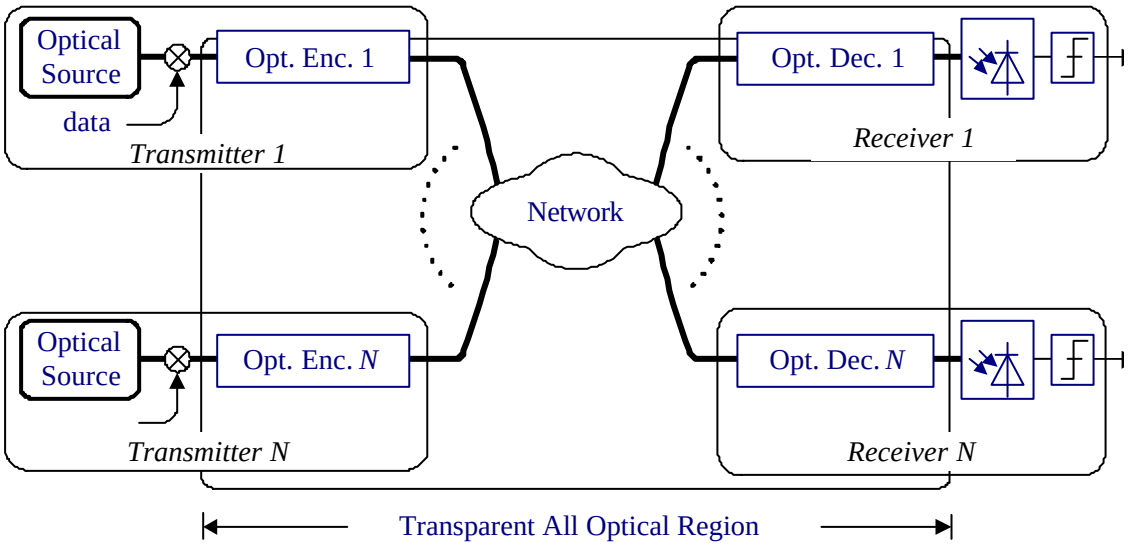

Figure 1.11: Typical Architecture of an All Optical CDMA System.

practical, and still far from commercialization in the short term.

It should be noted that the terminology used to describe optical CDMA techniques is often confusing and in need of standardization. Authors usually give new names to techniques, without reference to any agreement or standard.

1.5 Coherent Optical CDMA

In coherent optical CDMA systems, the complex form of the optical field is exploited in the encoding process, including amplitude and phase. Phase plays an important role in code design and properties. As in radio frequency, manipulation of the optical field phase, in addition to the amplitude, allows a sum of signals to at times be zero. The technology required for coherent optical processing, however, is significantly less mature than that for incoherent or amplitude processing.

1.5.1 Coherence-length based CDMA

In this scheme, the coherence length of the source is of key importance [16]. An incoherent source is usually utilized, yet a phase modulation is performed. This encoding/decoding principle was introduced before its application for a CDMA network [34]. In this approach, a ladder network of tapped delay lines is used as an encoder in order to insert a number k of phase

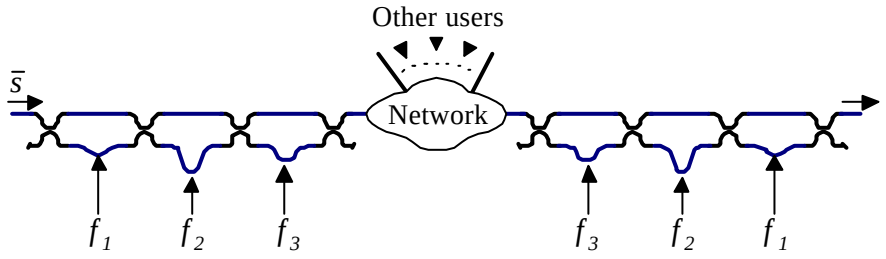

Figure 1.12: Coherence-length based multiplexing

shifts ϕ_1, ϕ_2… ϕ_k as shown in Figure 1.12. The signal at the encoder output is a sum of copies of the source signal $\bar{s}$, each copy having a phase shift. Those phase shifts represent all the possible

combinations (*i.e.*, sums) of the k phase shifts. At the decoder, an identical ladder network will compensate for these phase shifts so that only signal components originally from the same coherence length superpose creating a high autocorrelation peak. Otherwise, a noise-like signal will be observed.

In a CDMA system based on this principle, an important feature should be noted. Since each interferer uses a distinct incoherent source, their signals are inherently out of phase with respect to the desired user signal.

1.5.2 Coherent DS-CDMA

Coherent optical direct sequence CDMA is similar to its counterpart in wireless systems (Section 1.3.2). Hence, the *m*-sequence, Gold, and Kassami code families previously developed for wireless CDMA, are directly applicable for this architecture. As shown in Figure 1.13, the BPSK data bits are multiplied by a bipolar sequence delivered by a code generator. The encoded signal drives an electro-optic phase modulator, which shifts the electric field of the optical signal by a phase equal to 0 or π depending on the binary encoded spread spectrum signal. Since the phase of the optical signal is of importance in the system, the laser should have stable coherence properties.

At the receiver, another phase modulator and code generator are used. If the locally generated code is well synchronized with the desired user signal, the data will be restored. Otherwise, only noise-like bursts are observed. The dual balanced photodetector is used in order to generate a current proportional to the polarity of the data bit [32]. The local oscillator (or local laser: LL) provides an important amplification to the received signal, as it is the case in standard coherent detection systems [33]. The integration is performed over bit duration periods.

Hybrid WDMA/CDMA schemes have also been proposed where a number of low rate CDMA users can be superposed at each wavelength [45]. This is done in order to combine the advantages of both WDMA and CDMA systems.

Figure 1.13 represents only a simplified scheme of such hybrid systems. A real system should take into account many parameters including the phase drift due to the laser and the fiber, as well as polarization effects. It should be noted that the receiver is more complex; polarization maintaining components and fast phase locking loops should be included. This issue is not addressed in this context. The technique here does not fall in the category of all optical CDMA

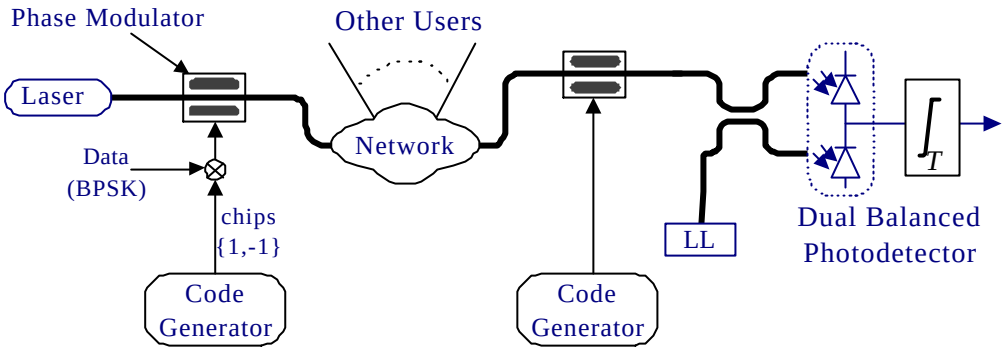

Figure 1.13: Simplified scheme of coherent DS-CDMA system with homodyne detection [32].

since the encoding is not performed in the optical domain.

1.5.3 Pulse-Based Coherent DS-CDMA

The development of femtosecond mode locked lasers delivering a train of ultra-short pulses with high coherence purity has motivated the emergence of new all-optical CDMA techniques. Each pulse is modulated by the value of the OOK data, and then split into identical sub-pulses along different optical paths. A combiner (passive coupler) gathers all the sub-pulses into the same fiber. The lengths of the optical paths are dimensioned so that the sub-pulses will be placed corresponding to a pre-determined pattern or code.

Figure 1.14 depicts a simplified reproduction of the experiment recently reported by Wada and Kitayama [30]. The encoder/decoder device, including all its elements, is monolithically integrated as a planar lightwave circuit (PLC). This includes tunable splitters, phase shifters, delay

lines, and combiners. The physical separation between the splitters defines the time-spacing between the chip pulses. The phase of each tapped pulse could be varied using an optical phase shifter consisting of an optical waveguide and a heater. The phase shifters adjust the tapped pulses as prescribed by the bipolar code. Tapped pulses are given a corresponding phase shift.

At the receiver, a similar setting is configured in order to match the desired user's encoded signal. The correlation between the receiver code and the desired user code leads to an auto-correlation peak. The interference signals, however, contribute by low-level peaks. Once decoded, the receiver may require some important and complex processing operations. This complexity is mainly due to the incapacity of electronics to make a set of very high speed processing required to complete the reception operation. The decoded signal should be compared to a threshold level in order to decide about the data bit value. The threshold value can be estimated using the statistics of the family of codes, and the number of active users. Furthermore, the desired part of the signal exists in a chip duration, over which integration should be performed. Since the original optical pulses are of sub-picosecond duration, it is not realistic to perform such

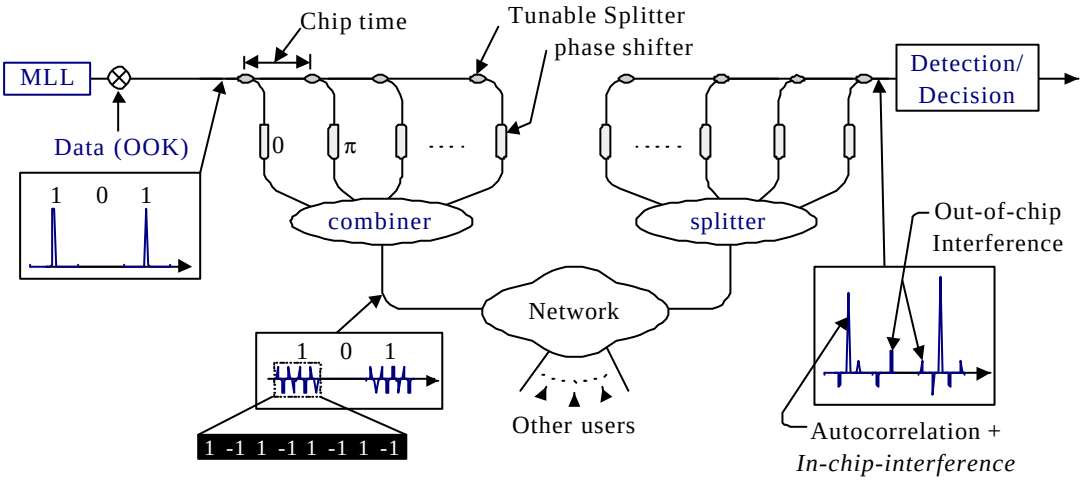

Figure 1.14: Coherent Pulsed DS-CDMA System [29-30].

operations in the electric domain.

Reception Issues

It is important to note a fundamental difference between decoded signal components in this optical coherent CDMA method and traditional (RF) coherent systems similar to the wireless counterpart. In wireless coherent CDMA, the decoded signal is a scalar product of the receiver code and the overall received signal (i.e. the desired signal plus interference). In this optical DS-CDMA system, however, the decoded signal is a sum of the whole auto- and cross-correlation functions and not only a scalar product. This explains the fact that, in this system, the autocorrelation peak corresponding to the desired user signal always appears without requiring any synchronization loop. Consequently, both the side-lobes of the auto-correlation function and the terms of the cross-correlation functions all appear in the decoded signal. Since integration for bit decisions should be performed within a chip duration only, stringent optical and electronic hardware is required.

Here we cite two propositions of so-called optical *time-gates*, which are applied on the decoded signal in order to pass only the autocorrelation peak. The first method [29], Figure 1.15 a), is inspired from the standard receiver architecture in optical coherent detection (Section 1.5.2). In place of a CW local laser signal, an optical clock signal, *i.e.*, the output pulse train of an MLL (mode locked laser) is used. An adjustable delay line is inserted inside the clock path in order to synchronize its pulses with the auto-correlation peaks.

Once this synchronization process is achieved, the output current of the balanced photodetector should present a high peak when the bit value is equal to one. It presents however a low level signal if only the interference is present; the corresponding bit is then decided to be zero.

On one hand, the mean value of the interference contribution can be assumed to be 0 for any coherent DS-CDMA system; this only requires good selection of the bipolar codes. On the other hand, for positive optical CDMA, specifically incoherent DS-CDMA, the value is always positive, and assumed proportional to the number of active users. Furthermore, the detection

threshold in coherent CDMA, is equal to half the voltage (or distance *d*) corresponding to the autocorrelation peak (see Figure 1.15). The signal representation in this figure assumes short propagation distance, otherwise a field representation is required for the signal in order to consider phase, polarization and dispersion effects.

The second method [29], Figure 1.15 b), includes local optical clock extraction, and time-gating. The latter operation uses semiconductor optical amplifier (SOA) based four wave mixing (FWM). The principle has been previously proposed for all-optical TDM multiplexing systems. The decoded signal is split into two replicas; the first is fed to an optical clock regenerating system. The latter exploits the auto-correlation peaks in order to generate a clock signal similar to that generated by an MLL, yet exhibiting better synchronization with the decoded signal. This clock and the decoded signal are both fed to the SOA, yielding the desired output.

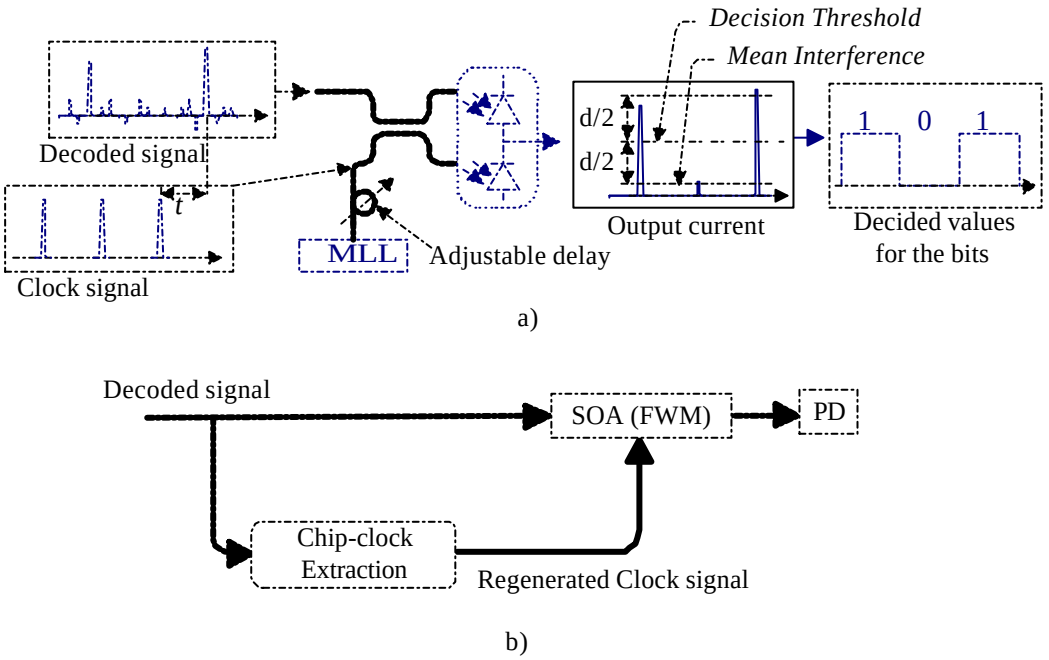

Figure 1.15: a) Optical Time-Gate using local clock and b) All-optical time-gate using clock regeneration [29, 30].

1.5.4 Time Spread Optical CDMA

Time spread-CDMA, developed by Salehi, Weiner et *al.* [55-61] in the late 80s, is considered among the most attractive implementations of optical CDMA (see Figure 1.16). This was the first time, to our knowledge, that the frequency axis itself was used as an encoding resource. This required an ultra-short pulse mode locked laser (MLL) providing a coherent broad bandwidth. The MLL output is modulated by the binary data in OOK format. The signal is then focused on a diffraction grating that spatially deploys the frequency components of the pulse. A phase mask, placed in the Fourier plain, introduces a phase-shift of 0 or π at each spectral component, according to a given bipolar frequency code. Following the mask, the frequencies are gathered using a second diffraction grating and injected into the fiber. The setting, including a phase mask, two lenses, and gratings, is usually referred to as a *4F*-diagram. This is especially used for pulse shaping applications.

The decoder has a similar *4F*-diagram. The phase mask, however, is configured with the phase conjugate of the encoder mask. The phase mask can be programmable if a Liquid Crystal Modulator (LCM) is used. Recent progress [55] published in 1998, reported a system including

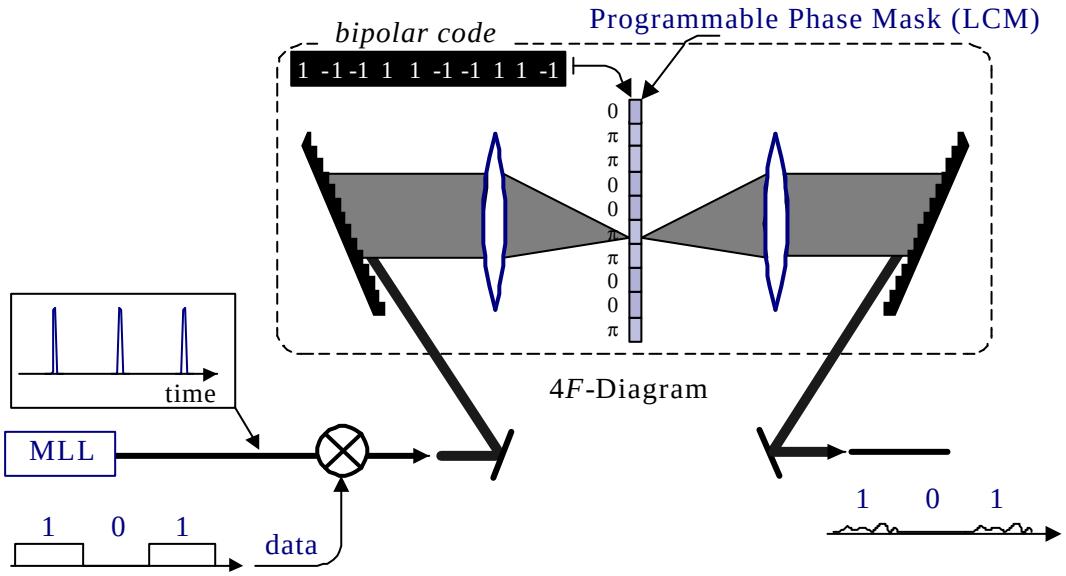

Figure 1.16: Time Spread-CDMA Encoder.

one encoder, one decoder, a 62 fs pulse MLL, a programmable fiber-pigtailed LCM with 128 pixels, DCF based dispersion equalization of 2.5 km link, and a high contrast nonlinear optical thresholder. The latter module is required after the decoder in any optical CDMA system using ultra-short pulses. Auto- and cross-correlation functions are measured with high fidelity in the absence of interference. In Section 7.3, we shall explain that a series of fiber Bragg gratings with accurate physical spacing can perform time spread-CDMA encoding.

1.6 Positive Optical CDMA

1.6.1 Incoherent DS-CDMA

Incoherent DS-CDMA is among the earliest and most well known optical CDMA proposals, and has attracted a significant research body for about fifteen years. The earlier encoder architecture consists of tapped delay lines as shown in Figure 1.17 a) [18-20, 35-54]. Optical data signals enter the encoder as short pulse trains modulated in the OOK format. When the data value is 1, each delay element delivers a chip sub-pulse from the incident bit pulse at a time-position fixed by the corresponding line length. The number of delay lines in the encoder (*i.e.*, number of ones in the code) is equal to the weight of the code.

The encoding process involves a double division of power while crossing the input and output couplers, which incurs significant loss. A ladder network has been proposed to overcome this power penalty, as shown in Figure 1.17 b). None of the two architectures allows reconfigurability, i.e., they only allow fixed codes. A ladder network where couplers are replaced by a 2:2 cross/bar switches allow such reconfigurability and eventually offer better power preservation (see Figure 1.17 c)).

The decoder at the receiver is identical to the encoder except that it performs the inverse function. Chip-pulses arriving in advance are delayed so that all the chip-components of the signal travel an equivalent path. The pulses coming from the desired transmitter will superpose in the same chip duration, thus requiring a fast time-gate.

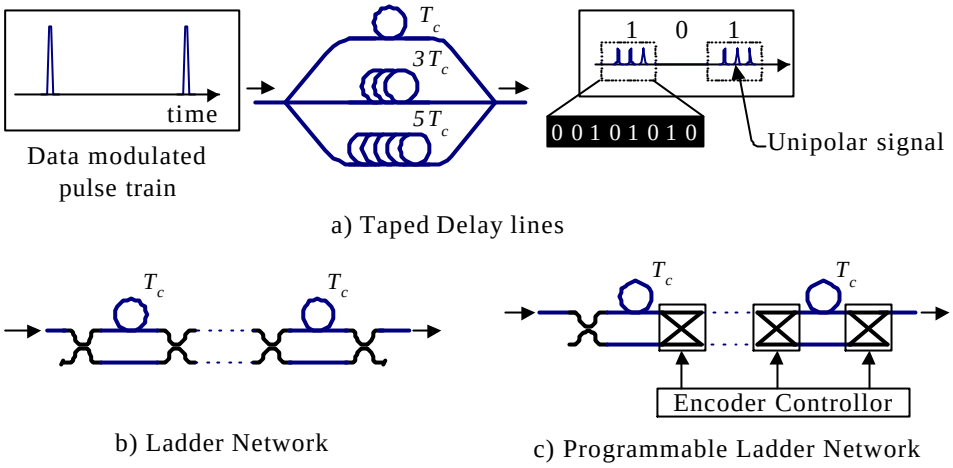

Figure 1.17: DS-CDMA Encoding/Decoding devices.

OOC Codes

The performance of any CDMA system strongly depends on the codes' properties. Since only positive chips are used in this system, very long codes with low weight are usually required in order to insure acceptable transparency (i.e. a low enough cross-correlation). When the cross-correlation between codes increases, the probability of error dramatically increases. To meet incoherent DS-CDMA requirements, researchers have developed various families of so-called *optical orthogonal codes* (OOC) [39-53]. It should be noted that those codes are not perfectly orthogonal, except for some less-practical synchronous systems.

The most popular OOC family is called prime sequences (PS) [46, 52]. It is known that these codes have optimal cross-correlation properties. Their auto-correlation function, however, presents very high side-lobes. OOC families are often presented by quadruplets (n, w, λ_a, λ_c). n, w, λ_a and λ_c are respectively the sequence length, weight, maximum side-lobe in the auto-correlation function, and the maximum value of the cross-correlation function.

To improve the orthogonality between codes, their weight should be minimized, which unfortunately decreases the signal to noise ratio. Reducing the code weight necessarily reduces the signal power of the user, hence inevitably decreasing the signal to noise ratio. To achieve an acceptable number of users, very long codes are required. That results in an excessive loss of channel resources.

1.6.2 Incoherent FE-CDMA

Since the pioneering work of Zaccarin and Kavehrad [64-69], incoherent frequency encoded-CDMA (FE-CDMA) has attracted a significant body of research. As shown in Figure 1.18, an amplitude-mask-based *4F*-diagram transmits a subset of frequencies from an incoherent source, *e.g.*, LED (Light emitting diode) or ASE (amplified spontaneous emission). Therefore, only unipolar codes are used, which seriously reduces the network capacity in terms of number of users.

At the receiver, the signal is split into two *4F*-diagrams. The first is configured for the desired code (branch D) and the second for its complement $\overline{D}$ (i.e., the i^{th} element of $\overline{D}$ is equal to 0 if that of D is equal to one, and vice-versa). When Hadamard codes, or cyclic shifts of any *m*-sequence code, are used, the interference signal is equally split among the D and $\overline{D}$ branch outputs, hence contributing to equal currents at the two photodetector outputs. Consequently, the interference in the resulting current is naturally removed, and only the desired user's signal remains. Some limitations were later studied, including the non-uniformity of the source spectrum, gratings

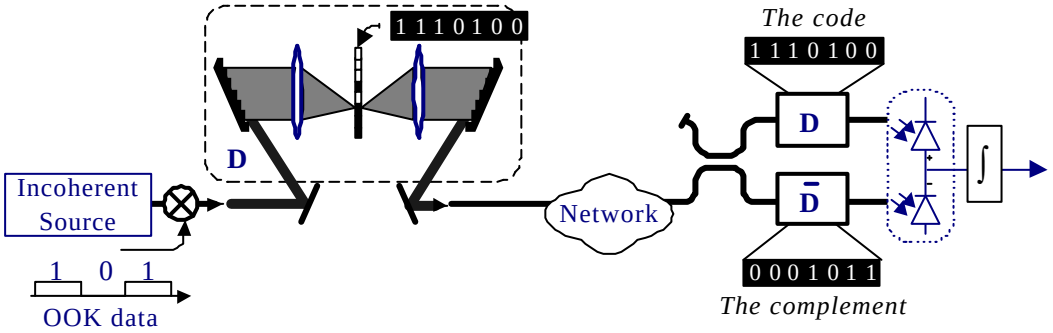

Figure 1.18: Incoherent FE-CDMA System.

and mask diffraction, misalignment, etc.

Due to its attractive properties, bipolar encoding has also been investigated in an incoherent FE-CDMA system. The idea is based on the emulation of bipolar encoding by transmission of the code complement, rather than no power, when the data bit value is zero. In Figure 1.19 a) and b) two transmitter architectures are shown. The first uses a balanced broadband source where modulation is performed by electrically alternating the sources [74]. In the second, the data drives an electro-optic 2:2 switch. By selecting the bar/cross states, depending on the incoming bit value, it selects which of the code or its complement should be transmitted [73]. The *4F*-diagram, as well as the AWG-based encoder/decoder of Figure 1.19 c), can be used at each of those transmitter architectures. The setting of Figure 1.19 d), demonstrated by Nguyen *et al.* [73], simultaneously operates as D and $\overline{D}$.

Other settings have been proposed to perform FE-CDMA encoding/decoding functionality. All are based on optical filters, Array Waveguide Gratings (AWG), multiple Bragg

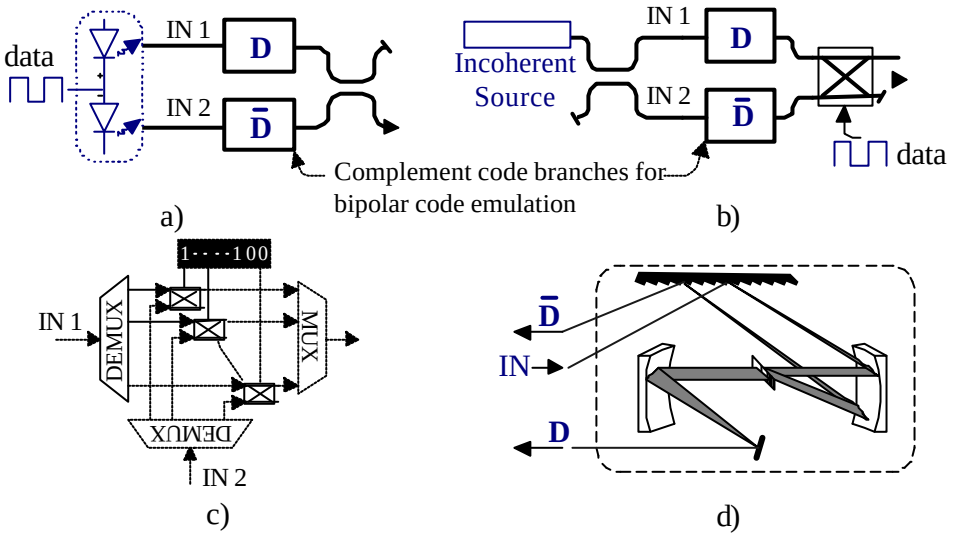

Figure 1.19: a) and b) two FE-CDMA transmitters' architectures including bipolar code emulation; c) Lam's principle [74], and d) Nguyen's setting [73].

gratings (MBG), and acousto-optic tunable filters [70-72, 79]. The latter have been experimentally demonstrated [70].

1.6.3 Wavelength-Hop/DS-CDMA

The adoption of incoherent DS-CDMA for real-networks has been handicapped mainly by the properties of its codes. The use of unipolar encoding results in very low code weights and very low cardinality of their families. Tancevski and Andonovic [123,124] have proposed to use the wavelength dimension as an additional encoding resource, thus performing a hybrid wavelength/time encoding. An obvious method consists of assigning a wavelength for each subgroup of DS-CDMA users. Such a system is called a hybrid DS-CDMA/WDM system.

A more sophisticated approach combines the frequency hopping spread spectrum codes with those of incoherent DS-CDMA. When the number of available wavelengths is equal or higher than the number of ones (or pulses) in the DS sequence, each pulse will be supported by a distinct wavelength. Each frequency hopping (FH) code can carry a whole family of DS codes, *i.e.*, the number of FH/DS codes is roughly the product of the number of FH by that of the DS codes. This allows an appreciable number of subscribers in the network. Moreover, it suppresses all the side-lobes of the auto-correlation function. The cross-correlation lobes are also reduced.

Figure 1.20 a) shows an example of a WH/TS sequence. Figures 1.20 b)-e) illustrate different encoder/decoder architectures suitable for FH/TS signal generation. All of them were proposed and discussed in [123-124]. The four architectures are arranged in increasing number of components and decreasing reconfiguration rate. This illustrates the trade-off between the number of components and the reconfiguration rate. In general, the use of tunable lasers and multiple switches highly complicates the hardware and increases the system cost.

We shall see in section 2.3 that the pulse placement and frequency selection operations which made the hardware heavy and costly were easily overcome by the emergence of multiple fiber Bragg gratings in optical CDMA.

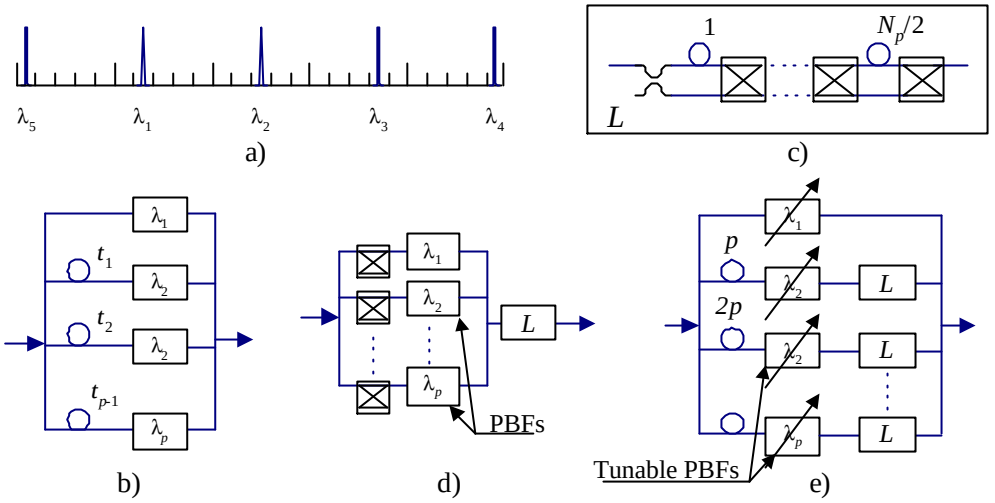

Figure 1.20: Possible architectures for FH/TS-CDMA signal generation: a) An FH/TS code; b) Fixed correlator using delay lines and PBFs; c) tunable laser (TL) and programmable ladder network (PLN); d) a bank of switched pass-band filters (PBF) and one PLN; and e) parallel network of PBFs and PLNs [123-124].

1.6.4 Periodic FE-CDMA

This scheme was first proposed by Möller in [75], and Pfeiffer et *al.* [76-78] with Alcatel in Germany. The most attracting point of this technique is that it uses commercially available low-quality filters and LEDs. A broadband spectrum is filtered by a standard periodic filter (e.g. Mach-Zehnder or Fabry Perot) and then multiplied by OOK data at the bit rate. By changing the free spectral range (FSR) of the filter, we achieve a different periodic spectrum, hence a different code, identifying a different subscriber. At the receiver, an optical periodic pass-band filter, matched to that of the desired user, can perform the decoding operation.

It has been determined that this technology should accommodate 32×155 Mb/s subscribers [76]. An experiment at rates of 12×155 Mb/s and 8×622 Mb/s has demonstrated high stability for a wide range of environment temperature variations (-40 ºC to 85 ºC) [78].

1.7 Space Optical CDMA

1.7.1 Fiber-array Space CDMA

Mendez et *al.* [136-141] proposed and demonstrated a hybrid Space/Time optical CDMA system. In such a system, the network consists of a number of passive N:N star couplers superposed so that a transparent, equal length, array of fibers exists between any encoder/decoder pair. The encoding principle is a set of tapped delay lines similar to that of incoherent DS-CDMA. The combiner is however removed, and each chip pulse travels in a different fiber of the array. At the receiver, the chip pulses, already separated in different fiber-paths, are injected into the decoder without splitting. This reduces the overall power loss in the system, as well as the auto-correlation side lobes, the cross-correlation terms, and the bit-to-chip duration ratio, hence alleviating the electronic speed requirement in the receiver.

1.7.2 Multicore-Fiber Space CDMA

In this system, the key component is the so-called *the multi-core fiber* [142], or the image fiber [144-147]. A multi-core fiber is composed of a high number of densely assembled parallel fibers of equal length. The images are spatially encoded so that each pixel is transmitted through a subset of parallel fibers. Two-dimensional space-codes can allow the multiplexing of a high number of images. An image fiber composed of thirty thousand fibers has recently been reported by Kitayama's group [143-146]. The experiment has demonstrated a system including two encoders with 8x8 2-D codes transmitting 4x4 bit matrices (pixels). At each transmitter, one 2-D spatial light modulator is used to insert the code, and a second SLM to insert the bit matrix (or the image) to be transmitted. At the receiver, one SLM is controlled in order to match the desired transmitter code, and a thresholding operation is performed. Potential applications of these techniques include future data links for massively parallel computer networks and data transfer between optical page oriented memories and processors [143].

1.7.3 Holographic CDMA

In this scheme, two-dimensional holographic masks are used as encoders/decoders. Due to the very high achievable spreading gain, the system has been predicted to support up to millions of users [148-149].

Chapter

2

Optical FFH

Concept and Implementation Solutions

The objective of this chapter is to introduce a new generation method (or concept) of optical fast frequency-hopping (OFFH) signal. A CDMA system that exploits this OFFH method is the focus of chapter 3. In addition, in this chapter, we describe some possible implementation solutions. In section 2.1, we review a mathematical model of the standard principle, which helps us introduce the new principle. In sections 2.2 and 2.3, we introduce the new processing principle to generate the optical FFH signal and discuss with block diagrams different possible architectures for the transmitter. In section 2.4, we mathematically analyze the new FFH-encoding concept and we exploit the duality between the filtering and modulation functions to highlight the fundamental differences between the new and the conventional principles.

In Section 2.5, we exploit the cascade of Bragg gratings to implement the new FFH principle. It is important to note that we first proposed the cascade of Bragg gratings to perform the FFH-encoding, and found later that the principle can be generalized, as explained in Section 2.1, as the dual of the well-known FFH-SS in radio frequency systems.

2.1 Optical FFH-SS Principle

In this section, we review the principle of the conventional FFH-SS technique and develop a mathematical model for the frequency synthesizer output. We analytically transform the FFH-SS signal expression to a form that will help us identify the signal processing operations and steps necessary to generate an FFH-SS signal. This will justify our idea that a fast frequency synthesizer is not fundamental for OFFH-SS transmission. Finally, we shall find that using our mathematical analysis, we precisely meet the conceptually expected results.

2.1.1 FFH-SS Signal Model

The encoding process in a conventional radio frequency FFH-Spread Spectrum technique was previously described in Section 1.2. Recall that it requires a rapid frequency synthesizer (FS) at both the transmitter and the receiver ends [1-11]. The FS should be able to deliver any among a number of F frequencies available in the spreading bandwidth. We

refer to theses frequencies (or carriers) as ω_1, ω_2 ... and ω_F, where $\omega_i=\omega_c+i\Delta\omega$ for $i=1\ldots F$. ω_c is a predetermined carrier, and $\Delta\omega$ is a constant frequency spacing between neighboring carriers. The frequency ω_i can be simply referred to by its subscript i denoting both its number among the available carriers and its separation from ω_c, *i.e.*, $i\Delta\omega$.

As depicted in Figure 2.1, the synthesizer of the transmitter should provide a periodic signal $s_{\boldsymbol{c}}$ with a period length equal to the data bit duration T_b. The subscript $\boldsymbol{c}$ is a vector designating the spreading sequence of the transmitter. Each period T_b in the FS output is composed of a concatenation of a number M of chips of duration $T_c=T_b/M$, during each of which the synthesizer generates a different sinusoid corresponding to the pre-selected sequence $\boldsymbol{c}$.

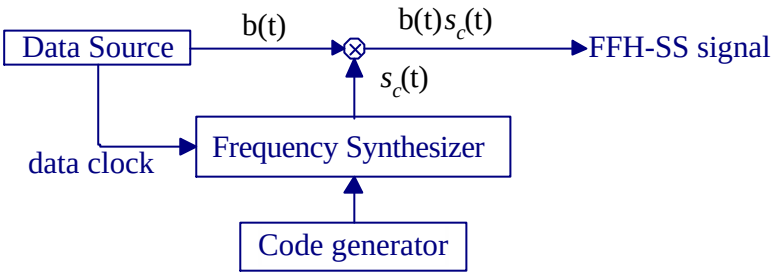

Figure 2.1: Conventional FFH-SS transmitter

In an FFH-SS transmitter, M frequencies among the available F are selected, corresponding to a sequence $\boldsymbol{c}=[c_1, c_2,..,c_M]$, where c_j, $j=1,..,M$ is an integer number corresponding to the carrier number used in the j^{th} chip interval of the sequence, *i.e.* $1 \le c_j \le F$.

Let us decompose the FS output into a linear sum of different orthogonal signals as described in Figure 2.2. This decomposition can be mathematically expressed as follows

$$s_c(t) = \sum_{j=1}^{M} s_{c_j}(t) \qquad (2.1)$$

where $s_{c_j}(t)$ denotes the part of $s_c(t)$ occurring in the j^{th} chip interval of the sequence $\boldsymbol{c}$,

and zero elsewhere.

The summation in equation (2.1) is achieved over all the chips of the sequence. Each chip periodic signal s_{c_j} can be expressed as a product of the j^{th} sinusoid in the sequence $\boldsymbol{c}$ and a periodic rectangular signal. The latter can be interpreted as a clock signal with low duty cycle.

Let $q(t)$ be a periodic square function (clock), with low duty cycle equal to $T_c/T_b=M^{-1}$, shown by the following equation

$$q\ t\ =\ \sum_{j=-\infty}^{+\infty}\Pi\left[t-jT_b\right],\quad \text{where}\quad \Pi\left[t\right]=\begin{matrix}1 & 0\le t\le T_c\\ 0 & \textit{elsewhere}\end{matrix} \tag{2.2}$$

The component s_{c_j} of the FS output can be written as

$$\begin{aligned} s_{c_j}\ t\ &= q\ t-\ \ j-1\ T_c\ \ s_c\ t\\ &= q\ t-\ \ j-1\ T_c\ \ \cos\left[\ \omega_c+c_j\Delta\omega\ t\right]\end{aligned} \tag{2.3}$$

where we used the equation

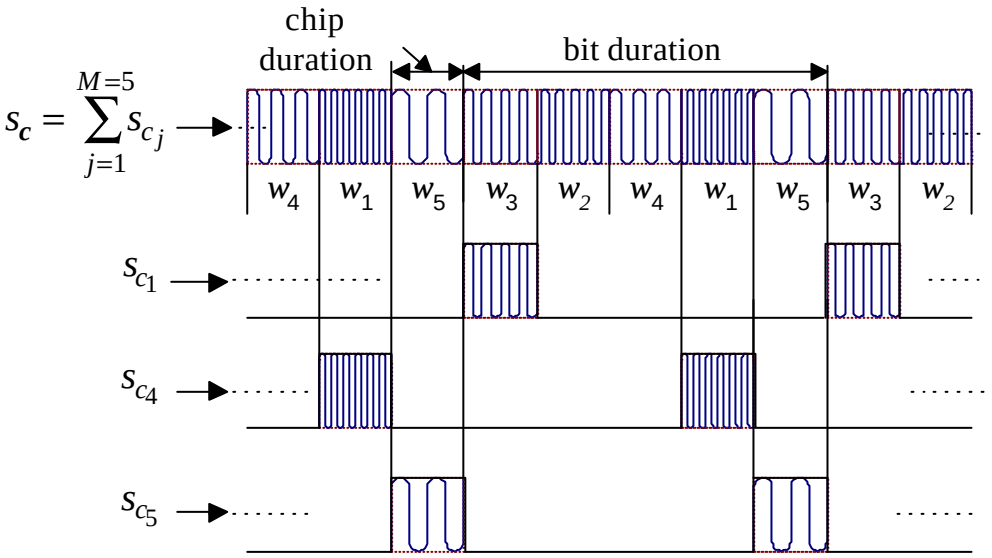

Figure 2.2: Frequency synthesizer output and its linear decomposition.

$$q[t-(u-1)T_c]\,q[t-(v-1)T_c] = \begin{cases} q(t-(u-1)T_c) & \text{if } u=v \\ 0 & \text{if } u\neq v \end{cases} \quad \text{for } u,v=1,..,M \tag{2.4}$$

Finally, using equations (2.1) and (2.3), the FS output can be expressed as

$$s_c(t)=\sum_{i=1}^{M} q[t-(j-1)T_c]\cos[(\omega_c + c_j\Delta\omega)t] \tag{2.5}$$

From equation (2.5), we can conclude that to generate the FS signal we can firstly proceed by generating each argument in the sum. Each of these arguments consists of a sinusoid switched ON/OFF in time by the low duty cycle periodic clock function. The clock function is the same for all terms; only its delay varies for each chip in the sequence.

It is important to note that once the spreading sequence is identified in the transmitter, the FS output becomes a deterministic signal, and does not change during transmission. Hence, the FS signal can be stored in a memory, for instance, and addressed when needed. This is recently proposed by Takakusaki in the patent document [13]. It was suggested to replace the FS in standard FFH-SS receiver by a ROM (read only memory) containing a digitized form of the FS signal. When a bank of ROMs containing time shifted copies of the FS signal is used, this can also provide a good solution to the synchronization problem between the received signal and the receiver sequence.

In the following section, we exploit Equation (2.5) to define the key signal processing operations necessary to generate the FFH-SS signal. Once the FS signal is generated, only multiplication by the data signal remains to produce the FFH-SS signal.

2.1.2 FFH-SS Signal Generation:

Equation (2.5) shows we can generate the FS signal if two tools are available: 1) the set of sinusoids selected by the code and 2) a clock signal with duty cycle M^{-1}. If we assume the required clock source and frequencies are already available in the transmitter that is sufficient, in principle, to generate the FS signal. In the optical domain, these frequencies can be provided by a laser array, a multi-wavelength source, or eventually

filtered from a broadband source. To generate the FFH-SS signal, the following four signal processing operations should be performed.

i. Selection of a predetermined subset of frequencies corresponding to the sequence.
ii. Time-switching each selected frequency so as to generate short pulses each of which is centered at a different frequency.
iii. Introducing relative time delays between the short sub-pulses as specified by the sequence.
iv. Multiplying the generated code sequence by the data stream.

This leads us to imagine that any device or system capable of performing these elementary operations can generate the FFH-SS signal. In our analysis, we emphasized that the frequencies can be already available and used upon demand instead of generating them as previously done by the frequency synthesizer. In optics, a continuously emitting laser can be considered as an already available frequency. Moreover, a broadband source can be considered as an available large bank of frequencies. In the following, we discuss some possible transmitter architectures using block diagram schematics. Note that the settings described in Figure 1.20 can theoretically implement the FFH-SS encoding but involves high complexity and cost.

2.1.3 Transmitter Architecture:

Depending on the exploited technology and the devices' built-in functionality, some of the operations ***i*** to ***iv*** listed previously can be performed either sequentially or simultaneously. In Figure 2.3, we show three possible transmitter architectures, which seem the most interesting. All of these exploit a broadband or multi-wavelength source (referred to as BB and multi-λ respectively,). In addition, they use wavelength selection and time delay block to perform operations ***i*** and ***iii***. Recall that BB is considered here as a large bank of frequencies always available in the network upon demand.

In Figure 2.3 a), the light source output passes through a gate achieving the operation ***ii***), which generates a stream of optical broadband short pulses. This signal is split

among a number of transmitters, each of which goes through the remaining transformations depending on its own code (or sequence).

In Figure 2.3 b), the data signal is provided with waveforms having a low duty cycle, and applied as a control signal for the gate at the light source output. Only in this scheme, the light source can be shared among various transmitters; operations ***i*** and ***iv*** are combined, and the use of a second gate is avoided. This scheme will be investigated throughout the remaining chapters.

In Figure 2.3 c), the light source itself provides the broadband or the multi-wavelength pulse stream, which can also be shared among different transmitters. The source signal propagates through a gate controlled by the data with conventional waveform, *i.e.*, low duty cycle is not required.

The block diagrams in Figure 2.3 show that three important sets of devices are required to build a complete transmission system based on our encoding principle: 1) A specific light source, 2) a device or system able to perform frequency selection and time delaying, and 3) time gates or optical switches.

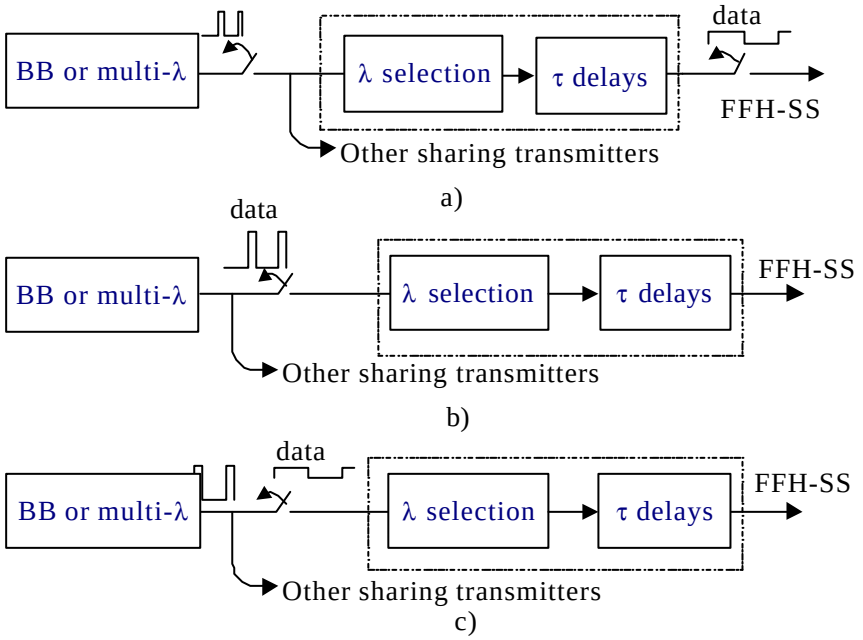

Figure 2.3: Three different architectures suitable for an optical FFH-SS implementation of the proposed encoding principle.

2.2 Suitable Optical Sources:

Several FFH-SS transmitter architectures are shown in Figure 2.1; all need specific devices to perform the required signal processing functions of the transmitter. Depending on the available device characteristics and built-in functionality, some functions can be implemented jointly or independently. In this section, we present light sources that can be used in the transmitter's architectures of Figure 2.3. In Section 2.3, we present some devices suitable to perform the λ-filtering and the time delaying functions.

One key feature of our encoding principle is the assumption of permanently available wavelengths or a bank of frequencies at any transmitter. Suitable sources should provide all spectrum frequencies or wavelengths necessary for encoding. The light sources can be coherent or a non-coherent sources. However, the coherence nature of the source has an important implication on the encoding technique itself as well as its overall performance. Although only non-coherent sources are used in the experimental part of this work, the encoding process of a broadband coherent source is illustrated in Figure 2.10.

2.2.1 Incoherent Broadband sources:

Non-coherent sources like LEDs, (Light Emitting Diodes), and the amplified spontaneous emission (ASE) of an erbium doped fiber amplifier (EDFA) have been previously used in frequency-encoded CDMA test-beds; (see section 1.6.2) and can be suitable for the FFH-SS system. Similarly, the ASE of a semiconductor optical amplifier (SOA) can be considered as an interesting broadband powerful incoherent source. In Table 1, we show some useful and conventional characteristics of these sources, such us full width at half maximum (FWHM) bandwidth (BW), total power (P_t), power spectral density (PSD), and approximate cost.

The SOA provides a high power compared to an LED [211, 212] and is less expensive than EDFAs. The SOA is also available in almost all the conventional communication wavebands, although they are more popular in 1300 and 1550 nm [211-212].

Source	λ_c	BW(FWHM) (nm)	P/PSD (dBm/dBm)	cost
LED	all bands	50÷80	-7/-40	<200 $
SOA (ASE)	1300/1550	70÷100	30/-15	~1k $
EDFA (ASE)	1550	30	25/-12	~10 to 15k$

All these sources can be used with the transmitter architectures (a) and (b) of Figure 2.3. In order to generate the optical broadband short pulses, a fast gate (or switch) is required at the source output. If an expensive source such as an EDFA is used, it can be shared among many subscribers using the architecture of Figure 2.3 a) and b).

It is known that the LED and SOA both have a power spectral density (PSD) with almost-Gaussian (or bell-shaped) form. This means that the elementary frequencies in the assumed bank do not have similar power. The power is an important parameter in every optical spectral-encoding based CDMA system. This problem has previously been encountered in FE-CDMA systems and two major solutions have been proposed: 1) source PSD flattening and 2) limiting the encoding in the central part of the PSD. Gain flattening of the EDFA using Bragg gratings can reduce the PSD non-flatness of an EDFA to a value lower than 1 dB over a 30 nm bandwidth.

Other important issues such as the limitation in direct modulation; the effect of coherence length and the intensity noise of the source on the pulse length and characteristics are not studied in this context.

2.2.2 Coherent Broadband Source:

The ultra-short pulse mode locked laser (MLL) is a coherent broadband source that is also suitable for FFH-SS. This was previously used for the first time by Salehi, et *al* [54-58] to implement the Time Spread-CDMA system (see Section 1.5.4). Recall this was the first time that the frequency axis itself was used as an OCDMA encoding resource.. He initiated a new trend in the optical CDMA field. These sources typically generate trains of

pulses with durations of few pico-seconds down to tens of femto-seconds. The pulse waveform is usually numerically modeled as the inverse Fourier transform of a Gaussian function. The FWHM of the assumed Gaussian PSD source rises as the pulse width decreases, *i.e.*, a 500 *fs* FWHM pulse width source occupies a FWHM BW of 15 nm. Some MLL sources use highly dispersive fiber (or material) and achieve more than 60 nm FWHM BW. These are usually referred as super-continuum sources.

The ultra-short pulse MLL usually has very low repetition rate (a few kilo- to mega-hertz). An optical multiplexing technique using fiber delay lines, similar to those used for DS-CDMA, is usually used to increase the repetition rate. This source is especially suitable for the transmitter architecture depicted by Figure 2.3 c). There is an increasing interest in these short-pulse lasers because they are suitable for all optical TDM and all optical packet switching [200-203,212-213]. This is because it is difficult to generate electrical pulses with comparable duration.

2.2.3 Multi-wavelength Source:

A multi-wavelength mode-locked laser (M-WMLL) is a coherent source that produces a comb of wavelengths, each of which can be considered as a different MLL [201,212]. Each MLL provides a train of pulses, with widths around a few picoseconds, respecting exactly the same rules as the ultra-short pulse-MLL laser described in the previous paragraph. The MLL's trains of pulses can be generated with relative delays prefixed by the M-WMLL architecture itself. For FFH-SS applications, these relative delays can be selected so that they correspond to an FFH-sequence. In such a case, the MW-MLL incorporates all the operations *i*, *ii* and *iii* of Section 2.1.2, and it cannot be shared between different users. If no predetermined delays are introduced among pulses, the source can generate all the system wavelengths; and can be shared among many users. Each of these users selects a subset of frequencies and introduces the correct delays corresponding to their own sequence.

2.2.4 Laser Array:

With the emergence of WDM systems, some companies have started to develop arrays of discrete lasers in the same substrate. Each of them is locked to one frequency corresponding to the ITU grid [206-209]. These arrays can be used as multi-wavelength sources in our system with the architectures a) and b) of Figure 2.3. The discrete lasers can be directly (or externally) and independently modulated to produce different frequency pulses corresponding to the code [210].

2.3 Optical Filtering and Delaying:

These two functions can be performed jointly or independently depending on the built-in functionality of the devices used. In Figure 2.4 a), we use band reflective-type filters (BRF), where each filter selects a precise wavelength or sub-band from the incident light. Due to their physical positions in the fiber, the filters should introduce relative delays between the reflected wavelengths.

If we are able to place the filters with a precise and predetermined physical spacing, it will be possible to introduce precise relative time-delays between the reflected

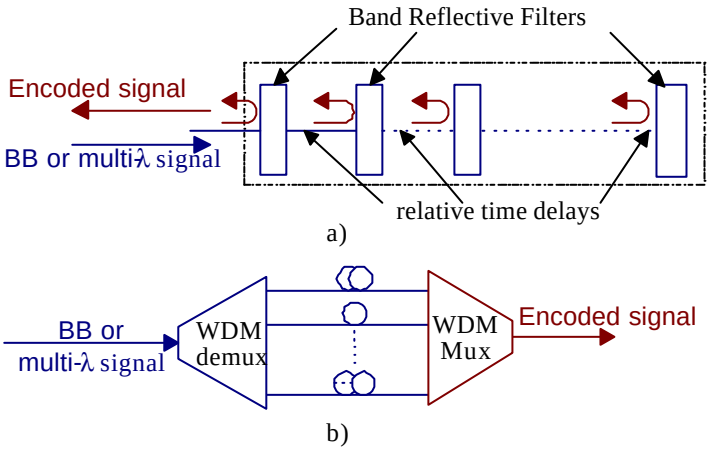

Figure 2.4: l-selection and time delay functions based on: a) Band reflective filters and b) WDM demultiplexing devices.

wavelengths. To perform this, two limiting parameters can be encountered: the proper physical dimensions of the filters and the accuracy of the positioning mechanism. If the used BRFs have high reflectivity, *i.e.*, ~100%, a second filter having the same central wavelength can be considered with no effect. This means that the in-line structure of the cascade of filters does not allow a wavelength to be reflected twice. Furthermore, it should be impossible to superpose two filters or more in the same physical location, *i.e.*, no more than one frequency can be reflected at the same time. The former affirmation depends in principle on the technology used because Bragg gratings, for example, can be superposed in the same location and simultaneously release a double reflection.

In Figure 2.4 b), a wavelength demultiplexer separates the wavelengths in different paths. One delay line should be inserted in each path as prescribed by the FFH sequence. BB and multi-λ source can be used with this architecture. The most popular demultiplexer is the AWG: Array Waveguide Grating. However, this remains an expensive solution. The demultiplexer can also be a passive power splitter cascaded with a bank of parallel pass-band filters, but this solution leads to a high loss of power. The WDM multiplexer in Figure 2.4 b) can be a passive coupler. This can also lead to a high loss of power.

In the case where an MLL is used as a multi-λ source with predetermined time delay between the pulses, the source itself combines the two functions: λ-selection and time delays. In such a case, the source can be very expensive and unstable. In addition, it cannot be shared among different transmitters. If a laser array is used as a multi-wavelength source, the wavelengths are naturally separated so the demultiplexer is not needed. Only delay lines are required.

2.4 Conventional *vs*. New Encoding Principles

In Section 2.1, we found that the generation of the FFH-SS signal does not require a frequency synthesizer because the frequencies (or carriers) become deterministic once the sequence is specified. In addition, equation (2.5) has shown that the FFH-SS signal is a function of only two parameters: 1) a set of sinusoids and 2) a low duty cycle clock. We have also proposed several transmitter architectures that are in principle capable of

generating an FFH-SS signal, eventually using passive components such as filters and delay lines. We assumed therefore that each filter selects a single frequency from a broadband source by considering their reflectivity as a single sinusoid.

When a multi-λ source or a laser array are used (Figure 2.5), the filter reflected bandwidths are wider than the lasers' linewidths and can be considered as having no spectral or temporal effect over the incident signal.

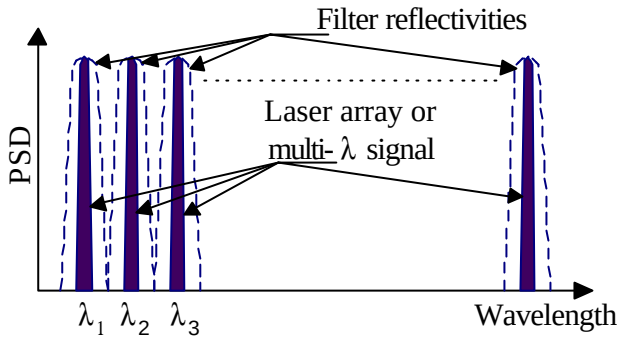

Figure 2.5: Filtering of a laser array or multi-wavelength signal; the filter's reflected bands are large enough, so that it does not affect the signal properties.

In the case where a broadband source is used however (Figure 2.6), the filters imprint their transfer functions in the incident signal. Therefore, the reflected signal results from an interaction between the filters on the incident signal. Practically, the time-frequency responses of the filters will shape the reflected pulse waveforms. Each of

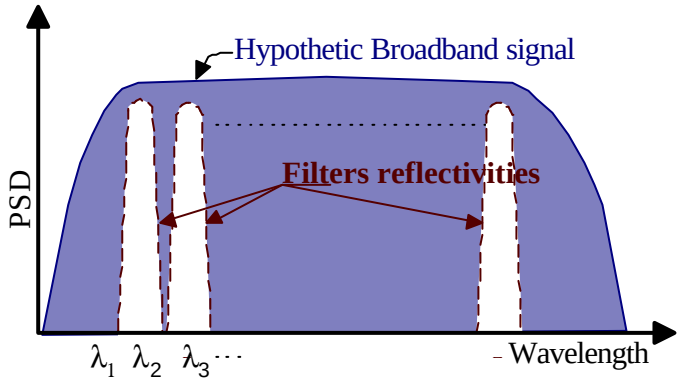

Figure 2.6: Filtering of Broadband signal.

those pulses corresponds to all frequencies contained in all the sub-band rather than a single frequency.

In the following, we analyze the encoding technique taking into account the filtering function effect when a broadband source is used. This analysis could be particularly interesting for both, optical FFH- or FE-CDMA.

2.4.1 Duality between Conventional and New principles

As described in Figure 2.1, the FFH-SS signal is the product of the FS periodic signal output and the data stream. In this section, we describe the spectrum spreading mechanism performed by this modulation.

2.4.1.1 Modulation Effect:

In Figure 2.7, we show the (time, frequency) space occupied by the base-band signal (before encoding) in the conventional FFH-SS transmission technique. This is distributed over a narrow frequency interval W_b and a data bit duration T_b. The encoding operation is performed by modulating the data signal by a number M of carriers. Hence, after decoding, it occupies a bandwidth $W_{ss}=M\times W_b$, M times larger than its original bandwidth. The time duration, however, remains the same. In the illustration of Figure 2.7, ω_c is omitted for simplicity.

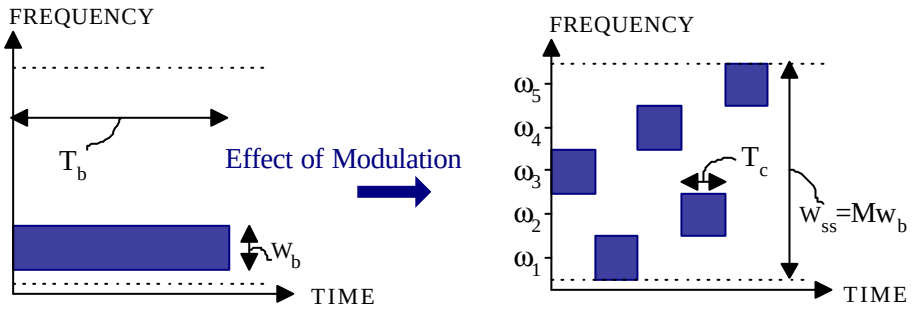

Figure 2.7: The effect of modulation by the frequency synthesizer signal in the conventional FFH-SS.

Mathematically, the modulation in conventional systems is simply a product, in the time domain, between the data signal and the hopping carrier sinusoids. Using equation (2.5), we derive

$$\begin{aligned} s_{ss}(t) &= d(t) \cdot s_c(t) \\ &= d(t) \cdot \sum_{i=1}^{M} q[t-(j-1)T_c]\cos[(\omega_c + c_j\Delta\omega)t] \end{aligned} \tag{2.6}$$

where d(t) and s_{ss}(t) are the data signal and the encoded signal, respectively. The other parameters have the same definition as in Section 2.1.

This is equivalent to convolving the Fourier transform of the data signal with a comb of Dirac pulses in the frequency domain, centered at the hopping carriers. In Figure 2.7, we show the spreading effect of the modulation with M=5 and the sequence is **c**=[3,1,4,2,5].

In the following we analyze the filtering effect of a broadband source and see how it performs the dual of the function performed by the modulation.

2.4.1.2 Effect of Filtering

Modified Data signal

In the architecture of Figure 2.3 a); a broadband source is transformed into a low duty cycle RZ (*i.e.*, return-to-zero) signal using a rapid modulation. This signal is then multiplied by the data. In Figure 2.3 b), the first gating operation is avoided, however the data itself is provided with RZ waveforms with low duty cycle. The data signal of equation (2.6) can be presented as

$$d(t) = \sum_{l} b_l p[t - lT_b], \quad \text{where} \quad p[t] = \begin{cases} 1 & 0 \le t \le T_b \\ 0 & elsewhere \end{cases} \tag{2.7}$$

and $b_l \in \{0,1\}$ is the l^{th} data bit value.

Using this expression, equation (2.6) can be transformed to

$$\begin{aligned} s_{ss}(t) &= \sum_{j=1}^{M} d(t)\, q\left[t-(j-1)T_c\right]\cos\left[\left(w_c + c_j \Delta w\right)t\right] \\ &= \sum_{j=1}^{M}\sum_{l} b_l\, p[t-lT_b]\, q\left[t-(j-1)T_c\right]\cos\left[\left(w_c + c_j \Delta w\right)t\right] \end{aligned} \tag{2.8}$$

where a good synchronization is assumed between the bit and chip streams. Using equation (2.2) we derive the product

$$p[t-lT_b]\,q[t-(j-1)T_c] = \Pi[t-lT_b-(j-1)T_c] \tag{2.9}$$

Thus, the spread spectrum signal (2.8) can be written as

$$\begin{aligned} s_{ss}(t) &= \sum_{j=1}^{M}\sum_{l} b_l \Pi\left[t-lT_b-(j-1)T_c\right]\cos\left[\left(w_c + c_j \Delta w\right)t\right] \\ &= \sum_{j=1}^{M} \tilde{d}\left(t-(j-1)T_c\right)\cos\left[\left(w_c + c_j \Delta w\right)t\right] \end{aligned} \tag{2.10}$$

where,

$$\tilde{d}(t_c) = \sum_{l} b_l \Pi\left[t-lT_{bc}\right] \tag{2.11}$$

which we call a modified data signal. This new form represents the electrical waveform applied to a BB output source signal in the architecture b) in Figure 2.3. Equation (2.11) means that when the data bit is equal to one the signal is ON during a time interval $T_c=T_b/M$, and OFF elsewhere. However, when the data bit is equal to 0, the signal is OFF during all the bit period. This symbol assignment is illustrated in Figure 2.8. The symbol can be considered as RZ waveform with low duty cycle M^{-1}.

Data modulated optical signal

The modified data signal $\tilde{d}(t)$ is used in architecture b), as a driving signal to the rapid switch at the BB source output. This generates the data stream modulated optical broadband short pulses.

$$\bar{d}(t, f) = \sum_{l} b_l\, \bar{\Pi}[t-lT_b, f] \tag{2.12}$$

where $\bar{\Pi}[t, f]$, is a two dimensional function, time and frequency, representing the short broadband pulses defined as follows

$$\bar{\Pi}[t, f] = \begin{cases} C & where\ 0 \le t \le T_c \quad and \quad f - f_c \le |W_{ss}|/2 \\ 0 & \text{elsewhere} \end{cases} \tag{2.13}$$

and C is a constant, W_{ss} is the whole bandwidth used for coding. As shown in Figure 2.9 a), the optical data signal before encoding occupies all the spread spectrum bandwidth (W_{ss}=W_b), and only a short slot of time T_c. Note that for a generalized case where pulses are generated by an MLL, it may be more convenient to consider that the optical pulse occupies a time duration T_p=T_c rather than T_c.

The encoding operation, consists of a convolution in the time domain and a multiplication in the frequency domain between $\bar{d}(t, f)$ and the (time, frequency) response of the encoder.

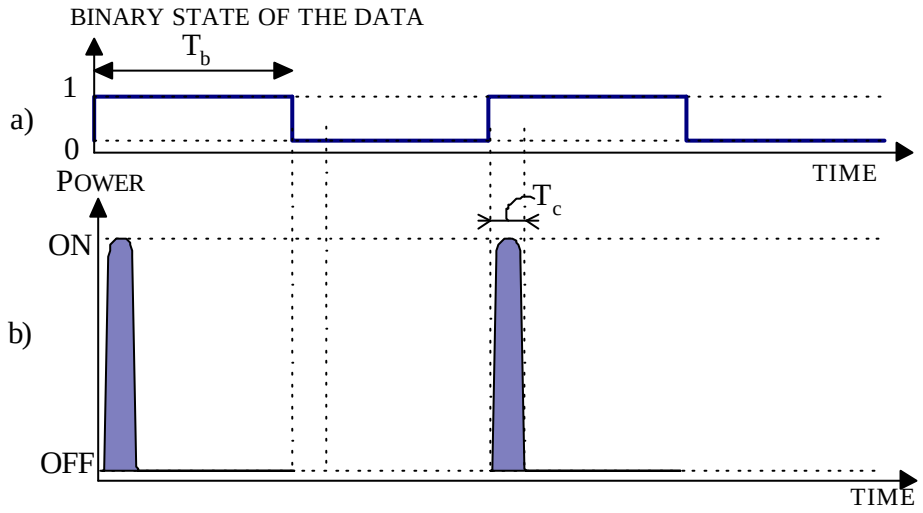

Figure 2.8: Low duty cycle RZ symbols assigned to the binary data

The Encoder Response

Let **C** be a $(F \times N)$ matrix representing a two dimensional sequence (or a hopping pattern); F and N denote the number of available frequencies and the number of time chips per code, respectively. The matrix elements $\mathbf{C}[i,j]$ can be equal to 1 or 0 depending on whether the i^{th} frequency is used in the j^{th} chip time or not. Let $c(t,f)$ be a two dimensional signaling function representing the (time, frequency) response of the encoder.

$$c(t, f) = \sum_{v=1}^{F} \sum_{u=1}^{N} \mathbf{C}[u,v] \Psi(t - uT_c, f - f_v) \tag{2.14}$$

where,

$$\Psi(t, f) = \begin{cases} 1 & where\ 0 \le t \le t_\Psi \quad and \quad f - f_c \le |\Delta f|/2 \\ 0 & elsewhere \end{cases} \tag{2.15}$$

f_v, for v=1,…,F, is the v^{th} available frequency carrier, *i.e.*, the center of the v^{th} sub-band from the F available in the shared spectrum. Δf is the frequency spacing between the disjoint carriers and/or a sub-band width. In our system, $\Psi(t, f)$ is a two-dimensional signaling waveform representing the (time, frequency) response of a single filter.

If the responses of the filters are relatively brief in time compared to the data signal waveforms $\bar{d}(t, f)$, *i.e.*, $\tau_\Psi << T_c$, they can be approximated by a series of Dirac functions in the time domain. The relative delays between the Dirac functions correspond to the relative delay introduced between frequencies in the encoding process.

The Encoded Optical FFH signal

The encoder output corresponds to a time-domain convolution and frequency-domain multiplication between the optical data signal $\bar{d}(t, f)$ and the response of the encoder. We denote this operation $*_t$. Using Equations (2.12) and (2.14), the encoder output signal is then

$$\begin{aligned} \bar{s}_{ss}(t, f) &= \bar{d}(t, f) *_t c_k(t, f) \\ &= \sum_{v=1}^{F} \sum_{u=1}^{N} \mathbf{C}_k[u,v] \bar{d}(t, f) *_t \Psi(t - uT_c, f - f_v) \end{aligned} \tag{2.16}$$

In Figure 2.9, we show the effect of the filtering-based encoding over the broadband data signal. In the figure, we considered that the filters do not increase the time duration of the pulses. It is known that a Bragg grating with high coupling coefficient exhibits very brief response duration, hence its response can be approximated as a Dirac function in time.

The encoding operation creates M independent frequency pulses and places each of them in the appropriate time-frequency square as determined by the FFH hopping pattern. The resulting transmitted signal has exactly the same structure as that generated by

conventional FFH-encoding techniques. This is the main reason for which we called the technique FFH-SS, avoiding the use of new expressions to describe the encoding technique itself. By referring to the encoding process, the technique can be called fast frequency hopping with time spreading (FWH/TS). Nonetheless, time-spread expression (TS) refers to another meaning in [127-128], where the time itself exhibits additional encoding.

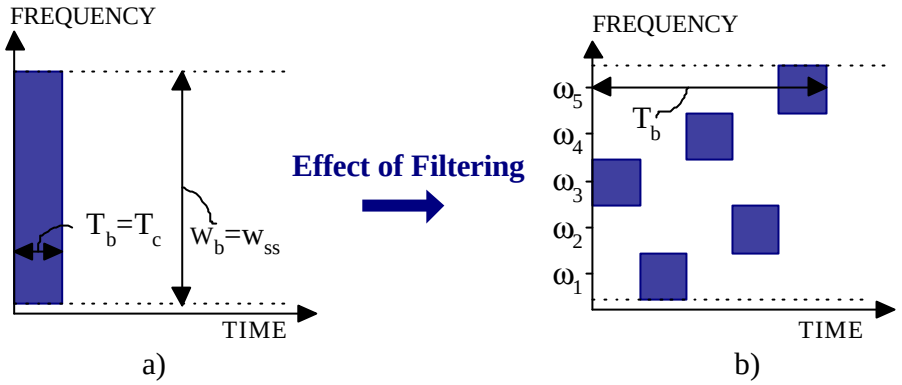

Figure 2.9: Effect of filtering of non-coherent BB source.

OFFH using Coherent Broadband Source

The interaction between a broadband signal and a filter or a set of filters leads to an output that strongly depends on the nature of the broadband source. The result illustrated in Figure 2.9 corresponds to an interaction with a non-coherent broadband source.

If an ultra-short pulse MLL is used within the architecture of Figure 2.3 c), the filtering operation will lead to a very different result. As described in Section 1.5.3, the ultra-short pulse of this laser is due to a given (deterministic) phase relationship between the spectral components of the signal. Any perturbation of this phase relationship leads a perturbation of the pulse. Hence, the energy will be spread in time, hence its broadening in time.

As previously reported by Salehi and Wiener [55-59], and recently by Jepsen [133], each filtered frequency slice will correspond to a low-level signal, which is spread in time over all the period. Figure 2.10 a) illustrates the time-frequency rectangles occupied by the short pulse of the MLL laser, and Figure 2.10 b) shows the time-frequency rectangles

occupied by the filtered frequency slices. In [133], laser pulses have 2.7 ps width and the chip pulses occupied 30ps.

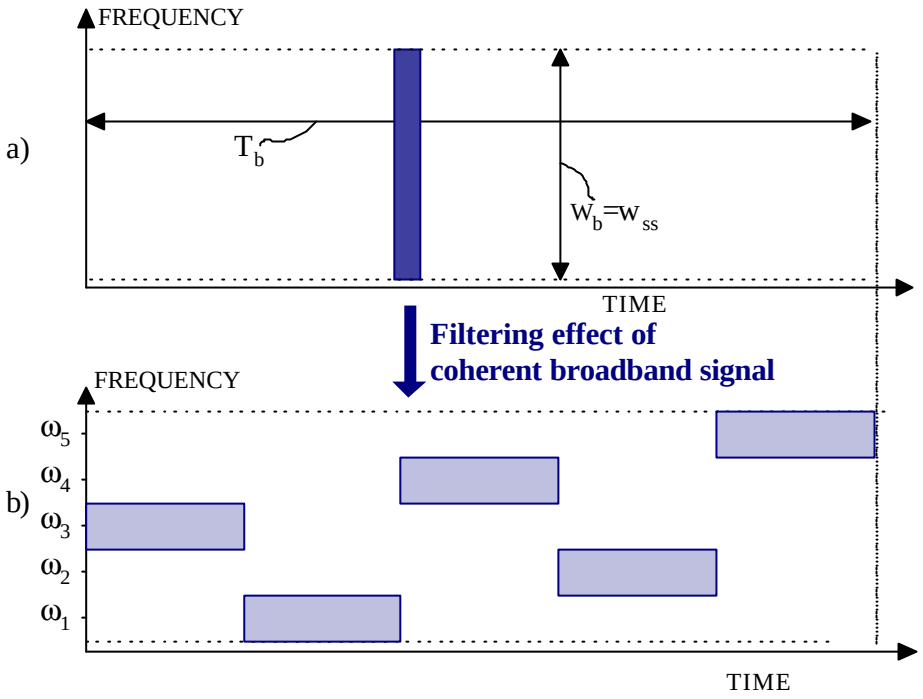

Figure 2.10: Effect of filtering of a coherent BB source.

2.5 FFH-SS using Multiple Bragg Gratings

We call multiple Bragg gratings (MBG) a series (or cascade) of Bragg gratings written with in-line configuration in the same fiber or waveguide [164-177]. Recall that the fiber Bragg grating is an exceptional highly selective band reflective filter (BRF) and can be easily and densely cascaded in the same fiber [164-170]. Due to its reflective nature, MBG is a good candidate to implement an optical FFH-SS transmitter with the architecture a) in Figure 2.3.

2.5.1 Simultaneous l-selection and time delaying using MGB

When a broadband signal is incident to the MBG, the reflected spectrum will be shaped by its overall reflectivity, provided the incident signal spectrum occupies a much larger bandwidth than the total frequency span of the MBG [177].

The space positioning of the gratings of the MBG structure, in the fiber, can be exploited to perform an in-time signal processing function (Figure 2.11). If the provided broadband signal is periodically ON/OFF keyed with a low enough duty cycle, discrete sub-pulses can be sequentially reflected. Each of those sub-pulses is contained in a different wavelength sub-band. The relative delay between two consecutive sub-pulses is equal to the round-trip time between the corresponding gratings.

To avoid time overlapping between the reflected sub-pulses, the duty cycle should be low enough for the ON interval duration to be inferior or equal to the round trip time between consecutive gratings. In addition, as explained in Section 2.3, if the short pulses originate from a non-coherent source, the slicing will have a negligible effect on the pulse width. On the other hand, if the pulses come from a MLL, the filtered pulses will have a substantially spread in time.

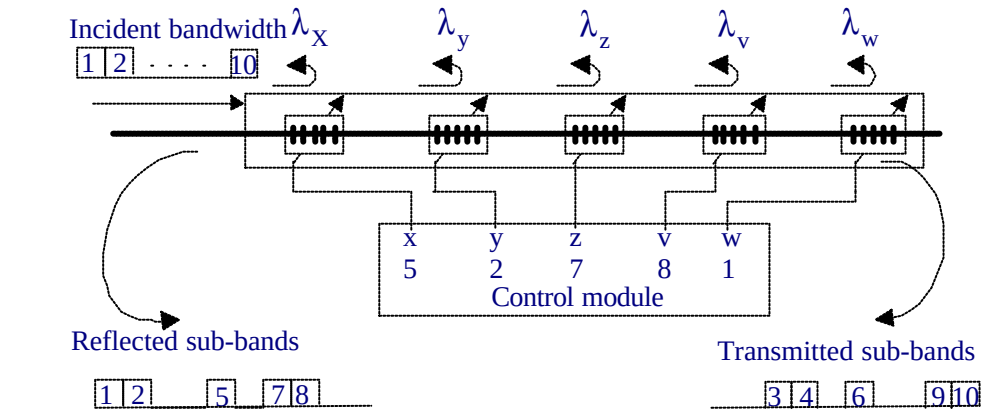

a) Multiple Tunable Bragg Gratings

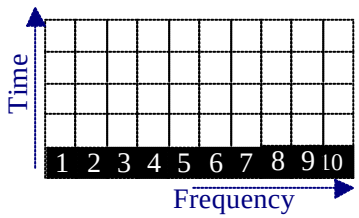

b) Incident signal

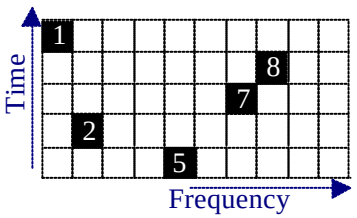

c) Reflected signal pulses train

Figure 2.11: l-selection and time delaying principle: using a multiple tunable Bragg grating (MTBG)

In Figure 2.11 a), we show that a multiple tunable Bragg gratings (MTBG) can simultaneously perform the two functions: frequency selection and in-time positioning. The MTBG can be programmed to reflect any sub-set of five wavelengths λ_x, λ_y … and λ_w, from the available ten in the incident short broadband signal (Figure 2.11 b). In the example shown, the MTBG is adjusted to reflect the sub-bands 5, 2, 7, 8 and 1; the transmitted signal will be composed of the remaining spectrum. Figure 2.11 c) shows the time-frequency space occupied by the reflected signal. Recall that the time duration of the short broadband signal should be less or equal to the round-trip time through the spacing between the gratings in order to avoid overlapping between the reflected sub-pulses.

If the reflected wavelength and the physical placement of the gratings themselves are selected corresponding to the FFH-SS sequence requirements, the MBG can imprint the code into the incident signal. In the following, we will describe the FFH-SS transmitter using the λ-selection and time delaying MBG based device including the overall functionality.

2.5.2 Optical FFH-SS Transmitter:

Using a non-coherent broadband source followed by an external intensity modulator directly that is controlled by an electric signal $\tilde{d}(t)$ with low duty-cycle RZ signal waveforms representing the data, we generate the data modulated optical broadband signal. When the bit value is equal to one, an optical broadband short pulse is transmitted to the MBG, and when the data is equal to 0, no power is transmitted. As described in the previous section, the first grating will reflect the sub-band centered at λ_3, the second in the line will reflect the sub-band centered at λ_1 and hence until the reflection of λ_5. The time delay between the reflected pulses is strictly determined by the physical separation distance L_c (see Figure 2.12). We assumed through all the document that L_c includes the length of the grating, hence the chip time also includes the traveling time through the grating.

Two points should be noted: 1) No frequency can be used more than one time, and 2) no more than one frequency can be used at once. This is due to the inherent in-line

structure of the multiple Bragg gratings. Incidentally, that also corresponds to the special category of radio frequency FFH codes called non-repeating frequency codes.

The encoding operation performed using the transmitter architecture of Figure 2.12 has some attracting features:

1. Encoding is achieved passively, *i.e.*, does not require any active device. This, in principle, provides high stability, reliability and long life time for the system.

2. The whole encoding signal-processing operation is performed in the optical domain and does not require electronic-to-optic or optic-to-electronic conversions.

3. Encoding is an in-fiber signal processing operation that substantially reduces the loss of power in the system.

4. Multiple tunable Bragg gratings allow the reconfiguration of the MBG reflected wavelengths and their order, allowing reconfiguration of the code in the transmitters as well as in the receiver.

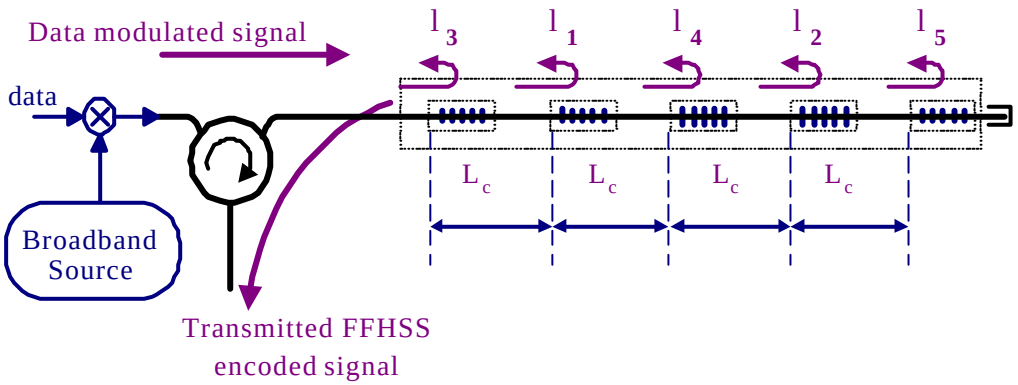

Figure 2.12: MBG based FFH-SS transmitter

2.5.3 Optical FFH-SS Receiver:

In the receiver, similar multiple Bragg gratings programmed in the reverse order as the encoder can compensate the relative delays between the received pulses. The example of Figure 2.12 uses an encoder with wavelengths order: 3, 1, 4, 2 and 5; this is the same configuration for the receiver but the Bragg gratings order is reversed (see Figure 2.13).

Suppose the receiver is matched to the desired user's signal, the first incoming pulse is reflected by the last grating, the second pulse is reflected by the last-but-one grating and so on. Hence, the pulses that come from the desired user will superpose (see Figure 2.14).

Similarly to the encoding process, the decoding can be modeled as a time-domain convolution and a frequency-domain multiplication between the received signal and the (time, frequency) two-dimensional function characterizing the decoder $dec(t, f)$. The decoded signal is then

$$y(t, f) = \bar{s}_{ss}(t, f) *_t dec(t, f) \tag{2.17}$$

In principle, the decoder should have a frequency domain response identical to that of the response of the encoder. In the time domain however, the decoder response is mathematically symmetric to that of the encoder. The decoder is a two-dimensional

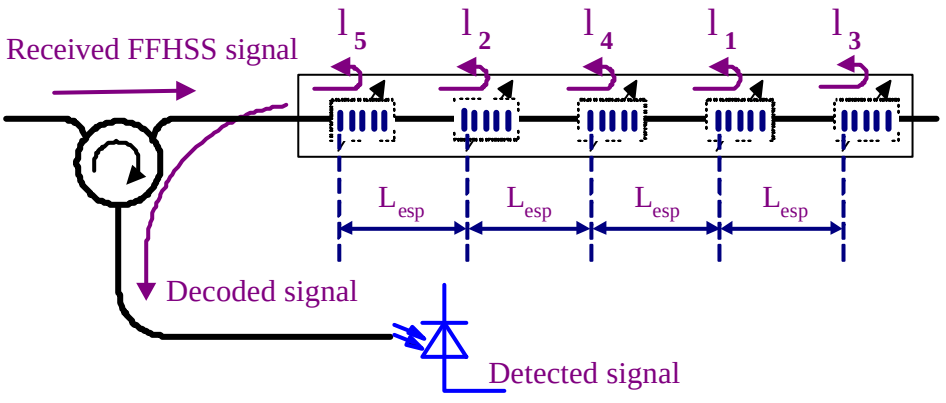

Figure 2.13: MBG based FFH-SS receiver

function can be written as

$$dec(t, f) = c(-t, f) \tag{2.18}$$

Perfect encoder/decoder is practically not possible, i.e., however this can be designed with enough precision in order to maintain a given performance and fidelity. Every grating in the encoder exhibits a certain amount of phase (or delay) dispersion inside the main-lobe that is difficult to compensate in the decoder. Furthermore, the signal exhibits a cumulative dispersion that can degrade the quality of the signal waveform.

Using equations (2.16-18) and we derive

$$\begin{aligned} y(t, f) &= d(t, f) *_t c(t, f) *_t dec(t, f) \\ &= d(t, f) *_t c(t, f) *_t c(-t, f) \\ &= d(t, f) *_t \int_t^{t+T_b} c(\tau, f) c(\tau - t, f) d\tau \end{aligned} \tag{2.19}$$

The integral in Equation (2.19) defines the so-called auto-correlation function. This can be interpreted as a measure of conformity or resemblance between the encoder and the decoder functions. The decoded signal hence is the convolution of the transmitted data signal with end-to-end encoder/decoder setting, which can be mathematically modeled by the auto-correlation function. In Figure 2.14, we considered the filter responses as brief in

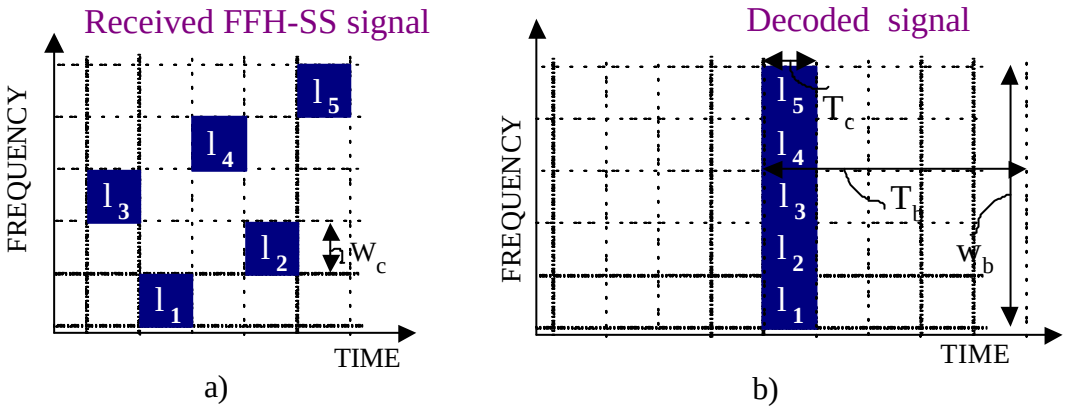

Figure 2.14 Decoding of a desired user signal

time compared to the data pulse duration. Hence, the recombined pulse has exactly the same duration as the original data. In the time domain, the autocorrelation peak can be mathematically expressed as a Dirac function, in the frequency domain however, only the frequency-bands used by the encoder are present.

When an interfering signal is received, its pulses' order does not match the receiver. The interfering signal pulses incidentally found in the same frequency bins as those the receiver is configured for will be reflected and reordered in the time (Figure 2.15). Furthermore, the interference pulses exhibit an additional spreading in the time, hence occupying a maximum time duration of $(2N-1)T_c$. The output of a decoder configured for a sequence different to that of the encoder is the so-called cross-correlation function. This is mathematically identical to the auto-correlation function however calculated between two different sequences. At the photodetector output, the electrical signal due to the cross-correlation will be much lower than the auto-correlation peak. The receiver will not be able to decode the signal unless it is tuned to the correct sequence.

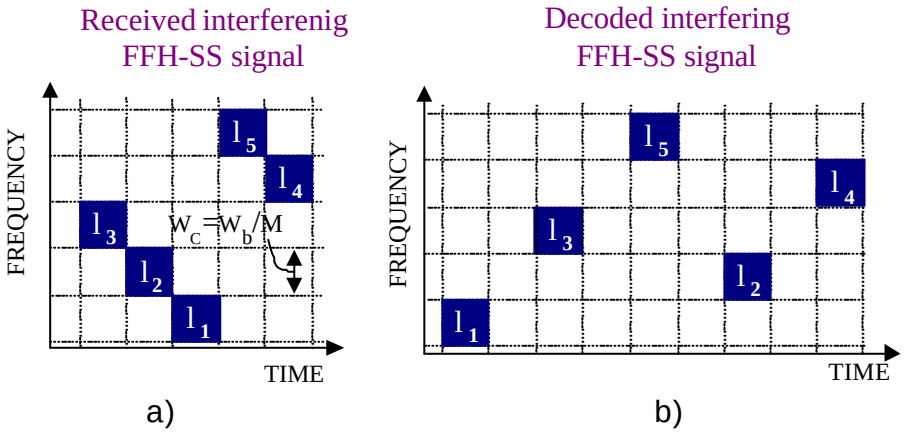

Figure 2.15: Decoding of interfering signal

Chapter

3

Optical FFH-CDMA

Theoretical Analysis

In this chapter we exploit the multiple Bragg gratings (MBG) based FFH-SS technique of Chapter 2 to develop an optical code division multiple access (OCDMA) system. In Section 3.1, we introduce the optical access system we refer to as OFFH-CDMA. In Section 3.2, we review the standard mathematical CDMA model in order to adapt that to the proposed OFFH-CDMA. The performance measures are defined in Section 3.3.

3.1. OFFH-CDMA System

The optical FFH-encoding principle introduced in Chapter 2 can be used for fiber optic CDMA networks once suitable sequences are selected and assigned for different access clients. As described in Figure 3.1, K users or user pairs can be connected to a passive star, each of which is assigned an FFH-sequence (or code). The code can be considered as the access key (or address) of the client.

The signal of each transmitter is broadcast to all the network clients. Hence, all clients receive a sum of all the broadcast signals. Moreover, each of them will be capable of extracting a desired users signal provided it is authorized to receive it, *i.e.*, provides the desired user's code is known.

The advantages of a Bragg gratings based OFFH-CDMA include its all-optical and its in-fiber signal processing operations. These important features make the technique promising for its potentially low-cost and robust implementation. We will see in Chapter 5

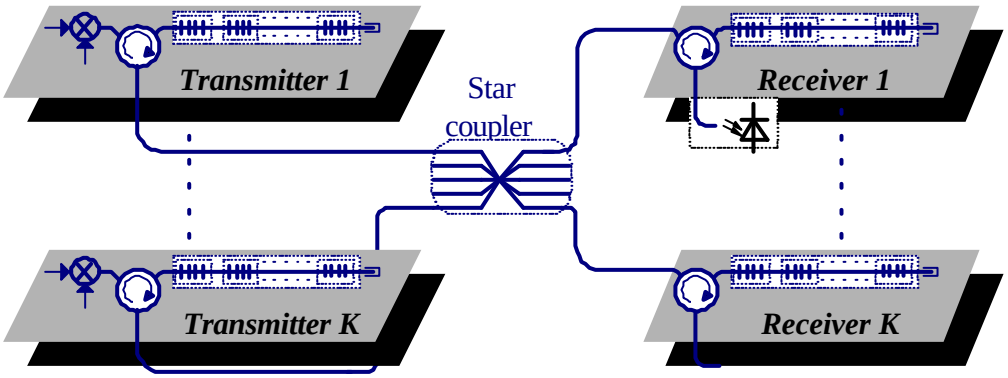

Figure 3.1: OFFH-CDMA network in star architecture

that OFFH-CDMA requires high reproducibility in Bragg gratings. The latter are considered as low cost components since their fabrication process can be automated.

Moreover, by use of piezo-electric devices, the order of the center frequencies of the Bragg gratings can be changed [185-189], effectively changing the hop pattern and therefore allowing for programmable codes. In the following section, we introduce the encoding process in radio frequency FFH-CDMA in order to adapt it to OFFH-CDMA.

3.1.1. FFH-coding

In an FFH-CDMA system, the available bandwidth is subdivided into a number F of contiguous frequency slots. The transmitted signal occupies one frequency slot in each chip signaling interval T_c, *i.e.*, the l^{th} chip pulse is carried by frequency f_l, so that

$$f_l = f_c + \mathbf{h}(l)\frac{B}{F} \qquad l = 1, \cdots, N \text{ and } 1 \le \mathbf{h}(l) \le F \tag{3.1}$$

where B is the available frequency bandwidth, $\mathbf{h}$ is the placement operator, and f_c is the frequency taken as a reference [87]. The placement operator is a sequence of N ordered integers determining the placement of frequencies in the N available time slots. Each user's code is a set of N frequencies from F available ones $S = \{f_1, f_2, \cdots, f_N\}$, where $N \le F$. As shown in Section 2.5, a convenient way of representing a frequency hop pattern is through an $N \times F$ matrix representing the time and frequency plane.

Most codes developed for radio FFH-CDMA assume $N=F$ [87-100]. Only a few code families can be generalized to $N<F$. In our system, the number N corresponds to the number of gratings written in the encoder. The number F of available frequencies is fixed by the tunability limit of the gratings (discussed further in section 3.2).

In [88], Bin proposes a construction algorithm for a new family of codes with $F \ge N$. Those codes fall into the category of so-called one-coincidence sequences, and are characterized by the following three properties. 1) All of the sequences are of the same length (in our case fixed by the number of gratings). 2) In each sequence, each frequency is used at most once. 3) The maximum number of hits between any pair of sequences and for any time shift is one. A good reference is the survey paper on one-coincidence sequences

written by Shaar *et al.* [87]. In the following section we see how these FFH-codes serve for a fiber shared access system.

3.1.2. Resources Accessibility:

Simultaneous utilization of the time and frequency domains in FFH-CDMA offers notable flexibility in the selection of codes, more easily satisfying the required quasi-orthogonality (or transparency) between the simultaneous users than previously proposed incoherent DS-CDMA systems.

Using OFFH-CDMA, we can take advantage of the huge bandwidth of single mode fiber and available broadband sources to make a very high number of frequency slices (or wavelengths). Moreover, the possibility of generating very short pulses in the optical domain is a second advantage that increases drastically the accessible space for FFH encoding (see Figure 3.2).

It is convenient to look at that space as a very large two-dimensional matrix to be shared by clients. The FFH-codes can be seen as very sparse matrices where the single-value elements represent the used time×frequency squares in the available space.

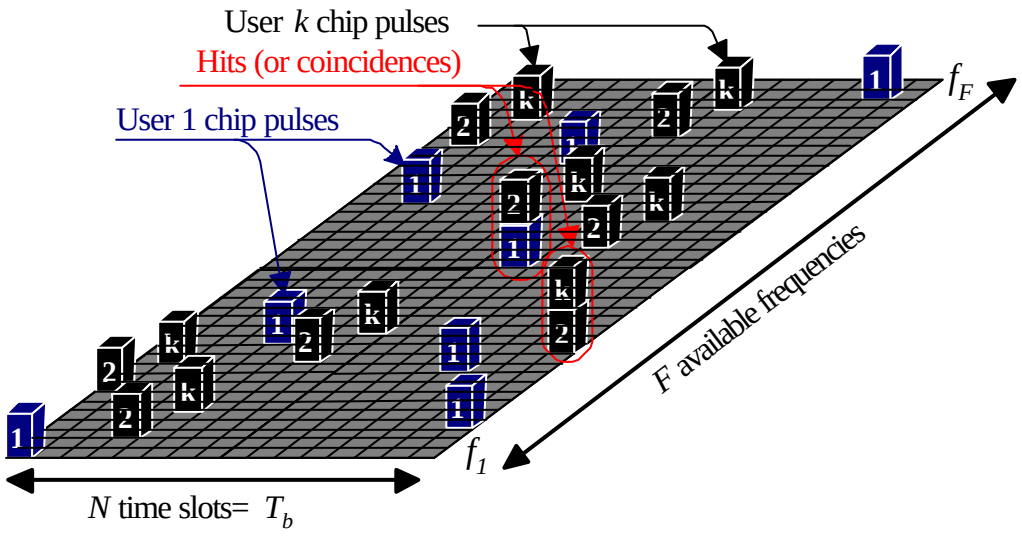

Figure 3.2: Frequency×time resource sharing in optical FFH-CDMA, *i.e.*, pulses marked by 1 relate to user number 1, and so on.

In Figure 3.2, we illustrate the sharing strategy in OFFH-CDMA. Chip pulses of users 1, 2… k are shown as cubic waveforms. The figure shows that the superposition of pulses coming from different users is possible; this is called a *hit* or coincidence. In the one coincidence code category introduced in Section 3.1.1, only one hit can occur between two different codes no matter what the time delay between the two transmissions. In Figure 3.2, we arbitrarily assume that the available number of frequencies is F=40, the number of chips is N=16, and codes contain w=8 pulses. w is usually called the *weight* of the code. For the simulations in Chapter 4 and the experiments in Chapter 5, we consider only the case where the weight is equal to the number of chips $w=N$.

It is important to note that code families previously developed for radio frequency (RF) communications are not directly applicable to an optical FFH-CDMA system. The MBG based encoding device imposes special constraints on code design. We will derive a new design criterion of codes that are unique to the optical FFH-CDMA system.

As explained in Chapter 1, three possible scenarios exist in typical access networks: 1) fixed transmitters and receivers; 2) fixed transmitters and tunable receivers; and 3) tunable transmitters and tunable receivers. The latter requires a network administrator to avoid output port retention. Implementing tunable transmitters and/or receivers allows the reconfiguring of destination address and/or the desired signal code. The ability to change the code either in the receiver or in the transmitter is always a desirable option.

In the following section, we address MBG-based encoder/decoder issues, including BG placement, bit rate, chip rate, and MBG tunability.

3.1.3. Bit and Chip Rate

As assumed in FFH-codes, chip pulses should be equally spaced at chip intervals T_c. That interval corresponds to the round-trip propagation time between any two gratings, and requires the gratings to be equally spaced.

Let L_c be the sum of one grating length and one spacing distance between adjacent grating pairs, c be the speed of light, n_{eff} be the average value of the effective refractive index, and n_g be the effective group index. Therefore the chip interval is $T_c=2n_gL_c/c$ (see Figure 3.3). The chip interval, pulse duration, and number of gratings will limit the data bit-

rate of the system. That is to assure that all reflections exit the fiber before the next pulse enters (to limit interference). Therefore, the total round-trip time in a structure of N Bragg gratings is given by $2(N\text{-}1)L_c n_0/c$. Recent works have showed the superposition of Bragg gratings possible with some compromises in their characteristics and properties. This is not considered in this thesis and we focused on the use of very high reflectivity gratings, their superposition is still difficult.

In addition, if the incident short pulse is assumed to have a duration $T_p = T_c$, this effectively determines the bit duration T_b, yielding

$$T_b = T_p + (N-1)T_c = NT_c \tag{3.2}$$

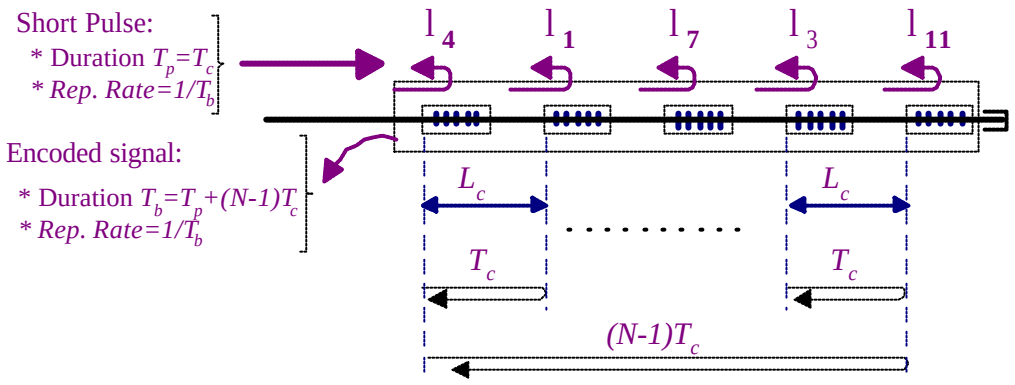

Figure 3.3: Physical parameters of the MBG

The passage of an incident pulse through a grating will necessarily lead to the smearing of the pulse in time, although it may come from a broadband non-coherent source. We neglect this effect and consider the time responses of the gratings to be ideal Dirac functions.

3.1.4. The Encoder Model

As introduced in Section 2.4, the encoder output signal inside one bit duration interval is the convolution of the optical broadband short pulse $\Pi(t, f)$ with the time-frequency response of the encoder $c(t, f)$. The convolution can be expressed as

$$\overline{\Pi}(t,f) *_t c(t,f) = \sum_{v=1}^{F}\sum_{u=1}^{N} \mathbf{C}[u,v]\,\overline{\Pi}(t,f) *_t \Psi(t-uT_c, f-f_v) \tag{3.3}$$

Recall that $\mathbf{C}$ is a matrix representing the hopping pattern, whereas F and N denote the number of available frequencies and the number of time chips per code, respectively. All single filters are assumed to have identical responses $\Psi(t,f)$ centered at different frequencies. The overall MBG response can be written

$$c(t,f) = \sum_{v=1}^{F}\sum_{u=1}^{N} \mathbf{C}[u,v]\,\Psi(t-uT_c, f-f_v) \tag{3.4}$$

where $\Psi(t,f)$ itself is a product of two independent single-variable functions

$$\Psi[t,f] = \Psi(t)\Psi(f) \tag{3.5}$$

Furthermore,

$$\Psi(t)\begin{cases}1 & 0 \le t \le T_\Psi \\ 0 & \text{elsewhere}\end{cases} \quad \text{and} \quad \Psi(f)\begin{cases}1 & f - f_c \le |\Delta f|/2 \\ 0 & \text{elsewhere}\end{cases} \tag{3.6}$$

For v=1…F, f_v is the v^{th} available frequency carrier, *i.e.*, the center of the v^{th} sub-band out of the F available in the shared spectrum. Δf is the frequency spacing between the carriers and/or the sub-bands.

In our system, if the Bragg gratings are designed so that their responses are relatively brief in time compared to the source short pulses $\overline{\Pi}(t,f)$, then we can assume that $\Psi(t) = \delta(t)$. In that case, the MBG response (equation (3.4)) can be approximated as a series of Dirac functions in the time dimension, and a single rectangular function in the frequency domain.

$$c(t,f) = \sum_{v=1}^{F}\sum_{u=1}^{N} \mathbf{C}[u,v]\,\delta(t-uT_c)\Psi(f-f_v) \tag{3.7}$$

The two-dimensional response of equation (3.7) is illustrated in Figure 3.4. Relative delays between the Dirac functions correspond to relative delays introduced between frequencies in the encoding process. When equation (3.7) is satisfied, equality in equation (3.2) holds; otherwise, the encoded signal duration will be

$$T_p + (N-1)T_c + T_\Psi > T_b \tag{3.8}$$

This would lead to an overlap between successive encoded bits. Moreover, it would cause an overlap between successive chips. In the remaining part of this document, we will always assume $T_{\Psi} = \mathbf{0}$. Chip pulse durations never exceed chip periods, and encoded bit durations consequently do not exceed a single bit time interval. By assuming that $T_p = T_c$, equation (3.2) will remain true.

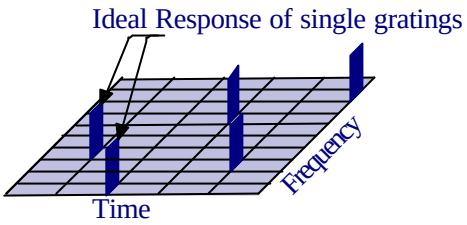

Figure 3.4: Ideal MBG based encoder response

3.1.5. Modulation Format

In radio frequency (RF) FFH-SS, modulation is typically either binary or M-ary FSK. In our system, we use binary ASK, since it is particularly suitable for optical communications. As depicted in Figure 3.5, a pulse is transmitted in the chip interval if the chip value is one; otherwise, no power is transmitted. Recall that binary ASK (or OOK) is also adopted at the data bit level, *i.e.*, power is only transmitted when the data bit is one.

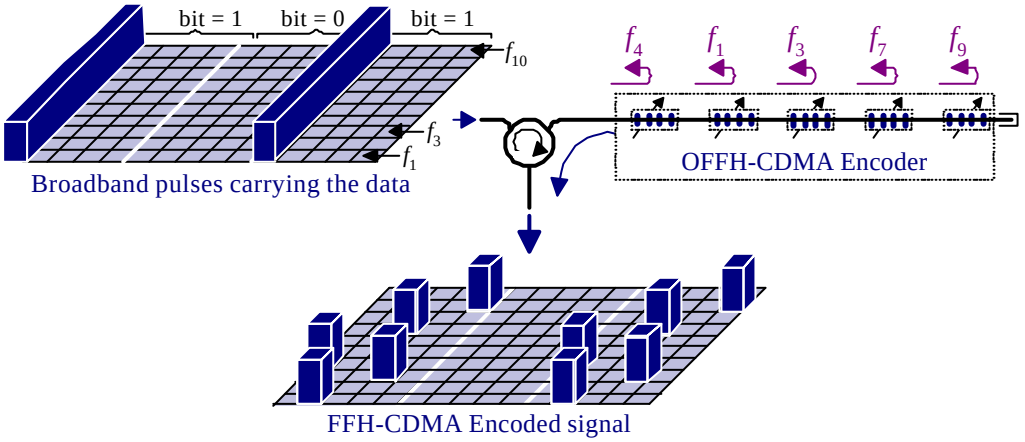

Figure 3.5: OFFH encoding process, using binary ASK modulation.

In the example of Figure 3.5, we use F=10 and N=5. An FFH-SS signal for the bit sequence "1 0 1" is illustrated with cubic chip pulses. The x-y plane sections represent the time-frequency dimensions, whereas the vertical (z-axis) histograms represent power.

3.1.6. Tunability:

As shown in Figure 2.11, the encoding device consists of a series of Bragg gratings all written at the same wavelength λ_B. Each grating can be tuned independently using piezo-electric devices, adjusting the Bragg wavelength from λ_B to a given wavelength defined by the corresponding placement operator. The tuning of each device is determined by the code used. Note that the tuning time only affects link setup time; it does not limit the bit rate.

Individual tuning of each grating requires one piezo-electric actuator for each. This can substantially increase the mechanical complexity, and hence the cost, of the system. Boulianne in [120] has observed that the Bin codes [88] we previously proposed in [112] maintain their one-coincidence property with any frequency shifted copy of itself. In other words, if we tune the whole MBG fiber implementing a Bin code, *i.e.*, we simultaneously shift all the frequency bins, the resulting set of codes would have acceptable properties among them.

For uniform gratings of a given reflectivity, the reflection bandwidth is inversely proportional to the grating length. For example, the grating bandwidth between the two first zero crossings of the reflectivity spectrum is given by

$$\Delta l_B = \frac{l^2}{n_{eff} L}\sqrt{1+\left(kL/p\right)^2} \tag{3.9}$$

where κ is the coupling coefficient, L is the grating length, and λ is the peak wavelength. For a given fiber stretching length ΔL, the shift in the peak Bragg wavelength $\Delta\lambda_s$ is a function of the applied strain. It is expressed as $\Delta l_s = 0.8 l\left(\Delta L / L\right)$ [187]. Therefore, the number of available frequency bins is related to the fiber stretching by

$$q = \frac{\Delta l_s}{m\Delta l_B} = \frac{0.8\Delta L n_{eff}}{m l\sqrt{1+\left(kL/p\right)^2}} \tag{3.10}$$

where m is a coefficient that takes into account the excess bandwidth left on each side of

the main reflection lobe. For a typical value of κL=2 (corresponding to 93% reflectivity), n_{eff}=1.452. This requires that $\Delta L \approx mql_B$. Depending on the available piezo-electric devices used for stretching, we can consider a tuning range of $0 \le \Delta L \le 50mm$ which can lead to $0 \le mq \le 33$. The compression of Bragg gratings, however, can allow up to 45 nm in tuning range [187]. Bragg grating tuning solutions exist in the literature; some of them are cited in Chapter 4.

Equation (3.9) shows that the bandwidth of a grating slowly depends on its length. Any stretching or compression induces a little change the grating length, hence affecting its bandwidth, however remains negligible for the practical tuning range of the grating. The reflectivity amplitude is also negligib ly affected by every tuning.

3.1.7. Code design for optical FFH-CDMA

Codes previously developed for frequency hopping in RF applications have mainly been selected 1) to reduce the Doppler effect, 2) to minimize frequency synthesizer agility, and 3) to reduce MAI in asynchronous systems. In addition, most of them assume that the number of available frequencies q is exactly equal to the number N of chips (or hops) per bit. For OFFH-CDMA, only criterion 3) applies in addition to the constraint $N<q$. Furthermore, the maximum number of hops is determined by the maximum number of gratings N that can be written in a fixed fiber length. N is dictated by 1) the required bit rate, 2) the grating length, and 3) the physical spacing needed to allow grating tunability. The number of frequencies is determined by the tunability limitation of the gratings. These points lead to a new optimization criterion in code design for optical frequency hopping.

The algorithm developed by Bin [88] allows the generation of one-coincidence codes defined in Section 3.1.1, which guarantee a minimum distance d between adjacent symbols (or pulses). For our system, this means that the reflected frequencies from adjacent pairs of gratings, (leading to two reflected pulses adjacent in time), are separated by a specified minimum number of bins. In our case, this reduces the effect of side lobes in the reflectivity of each grating.

New code optimization criterion:

The proposed codes cannot be considered as optimal codes for fiber optic CDMA. Indeed, those codes have been developed for mobile and satellite communications, and optimized to minimize cross-correlation in mobile radio communications due to the Doppler effect. In optical fiber communications, the Doppler effect can be neglected, while dispersion must be accounted for. The development of code families that are robust to fiber dispersion and ignore the Doppler effect is a relevant axis of research.

3.2. System Modeling

In order to estimate the optical FFH-CDMA system performance we focus in this section on the development of a mathematical model for the optical FFH-CDMA system. This is essential in order to estimate system performance. We start by a model usually used for standard wireless direct sequence-CDMA systems, or more accurately non-coherent optical DS-CDMA introduced in Section 1.6.1

3.2.1. Standard CDMA system model

We consider a typical fiber optic CDMA communications network with K transmitter and receiver pairs, *i.e.*, K users sharing the same optical medium. Usually, but not exclusively, the shared medium is a star architecture. Each information bit from user k is encoded onto a code sequence or "address"

$$c_k(t) = \sum_{j=1}^{N} d_{k,j}\, p_{k,j}\left(t - jT_c\right) \tag{3.11}$$

where N is the length of the code (or the number of chips per bit), T_c is the chip duration, and $d_{k,j} \in \{0, 1\}$ is the j^{th} chip value of the k^{th} user code, for $1 \le j \le N$. Let $\boldsymbol{c}_k = [d_{k,1}, d_{k,2}, \ldots, d_{k,N}]$ be a vector representing the discrete form of the code. The chip signaling waveform $p_{k,j}(t)$, for $1 \le j \le N$, is usually assumed to be rectangular with unit energy.

In our FFH system, the chip pulses are generated in different and disjoint frequency sub-bands (they have different colors). Each transmitter broadcasts its encoded signal to all

the receivers in the network. The received signal is a sum of all the active users' transmitted signals.

$$r(t) = \sum_{k=1}^{K} A_k b_k c_{k,j}\{t - \tau_k\} \tag{3.12}$$

For k=1...K, $b_k \in \{0,1\}$ and $0 \le \tau_k \le T_b$ are the k^{th} user information bit and time delay respectively. The parameter A_k denotes the k^{th} user signal amplitude seen by the receiver of interest, *i.e.*, after all splitting and coupling losses along the path of the k^{th} user signal occur.

Figure 3.6 shows a diagram describing the logical functionality of a typical asynchronous optical CDMA link. The codes, as well as the delays, are fixed by the transmitters. Amplitudes, however, are fixed by the network architecture. Detection, including the interference rejection strategy, is performed at the receiver end.

The receiver applies a matched filter to the incoming signal to extract the desired user bit stream. For notational simplicity, it is usually assumed that the user number one (k=1) is the desired one. Furthermore, without loss of generality, we assume the receiver is synchronized to the desired user signal, *i.e.*, τ_1=0. The matched filter output for a bit duration T_b is thus

$$\begin{aligned} y &= \int_0^T c_1(t) r(t) \\ &= A_1 \int_0^T \{c_1(t)\}^2 dt + \sum_{i=2}^{K} A_k b_k \int_0^T c_1(t) c_k\{t - \tau_k\} dt \\ &= A_1 b_1 N + MAI \end{aligned} \tag{3.13}$$

$T_b = NT_c$ is the duration of one data bit, neglecting the effects of quantum and thermal noise. The first term in (3.13) corresponds to the desired user; the second is multiple access interference (MAI). In most CDMA systems, MAI is the most important noise source.

For a large number of interfering users, the probability density function of the MAI is usually approximated as a Gaussian density, using central-limit-theorem arguments. To reduce the effect of MAI, orthogonal (or nearly orthogonal) codes are required. For non-coherent DS-CDMA, different families of codes, including so-called optical orthogonal codes (OOCs), have been developed with acceptable levels of cross-talk between users [53].

Furthermore, MAI statistics strongly depend on the network architecture. In a star architecture, the splitting and coupling losses seen by different transmitted signals are almost equal. If the transmitted signals' powers are the same, the different users signal amplitudes, A_k, k=1…K, are consequently roughly equal.

In bus or ring architectures, however, the splitting loss differs from one user signal to another depending on its relative position in the network. In such a case, the received signals have different amplitudes. That can lead to serious degradation in signal quality at the decoder output. The problem becomes especially serious when the desired signal is among the most attenuated (or split) ones. This problem is well known in radio frequency CDMA system as the *near-far* problem. A significant body of research has investigated this issue since the pioneering work of Verdú [151] that relates to the CDMA-related field called *multiuser detection* [150-163].

We previously used the standard mathematical model of Equation (3.13) for our OFFH-CDMA in [112-113]. We have noted, however, the importance of keeping in mind that the chip pulses are supported by different frequency bands, *i.e.* are all transparent (or orthogonal) among themselves. The weakness of the model in Equation (3.13) is that it does not clearly reflect the two-dimensional nature of the signal, and the FFH-CDMA correlation operation.

3.2.2. OFFH-CDMA system model

Equation (2.16) represents the transmitted signal from one user, which we refer to as $s_k(t)$. The received signal is the sum of all the active users' transmitted signals

$$\begin{aligned} r(t,f) &= \sum_{k=1}^{K} A_k s_k(t-t_k, f) \\ &= \sum_{k=1}^{K} A_k \bar{d}_k(t,f) *_t c_k(t-t_k, f) \end{aligned} \tag{3.14}$$

At the receiver, the decoder output is then

$$
\begin{aligned}
y(t,f) &= r(t,f) *_t dec_1(t,f) \\
&= \sum_{k=1}^{K} A_k \bar{d}_k(t,f) *_t c_k(t-t_k,f) *_t dec_1(t,f)
\end{aligned}
\tag{3.15}
$$

$$
\begin{aligned}
y(t,f) &= \bar{d}_1(t,f) *_t c_1(t,f) *_t c_1(-t,f) \\
&\quad + \sum_{k=2}^{K} A_k \bar{d}_k(t,f) *_t c_k(t-t_k,f) *_t c_1(-t,f) \\
&= A_1 \bar{d}_1(t,f) *_t \int_t^{t+T_b} c_1(t,f)\, c_1(t-t,f)\, dt \\
&\quad + \sum_{k=2}^{K} A_k \bar{d}_k(t,f) *_t \int_t^{t+T_b} c_k(t-t_k,f)\, c_1(t-t,f)\, dt
\end{aligned}
$$

Equation (3.15) shows that the decoder output is the sum of the auto- and cross-correlation functions subject to time-delays t_k and amplitudes A_k. This is somewhat similar to the case of the WH/TS system developed by Tancevski and Andonovic in [123-124].

The optical signal *y(t,f)* is be received by the photodetector which, in turn, generates a current proportional to the squared value of *y(t,f)*. In order to make a bit decision, the chip interval where all the desired energy exists should be isolated using an electronic synchronization loop. Integration and thresholding should be carried out within this chip interval.

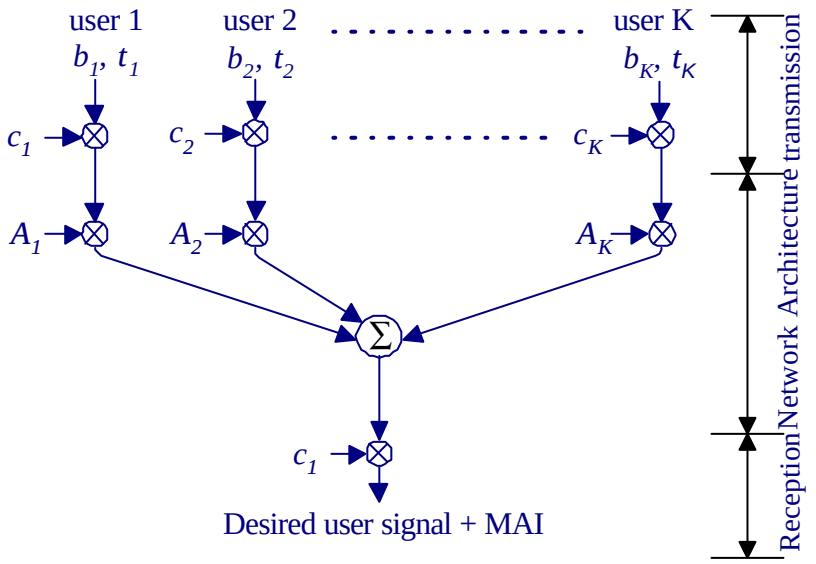

Figure 3.6: Logical diagram of a CDMA link

3.3. Performance Measures

Since the principal source of noise in CDMA systems is multiple access interference, the correlation among codes plays a major role in system performance. The auto- and cross-correlation are important functions to evaluate code efficiency.

3.3.1. Auto and Cross-correlation Functions

As in any CDMA system, user codes should be selected to satisfy three fundamental conditions. Firstly, the peak of the auto-correlation function

$$R_{c_m c_m}(t, f) = \int_t^{t+T_b} c_m(\tau, f)\, c_m(\tau - t, f)\, d\tau \quad -T_b \le t \le T_b \tag{3.16}$$

should be maximized for each code; secondly, its side-lobes should be minimized; finally, the cross-correlation function

$$R_{c_m c_p}(t, f) = \int_t^{t+T_b} c_m(\tau, f)\, c_p(\tau - t, f)\, d\tau \quad -T_b \le t \le T_b \tag{3.17}$$

of each pair of sequences $\boldsymbol{c}_m$ and $\boldsymbol{c}_p$ should be minimized for all delays *s*.

The discrete form, using matrix representation of codes, is useful. The discrete auto-correlation function

$$R_m(s) = \sum_{i=1}^{F} \sum_{j=1}^{N} \mathbf{C}_m(i, j)\, \mathbf{C}_m(i, j-s) \quad -N+1 \le s \le N-1 \tag{3.18}$$

and cross-correlation function

$$R_{m,p}(s) = \sum_{i=1}^{F} \sum_{j=1}^{N} \mathbf{C}_m(i, j)\, \mathbf{C}_p(i, j-s) \quad -N+1 \le s \le N-1 \tag{3.19}$$

of each pair of sequences $\mathbf{C}_m$ and $\mathbf{C}_p$ should be minimized for all delays *s*.

In the auto- and cross-correlation functions expressions (3.18) and (3.19), we sum over all the available *F* frequency bins. Hence, the frequency dimension disappears, and R_m and $R_{m,p}$ turn out to be one dimensional vectors, *i.e.*, they only depend on the time-shift, although the codes occupy two dimensions. Note that in these equations, no shift is considered in the frequency dimension. For DS-CDMA, by contrast, the summation over the *F* frequencies is absent.

In [112], we present formulas without the summation over the frequency dimension. They had been considered to be inherent to the FFH-code definition. The equations given here better describe the operation performed.

The three auto- and cross-correlation conditions mentioned above constrain the physical positioning of the gratings on the fiber as well as their bandwidth. The relative distances between the gratings must be chosen to satisfy a given level of auto- and cross-correlation among the codes. This distance, in turn, determines the achievable bit rate as discussed in Section 6.4.

3.3.2. Signal to interference ratio

Let $\overline{R}_{m,p}$ be the delay-averaged value of the cross-correlation between codes m and p. The variance of the cross-correlation between codes m and p is then

$$\sigma_{m,p}^2 = \frac{1}{2N-1} \sum_{s=-N+1}^{N-1} \left[R_{m,p}(s) - \overline{R}_{m,p} \right]^2 \tag{3.20}$$

Since we do not know which codes will be active at any given time, we further average over all code pairs. We obtain

$$\sigma^2 = \overline{\sigma}_{m,p}^2 = \frac{2}{K^2-K} \sum_{m=1}^{K} \sum_{p=m+1}^{K} \sigma_{m,p}^2 \tag{3.21}$$

$$\sigma_{MAI}^2(k) = (k-1)\sigma^2 \tag{3.22}$$

The signal to interference can then be easily derived

$$SIR(k) = N^2 / (k-1) s^2 \tag{3.23}$$

3.3.3. Probability of Error

The output of the matched filter is compared to the threshold $h = N/2 + m_{MAI}$ to decide if a one was transmitted. Using the Gaussian assumption for MAI, and assuming the system is MAI-limited, *i.e.*, neglecting other noise sources, the probability of error for equiprobable data is given by

$$\begin{aligned} P_e &= \text{Prob}(y \geq h | b_1 = 0) \cdot \text{Prob}(b_1 = 0) \\ &\quad + \text{Prob}(y \leq h | b_1 = 1) \cdot \text{Prob}(b_1 = 1) \\ &= \frac{1}{2}(\text{Prob}(y \geq h | b_1 = 0) + \text{Prob}(y \leq h | b_1 = 1)) \\ &= Q\left[N / \sqrt{(K-1)s^2}\right] = Q(\sqrt{SIR}) \end{aligned} \tag{3.24}$$

where $Q(x) = \frac{1}{\sqrt{2p}} \int_x^{+\infty} e^{\frac{-u^2}{2}} du$

We note the result of Salehi *et al.* in [36-37] demonstrating that synchronous DS-CDMA offers an upper bound on the exact probability of error

$$P_e(\text{exact}) \leq P_e(\text{chip synchronous case}) \tag{3.25}$$

This relationship holds for one-coincidence sequences, hence also for our OFFH-system.

Chapter

4

OFFH-CDMA

Numerical Simulation

This chapter is dedicated to a numerical simulation of the OFFH-CDMA system based on multiple Bragg gratings (MBG). In Section 4.1, we focus on multiple Bragg grating characteristics designed for an encoding/decoding operation. Parameters corresponding to a transmission rate of 500 Mb/sec per user, in a system with up to 30 simultaneous users, are determined and used in the simulation as system constraints. The encoder/decoder programmability problem is addressed and some solutions are briefly described in Section 4.1.3. For simulation, we assumed that each single grating wavelength could be independently tuned within a range of about 4.5 nm. This is a reasonable value for stretching-based tuning [185]. It is known that compression allows up to 45 nm, although it requires complex mechanics.

Furthermore, we determined grating parameters to enhance the capacity of the network and minimize the cross-correlation between codes. We found that a main-lobe *sinc* apodization can be used in writing the gratings to increase the system capacity and the spectrum efficiency. This result has been recently demonstrated experimentally by P.Y. Cortès in our laboratory.

In Section 4.2, we summarize the performance results. Simulation has shown that the encoder efficiently performs the FFH-CDMA signal generation and that the receiver easily extracts the desired signal from a received signal, for several multiple access interference scenarios. We measure the system performance in terms of bit error rate, as well as auto- to cross-correlation contrast.

It should be noted that we analyze only the performance degradation due to the presence of multiple access interference. The effects of quantum noise and thermal noise are neglected. The interferometric beat noise effect between frequency slices is not addressed here [79-86]. In the theoretical calculation of the variance of the multiple access interference [123-124] we assumed chip synchronization, while for simulation, we have considered an asynchronous system. In any positive CDMA system, the exact variance of MAI with arbitrary timing delays between users is less than its variance in a chip synchronous case.

4.1. Encoding/Decoding System

An MBG based encoder/decoder was described in Section 2.4. We keep the same definitions and assign numerical values for the system parameters. Typical numerical values of coupling coefficient of κL=2 (corresponding to 93% reflectivity) and effective refractive index of n_{eff}=1.452 are assumed. Equation 3.10 implies that $\Delta L \approx mql_B$.

Depending on the available piezo-electric devices used for stretching, we can consider a tuning range of $0 \le \Delta L \le 50mm$ which can lead to $0 \le mq \le 33$. For our calculations we selected parameters leading to a nominal data rate of 500 Mb/s, fixing the total round trip time in the grating structure to $2 10^{-9}$ sec=2(N-1)$L_c n_g/c$. Taking into account physical constraints in writing Bragg gratings (length L) and the spacing required between gratings to perform strain tunability, we selected L=10 mm (κL=2.2) with 8 mm spacing as reasonable values. This leads to N=12 for the number of gratings and a chip rate of $N\acute{}$500 MHz=6 GHz. These numerical values correspond to the series of reflected pulses depicted in Figure 4.1.

4.1.1. Encoder/Decoder Simulation:

The gratings will spectrally and temporally slice an incoming broadband pulse into several components as demonstrated by Chen, *et al.* [177]. As illustrated in Figure 4.1, each

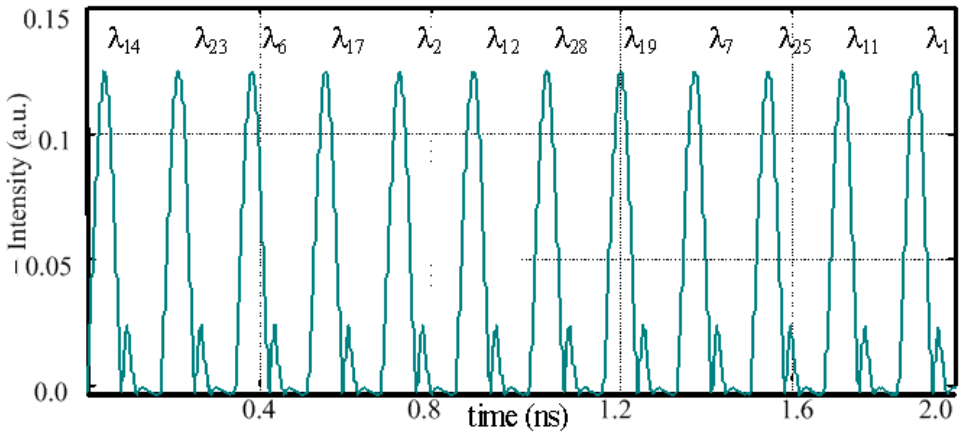

Figure 4.1: Reflected series of pulses from particular encoder with placement operator [14 23 6 17 2 12 28 19 7 25 11 1].

grating contributes a single reflected pulse. Pulses are equally spaced at chip intervals T_c corresponding to the round-trip propagation time between two gratings, due to gratings being equally spaced. Figure 4.1 corresponds to a particular user code with placement operator [14 23 6 17 2 12 28 19 7 29 11 1]. The sub-pulses following the chip pulses correspond to the power reflected by the side-bands of the gratings. The importance of these ghosts diminishes as we apodize the gratings and avoid saturation of the refractive index modulation.

Figure 4.2 a) depicts the reflected spectrum components for a MBG with the same placement operator. Each grating bandwidth is constrained so that the time overlap of the reflected pulses does not degrade the cross-correlation function. The time delay between the frequency components of the simulated MBG with this placement operator is presented in Figure 4.2 b).

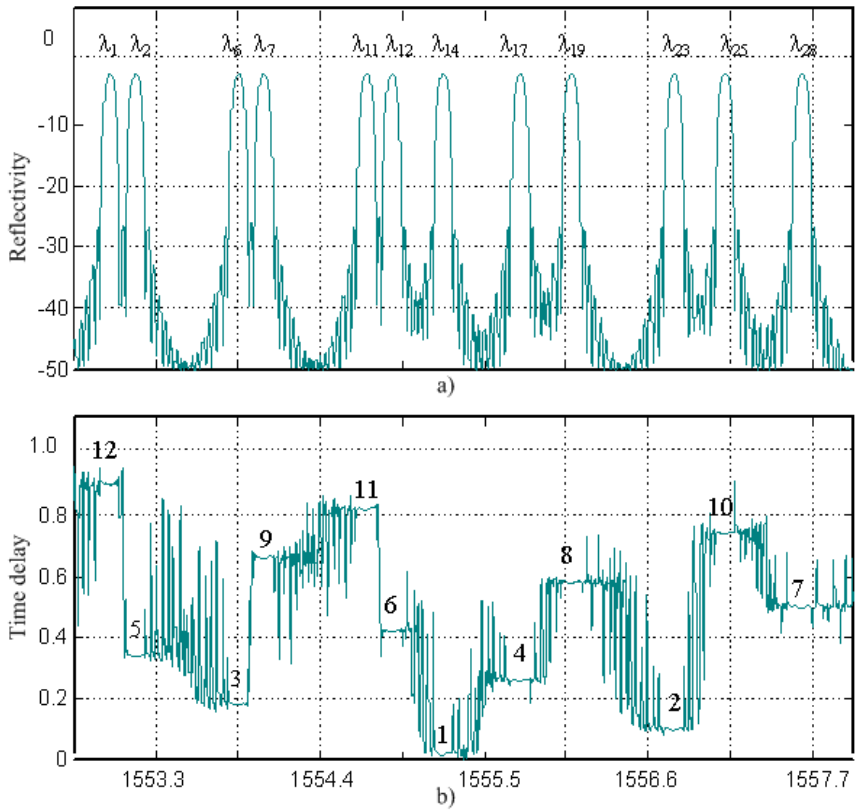

Figure 4.2: Reflectivity and group delay of an MBG based encoder/decoder.

As explained in Section 2.5, at the decoder, the peak wavelengths are placed in reverse order of that of the encoder to achieve the decoding function. The proposed decoder removes the translation between the frequency components and realigns all chips into a single pulse. Note that the chip synchronization loop is unnecessary in this scheme.

4.1.2. Apodization and Spectral Efficiency

In theoretical FFH-CDMA, the frequency components are assumed to have a rectangular shape. In our system, the gratings must be optimized to achieve near-rectangular spectrum slicing. This problem is known as band-pass (or band-stop filtering) in optical components design, *e.g.* as multiplexers/demultiplexers, WDM sources, etc. In our system, gratings with near-perfect rectangular band-pass filtering are required to achieve a high density of frequency bins in the available spectrum [170-176]. The higher the number of available frequency bins, the higher the number of near-orthogonal codes (i.e., the larger the number of simultaneous users).

Apodized Bragg gratings differ from the uniform grating in that their coupling coefficient varies along the propagation axis. The coupling coefficient as a function of position along the propagation axis, $k_0(z)$, is called the apodization profile. Recently, Storoy *et al.* [174] demonstrated a very long grating with a *sinc* apodization with nearly ideal rectangular reflectivity. Recall that grating length and separation are limiting factors for the data bit rate. Near ideal rectangular reflectivity can be achieved only by using 1) a long grating with a *sinc* apodization including many side lobes [179], 2) the inverse Fourier transform of the raised cosine [114]. We have examined several apodization profiles to achieve nearly disjoint and high-density frequency slices under the limited length constraint.

Figure 4.3 depicts the reflectivity of gratings with different apodization profiles: uniform, hyperbolic tangent (tanh(z)), $sinc_{ML}$ (sinc main lobe, *i.e.* sinc function with zero side lobes), Gaussian and Hamming window; all for 10 mm length and 220 m^{-1} coupling coefficient.

Apodization profiles:

All apodization profiles are normalized to have the minimum equal to zero and the maximum equal to κ_0=220. In our simulation, we calculate the different profiles of Figure 4.3 using the following definitions:

$$\kappa(z) = \kappa_0 \frac{g(z) - g_{\min}}{g_{\max} - g_{\min}}, \text{ where } g_{\max} = \max\{g(z)\} \text{ and } g_{\min} = \min\{g(z)\}$$

1) For Tanh(z) profile: $g(z) = 1 + \tanh\left[\beta(1 - 2|2z / L|^{\alpha})\right]$, with α=3 and β=4

2) For Gaussian profile: $g(z) = \exp\left[-G(z / L)^2\right]$, with G=1

3) For Blackman window profile:

$g(z) = \left[1 + (1 + B)\cos(2\pi z / L) + B\cos(4\pi z / L)\right] / (2 + 2B)$, where B=0.18

4) For Hamming window: $g(z) = \left[1 + H\cos(2\pi z / L)\right] / (1 + H)$, where H=0.55

Among the simulated profiles, the uniform grating has the narrowest main lobe (allowing for tighter frequency bins), but has the worst side lobes. The Hamming window has low side lobes, but an extremely wide main-lobe. The Gaussian and $sinc_{ML}$ profiles have similar main lobe widths, but the $sinc_{ML}$ has lower side lobes, achieving -25dB. We

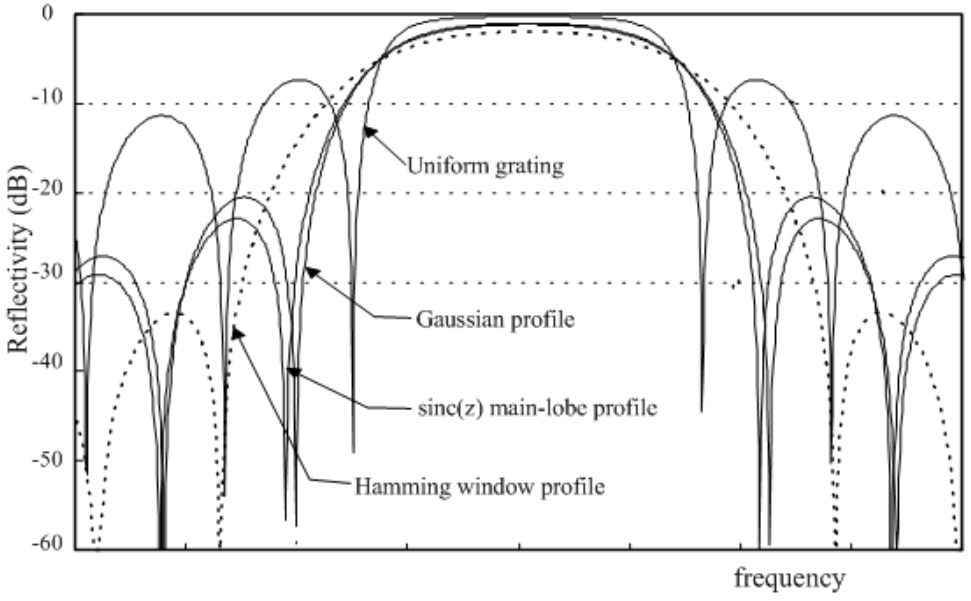

Figure 4.3: Reflectivity of gratings for differe nt apodization profiles.

therefore opt for the $sinc_{ML}$ apodization for our simulations.

In Figure 4.2 a), we depict the reflectivity of 12 gratings each with a $sinc_{ML}$ apodization profile, *i.e.*, one user code (user number 1) from Figure 4.6. The central resonance wavelengths are selected allowing the first and second side lobes of successive gratings to overlap, in order to increase bin density. Simulation results presented in this chapter use MBG with $Sinc_{ML}$ apodization.

4.1.3. Programmability Solutions

The ability to reconfigure the encoder/decoder pair is essential for the modularity, survivability and the resilience of the network topology. To that end, several approaches can allow reconfiguration of the encoding/decoding device. One approach would be to tune the period of each Bragg grating so that the reflection spectrum of the grating moves within the available bandwidth, effectively changing its resonance wavelength. Therefore, while each grating can be written to a common center frequency, it can later be tuned to a particular frequency as prescribed by the code.

Two popular methods can be used to tune the Bragg grating: stretching and heating [179,189]. We report here solutions previously proposed to tune single Bragg gratings for applications like reconfigurable Add/Drops in wavelength division multiplexing systems. We think these are among the most elegant solutions. None of them, however, is commercial at this time. Numerous tuning solutions have been studied in the literature. Figure 4.4 a) describes one possible method where the fiber coating is made with metallic material to which an electric voltage is applied to heat the grating and change its central wavelength. Figure 4.4 b) describes another method where we coat the fiber grating using piezoelectric material and apply an electric voltage to the two electrodes placed in the ends.

Several integrated photonics devices in chalcogenide glasses could also be used to erase/write Bragg gratings, to the center frequencies. Voltage controlled electro-optic devices can also achieve the same functionality by changing the refractive index of the grating. The latter device can only be implemented in materials with large electro-optic coefficient, and thus require special polymer fibers or gratings on integrated optical devices

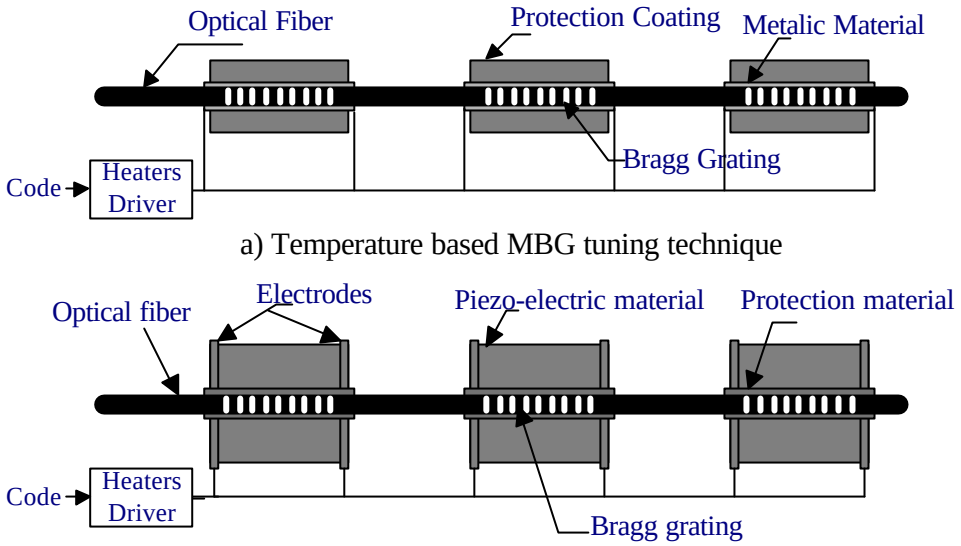

Figure 4.4: Temperature and Piezo-electric programmable encoders decoders.

such as $LiNbO_3$. A combination of other optical spectrum slicing (or filtering) devices together with a bank of delay lines can also be used to achieve the same functionality.

Figure 4.5 shows a programmable transmitter where a bank of useful codes and a multi-position optical switch are used. The optical switch selects the position, which corresponds to the selected code as prescribed by the code generator.

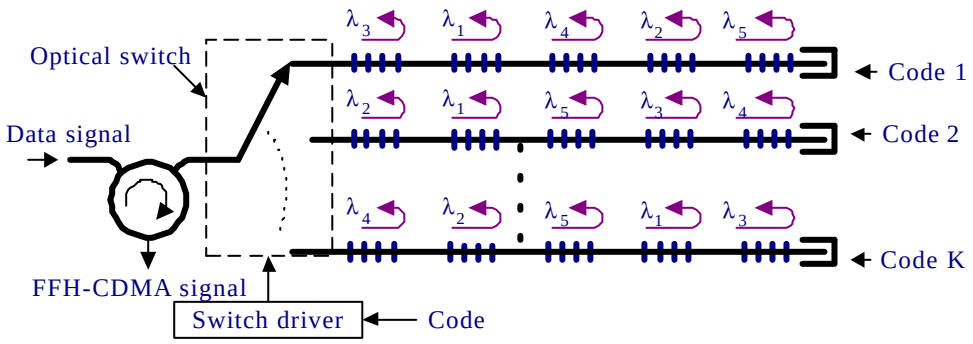

Figure 4.5: Switch based programmable encoder/decoder.

4.1.4. Code design for optical FFH-CDMA

Bin [88] recently proposed a novel FFH-code generation algorithm. These codes fall into the category of one-coincidence sequences introduced in Section 3.2, and guarantee a minimum distance, *d*, between adjacent symbols (or pulses). For our system, this means that the reflected frequency bins from adjacent pairs of gratings, (leading to two reflected pulses adjacent in time), are separated by a specified minimum number of bins. In our case, this reduces the effect of side lobes in the reflectivity of each grating. In the following, we describe the main steps of the algorithm.

Codes Generation Algorithm:

Let q be an odd integer, and define $N = 2k = q - 2d - 1$. Let **C**=(c_0, c_1, ..., c_{2k-1}) be a permutation of **D**=(d+1, d+2, ..., q-d-1).

Let $D_n(j) = \left(\sum_{i=n}^{n+j-1 \bmod 2k} c_i \right) \bmod q$, for $0 \le n \le 2k-1$, and $2 \le j \le k$.

We select **C** among the all the possible permutations of **D**, which satisfies:

$c_i + c_{i+k} = q$, *and* $0 \le i \le k-1$

1. For each $j, 2 \le j \le k$, all the $D_i(j)$ are different for $0 \le i \le 2k-1$.
2. If the vector **C** exists, it is called the generator sequence, and a set of q sequences are generated by $F_j = (D_0(1)+j, D_0(2)+j, D_0(3)+j, \cdots, D_0(2k)+j)$, where $0 \le j \le q-1$, and "+" is modulo-q addition.

Using q=29, N=12, and d=8, we derive 29 one-coincidence sequences, including $\mathbf{c_1}$=[14 23 6 17 2 12 28 19 7 25 11 1] and $\mathbf{c_2}$=[15 24 7 18 3 13 0 20 8 26 12 2]. Figure 4.6 illustrates the frequency-hop patterns of codes 1, 2 and 7. The example of reflectivity and delay time curves shown in Figure 4.2 corresponds to the frequency-hop pattern of code 1.

The codes used here cannot be considered as optimal codes for fiber optic FFH-CDMA. Indeed, these codes were developed for mobile and satellite communications, and optimized to minimize cross-correlation in mobile radio communications due to the Doppler effect. In optical fiber communications, the Doppler effect can be neglected, while dispersion must be accounted for. Furthermore, we studied other radio frequency FFH-

CDMA families of one-coincidence codes in order to adapt them to our optical system. In [118] we used the so-called hyperbolic codes.

4.2. Performance Results

4.2.1. Auto- and cross-correlation

To estimate the performance of the proposed FFH-CDMA encoder/decoder we calculate the auto- and cross-correlation functions for different numbers of simultaneous users. In Figure 4.7 a) we present the auto and cross-correlation for a single interfering user (simulated with code 2 of Figure 4.6) and code 1 for the desired user). The auto-correlation has an easily identifiable peak compared to the cross-correlation function. Recall that the high auto-correlation peak is also used by the receiver to determine the time of the detection window for the desired signal. In the remaining time of the bit, *i.e.*, outside the detection window, only the interference energy is present. This interference energy is useful for the receiver to dynamically estimate the number of active users, which in turn determines the detection threshold.

It is worth mentioning that in the code set used for this simulation, the different code pairs do not have the same number of shared frequencies; hence the interference

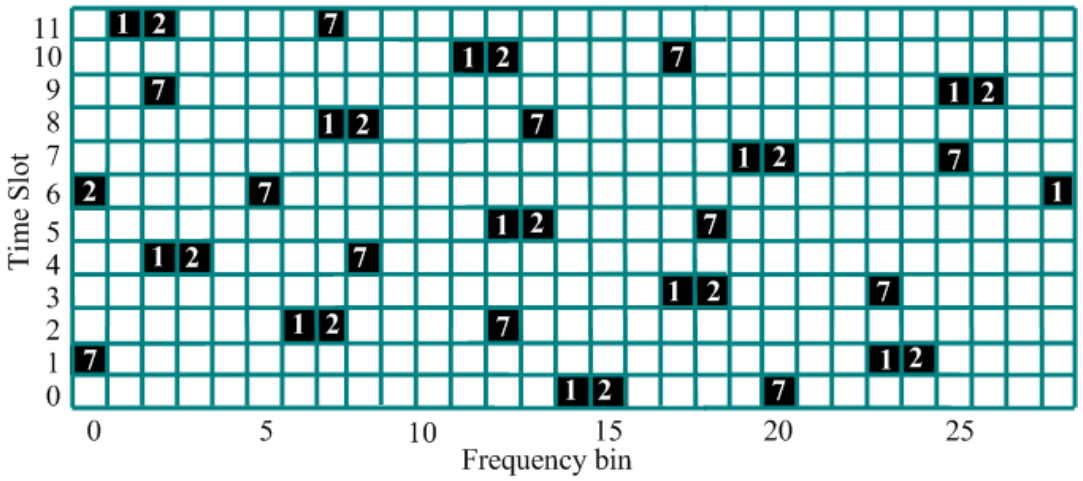

Figure 4.6: Three hopping patterns in a system with 12 time slots and 29 hop frequencies

energy is not proportional to the number of interferers. Optimized codes could minimize the variance of the number of coincidences between code pairs to improve threshold estimation. Similarly, in non-coherent DS-CDMA systems, preferred OOC families had code pairs with similar number of shared chips.

In Figure 8 (b-d), higher numbers of interfering users (5, 10 and 15) are present, and the cross-correlation function presents higher peaks, but the auto-correlation peak remains easily distinguishable. The largest cross-correlation peak slightly exceeds half of the auto-correlation peak. This means that the maximum number of active users is roughly equal to half the code capacity. This is consistent with 16 simultaneous users (1 desired user +15 interferers) in a system with 29 unique codes available.

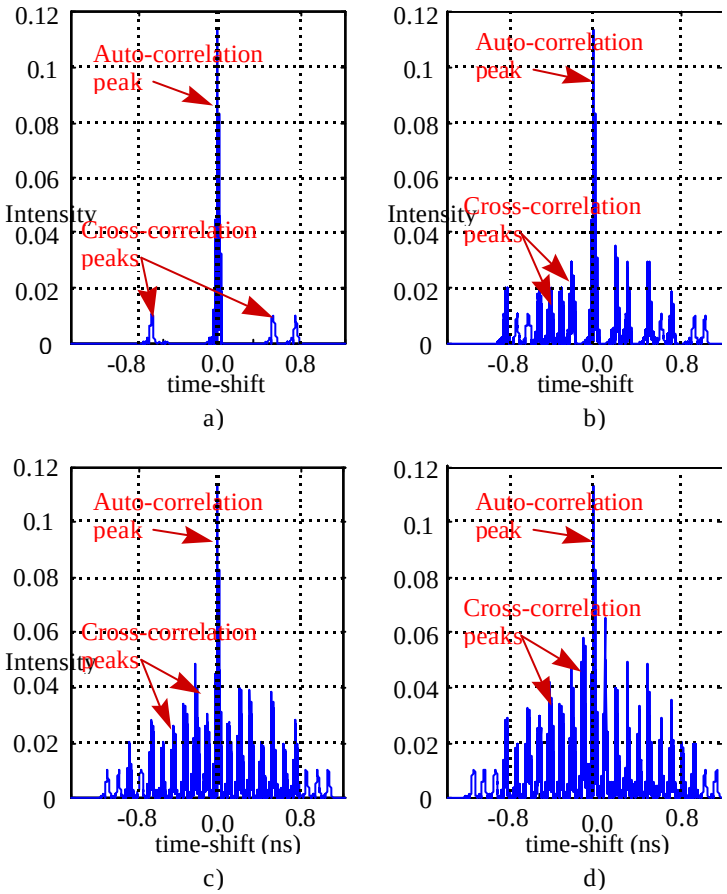

Figure 4.7: Auto- *vs.* cross-correlation functions for different numbers of simultaneous interferers: a) only one interferer, b) 5 simultaneous interferers, c) 10 interferers and d) 15 interferers

4.2.2. Probability of error

Recall the simulations were run for Bragg gratings of length 10 mm, spacing of 8 mm and a main-lobe *sinc* apodization. The average variance for codes implemented in the simulated gratings is given by equation (3.23). For N=12, q=29, Figure 4.8 depicts the probability of error (Equation 3.24) versus the number of asynchronous simultaneous users; the interference contribution is assumed to have a Gaussian distribution. The variance is calculated using equation (3.21). The upper bound (solid line) is derived assuming ideal reflectivity, and perfectly rectangular, disjoint, time *contiguous* chip pulses. The simulated gratings (points) use non-ideal reflectivity and non-contiguous chip pulses.

As shown in Figure 4.1 the chip pulse energy is not constant during the chip interval, *i.e.*, the transmission pulse shape $<T_c$, but rather compressed in time, allowing for guard times between chip pulses. This arises from the physical spacing required between the gratings.

In systems applications where the encoding/decoding device is not required to be programmable, especially broadcast and sensors multiplexing applications, physical spacing between gratings can be reduced to enhance the system capacity and efficiency. Nonetheless, the spacing between chip pulses reduces the probability of coincidence between users in an asynchronous transmission system, and reduces the interference

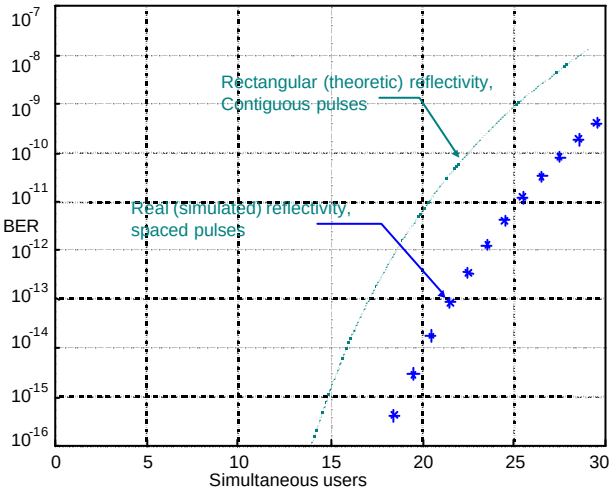

Figure 4.8: Probability of error *vs.* number of simultaneous users: simulation vs. ideal reflectivity

contribution and leads to better probability of error than a system with contiguous chip pulses. This phenomenon is illustrated in Figure 4.8, where simulated gratings (points) with non-contiguous chip pulses have better performance than the ideal closely packed pulses (solid line). Thus, simulation results confirm good performance for real (simulated) reflectivity. Furthermore, the probability of error can be further reduced by selecting codes better matching the new constraints. It should be noted that introducing guard time between bits substantially reduces the inter-symbol interference (ISI) hence increasing the performance.

Recall that the probability of error depicted in Figure 4.8 relays only on the assumption of interference limited performance. The performance difference between contiguous and non-contiguous chips based transmission reflects the effect of varying the chip duty cycle on the interference amount, but not on the overall signal power or other noise sources. The study of the duty cycle effect on all these noises and power parameters is necessary to have an accurate picture on the overall performance of the system.

4.2.3. Optical FFH-CDMA vs. non-coherent DS-CDMA

In radio frequency systems, a FH signal does not require the stringent synchronization inherent in DS spread spectrum signals. We compare the capacity of optical FFH-CDMA and non-coherent optical DS-CDMA in terms of simultaneous number of users, *i.e.*, the number of codes with specified cross-correlation.

Each family of optical orthogonal codes (OOC) for DS-CDMA are usually characterized by the quadruple $(n, w, \lambda_a, \lambda_c)$. n denotes the sequence length, w is the sequence weight, λ_a is the maximum of the auto-correlation side-lobes and λ_c the maximum cross-correlation [35]. As FH codes are two-dimensional the effective length of codes is $n = N \times q$, N being the number of gratings and q the number of available frequencies.

In Figure 4.9, we reproduce results from [89] which compare some DS-code families in terms of achievable probability of error as function of the simultaneous number of users and compare them with our sub-optimal codes. FH-codes for N=12 and q=19, 23, 27 and 29 corresponding respectively to quadruples (12×19=228, 12, 0, 1), (12×23=276, 12, 0, 1), (12×27=324, 12, 0, 1), (12×29=348, 12, 0, 1) , clearly outperform DS-codes of even

greater length, including prime sequences (PS), quadratic congruence codes (QC), extended quadratic congruence codes (EQC) and truncated Costas array codes (TC).

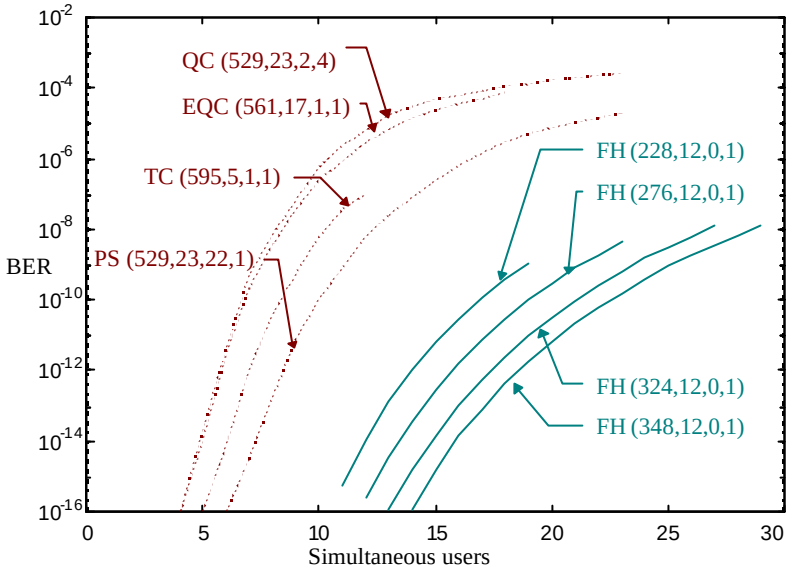

Figure 4.9: Probability of error *vs*. simultaneous number of users: FH and DS-CDMA

Chapter

5

Robust OFFH-CDMA

Theoretical and Numerical Analysis

In WDM, transmitters (DFBs) require stringent and complex frequency control loops to avoid wavelength drifts due to environmental fluctuations. This makes the transmitters heavy, bulky and inappropriate for local and short-haul communications networks. In this chapter we propose and analyze a technique we call robust FFH-CDMA, particularly suitable for severe, non-controllable environments. We avoid all conditioning and frequency stabilization loops in the transmission end. We develop a modified version of Extended Hyperbolic Congruence codes to achieve environment-resistant codes. We evaluate probability of error versus capacity for a single user and as an average over all users. The robust FFH-CDMA system avoids the stabilization problems of WDM and non-robust FFH-CDMA (see Chapter 4) at the cost of lower overall capacity.

5.1 Introduction

In WDM (Wavelength Division Multiplexing), optical sources must transmit at precise, distinct wavelengths. The environmental fluctuations at a transmitter, above all the temperature, can lead to significant wavelength drift. Stringent frequency control loops and complex tracking systems are required to avoid this drift [204-205], involving optic-to-electronic and electronic-to-optic conversion devices. The result is heavy, cumbersome transmitters that are unsuitable for local area networks (LANs), fiber-to-home access networks, short-haul interconnecting and multiplexing, and on-board naval and avionics communications.

To avoid frequency stabilization we employ OFFH-CDMA communications. In frequency-hopped CDMA the coding is done in two dimensions: time and frequency. During each time slot within a bit a certain frequency is transmitted. The decoding operation is similar, and the two-dimensional code is translated in the time dimension to achieve synchronization. Typically, an absolute frequency reference is assumed, *i.e.*, frequency synchronicity. In RF frequency-hopped CDMA, Doppler shift can corrupt the frequency reference so that the decoder must seek the auto-correlation peak while shifting over both the time and frequency domains (see Figure 5.1).

In optical communications, there is no Doppler shift, however frequency drift of source lasers due to environmental affects, above all temperature, is in some ways similar. Frequency-hopped CDMA allows communications despite drift, therefore obviating frequency-stabilization routines. In this chapter we propose such a system and address two major concerns. The first is the encoding/decoding device which can easily perform the correlation while shifting the code (or hop pattern) over both the time and frequency domain. The second consists of codes which have the necessary auto-correlation peak over two dimensions and that also conform to the physical constraints of the coding device.

The system proposed is robust to environmental effects that can be modeled as non-frequency selective; whenever the environmental effect has the same behavior at each frequency in the communications band, communications are possible despite the frequency drift. Bragg gratings (BG) and several BG based devices such as distributed feedback (DFB) lasers exhibit non-frequency selective drift. The OFFH-CDMA encoding/decoding device studied in chapters 2 and 3 is based on BG, and therefore has non-frequency selective drift. In that system, the transmitters require stabilization to the environment parameters' fluctuations. In contrast, the version proposed in this chapter is called robust FFH-CDMA, as we avoid stabilization and frequency-control loops, at the cost the decreased overall capacity.

In Section 5.2, we discus the frequency drift problem and control complexity in WDM systems. In Section 5.3, we explain how BG exhibits non-frequency selective drift. The basic mathematical formalism of the robust optical FFH-CDMA system is presented in Section 5.4. The environmental effect on the FFH-CDMA signal, in cases of BG and DFB

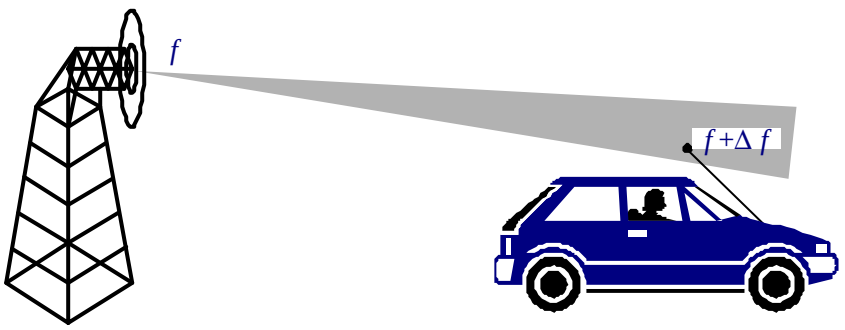

Figure 5.1: Frequency shift in radio-mobile systems due to Doppler effect.

lasers based encoders, are discussed in Section 5.5. In Section 5.6, we study the performance of the robust FFH-CDMA system. We derive suitable environment-resistant codes, calculate its maximum capacity in terms of number of users and we evaluate the probability of error both in mean and for a single user.

5.2 Frequency Drift in WDM

In DWDM (Dense Wavelength Division Multiplexing) communications, each wavelength is dedicated to one independent transmitter/receiver pair. The wavelengths coincide with a predetermined grid, fixing their values and spacing. In such systems, each transmitter must generate a very precise wavelength. Physical characteristics of the optical devices in the transmission end, especially source lasers, can lead to wavelength drift due to environmental fluctuations, especially changes in ambient temperature.

Figure 5.2 a) shows a branch of a hypothetical access DWDM network. Three sites are shown connected to the network each uses a dedicated frequency (or wavelength). Figure 5.2 b) illustrates the frequency drift problem. A client transmitting at f_2 that exhibits a shift and embarks in its neighbor's zone hence disturbing its communication. One obvious solution is the absolute control of semiconductor laser wavelengths for DWDM applications.

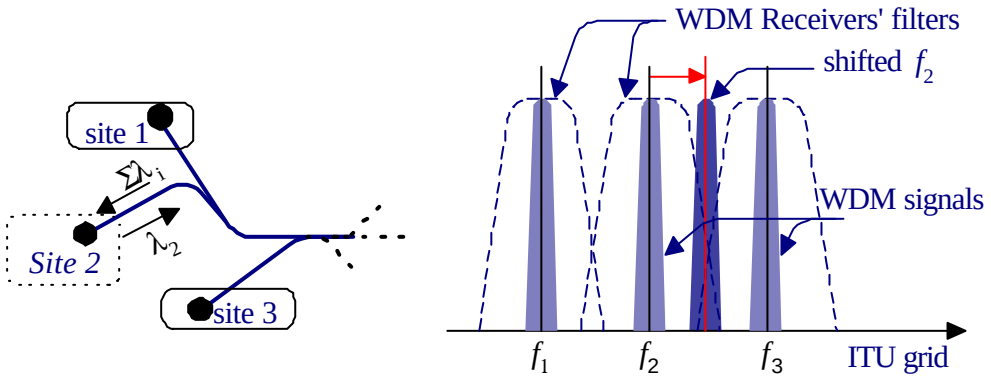

a) DWDM based tree network b) Power spectral density of the received signal

Figure 5.2: Frequency drift problem in typical dense WDM system.

5.2.1 Distributed Grating Based Lasers

For telecommunication systems, the most commonly used laser sources are distributed feedback (DFB) or distributed Bragg reflector (DBR) lasers [208]. This is due to their highly monomode spectrum where the emission frequency is set by the selective reflectivity of the distributed grating. When the ambient temperature changes, the distributed grating characteristics change and hence the emission frequency of the laser changes. Two parameters are usually used to control the frequency of a semiconductor laser, the junction temperature and the injection current. In Section 3, we further address the temperature dependency of the DFB laser frequency.

Temperature fluctuations affect not only source lasers, but also any Bragg grating devices. Gratings are widely used in communications for filtering, multiplexing, and waveform shaping, encoding/decoding and channel equalization. The performance of these devices is also sensitive to the ambient temperature variation and requires stringent control of their environment. Note that passive Bragg gratings are almost 10 times less sensitive to temperature than DFB lasers. Moreover, their stability can be enhanced again 10 times more if encapsulated in athermal packaging.

5.2.2 Frequency Control Problem

One popular way to stabilize the frequency of a laser source is to lock it to a stable optical reference. High precision is usually obtained using an atomic or molecular transition as an optical reference in the transmitter. Many atomic and molecular transitions are available at both 1.3 and 1.55 μm, which are usually observed using optogalvanic detection or optical pumping techniques [209]. These frequency stabilization techniques are typically very complex and require a stringent control of environmental parameters at each transmission site. Control loops require additional optic-to-electronic and electronic-to-optic conversion devices, making the transmitter heavy and cumbersome.

While a surmountable impediment for long-haul communications, the complexity and bulk of frequency stabilization has limited the success of WDM for Local Area Networks (LANs), fiber-to-home access networks, short-haul communications, security and

surveillance systems, on-board naval and avionics communications. In these applications, we must 1) reduce the system bulk and weight, 2) avoid environmental conditioning, and 3) reduce system complexity, especially the number of active devices. The last requirement is critical to ensure system reliability.

5.3 Non-Frequency Selective Environmental Effects

As an alternative to frequency control techniques we propose a coded communications system that is robust to environmental effects that can be modeled as non-frequency selective. Whenever the environmental effect has the same behavior at each frequency within the communications band in use, communications is possible despite frequency drift. There are several devices which exhibit non-frequency selective drift. Our approach is predicated on having a laser source and encoding/decoding device with non-frequency selective drift. Bragg gratings can be modeled as having non-frequency selective drift in their reflectivity. DFB lasers based on Bragg gratings also have this property. In order to insure that source frequency drift is independent of operating frequency, the source must not undergo any mode-hopping in response to environmental effects. For this reason Fabry-Perot lasers would not make suitable sources.

5.3.1 Bragg Gratings

Recall that Bragg grating operates as an optical band-pass (or band stop) filter centered at the so-called Bragg wavelength given by the expression $\lambda_B = 2n_{eff}\Lambda$, where Λ is the grating period and n_{eff} is the effective index of the core. The Bragg grating wavelength is particularly sensitive to two parameters: strain and temperature, which are usually used to tune Bragg gratings and also makes them attractive devices for fiber based sensors. While our results apply equally to drift due to strain, temperature variations are most common, and hence from this point forward we only refer to temperature affects.

The wavelength shift due to temperature variation ΔT can be expressed as

$$\Delta\lambda_B = \left[\left(dn_{eff}/dT\right)/n_{eff} + \left(d\Lambda/dT\right)/\Lambda\right]\lambda_B \Delta T \qquad (5.1)$$

where the first term arises from the temperature dependency of the refractive index, and the second term is due to the thermal expansion of the fiber. The former is dominant and accounts for about ~95% of the total shift. Experimental observations show that [185]

$$\frac{\Delta\lambda_B}{\lambda_B} = 6.67 \times 10^{-6} \Delta T \tag{5.2}$$

for the communications band. This equation indicates that wavelength shift $\Delta\lambda_B$ is frequency selective, *i.e.*, the constant of proportionality between $\Delta\lambda_B$ and ΔT is frequency dependent. However, in practice, the wavelength drift is much narrower than the wavelength itself, (~30 nm in the 1550 nm band), and therefore we can approximate $\Delta\lambda_B(nm) = 6.67 \times 10^{-6} \times 1550 \times \Delta T$.

5.3.2 DFB lasers

The operating wavelength of a distributed feedback (DFB) laser is determined by the etched grating through the Bragg wavelength given by $\lambda_B = 2\bar{\mu}\Lambda / m$, where $\bar{\mu}$ is the mode index, Λ is the grating period, and *m* is the diffraction order of the grating. Therefore, DFB lasers have the same temperature dependence as Bragg gratings. In our analysis of an environmentally resistant FFH technique, we assume that no mode hops can occur in the transmission. This is a reasonable assumption for DFB lasers as the built-in grating provides high stability of the longitudinal mode over a wide range of temperature (20-108$^\circ C$ reported in [208]). The wavelength of a DFB laser changes with temperature at a rate $\Delta\lambda_B / \Delta T \cong 0.1 nm/^\circ C$ without mode hopping. In [207], it was recently demonstrated that DFB lasers designed from erbium doped fiber also present a stable longitudinal and polarization single-mode operation without mode hopping in a range of temperature as wide as (-196 to 200 °C). Fabry-Perot lasers are generally less stable than DFB lasers and frequently exhibit mode jumps with the temperature variation.

5.4 Robust OFFH-CDM

In Chapter 4, we introduced the mathematical formalism for OFFH-CDMA. In this section, we exploit the same formulation and adapt this to the new context, where we take into account the frequency shift due to the environment temperature fluctuation. In Figure 5.3, we show a robust OFFH-CDM system in star topology. The transmitters are shown with fixed codes, the receiver however is programmable. The broadband source and fast external modulator are shown shared among all transmitters. Note that the data signal need to be synchronized with the low-duty cycle clock generating the optical short broadband pulses.

5.4.1 Time & frequency domain characteristics

In FFH-CDM system, the information bits are encoded with two-dimensional matrix codes simultaneously exploiting the time and frequency domains. The matrix codes are chosen to be as transparent (or mathematically orthogonal) as possible. We use codes adopted for radio frequency (RF) FFH-CDMA as a starting point for our analysis. These codes have their transparency optimized to combat two affects: time domain asynchronicity

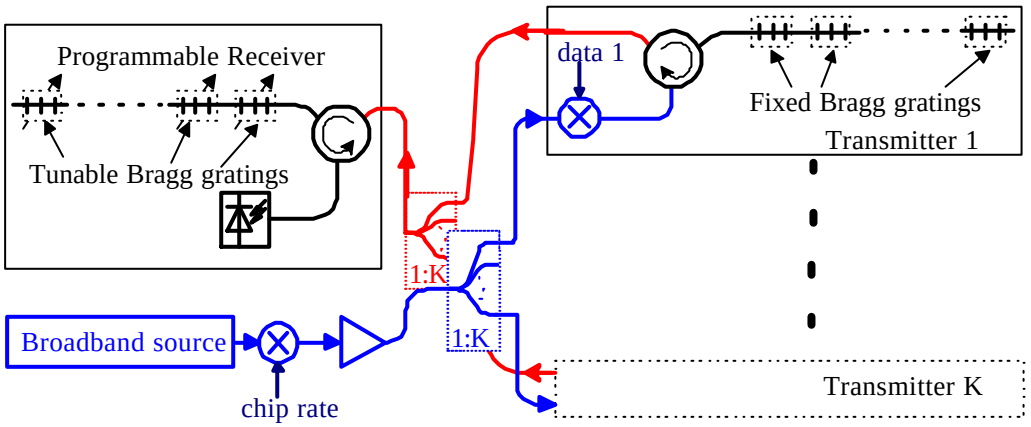

Figure 5.3: Robust FFH-CDM system.

(i.e., user transmissions have a random relative delay modeled with a uniform distribution) and frequency domain Doppler shift (due to relative motion of transmitter and receiver).

Temperature-induced frequency drift in optical systems will have characteristics different from those of Doppler-shifted RF communications, and therefore the codes used will be sub-optimal. In order to assess the performance of these codes via the signal-to interference ratio (SIR) and bit error rate (BER) (discussed later in section 5.4.4) we will average over the distribution of the temperature variation.

5.4.2 Coding and decoding

We introduce a special notation to express the sensitivity of the FFH code to environmental conditions, especially temperature. Let c_k^{α} be the transmitted FFH sequence at the temperature $T_\alpha = T_0 + \alpha\Delta T$, where T_0 is an arbitrary nominal temperature, ΔT is the amount of temperature variation which can change the transmitted wavelength by one increment, B_0, *i.e.*, one frequency slot, and α a coefficient which quantifies the temperature variation in the system. While in practice temperature variation will be continuous and not in discrete steps, we present a discrete form of our analysis for heuristic reasons only. The results apply equally to continuous temperature variation for ambient temperature.

When the temperature of the desired user's environment shifts from the nominal temperature T_0, the coefficient $\alpha_1 \neq 0$, *i.e.,* the locally generated desired user's code, $c_1^0(t)$ is spectrally shifted with respect to the transmitted code. The receiver should continuously and simultaneously shift the frequency components of the locally generated desired user's code to accurately match its frequency components, *i.e.* the receiver should generate $c_1^{\alpha_1}(t)$. The tuning of the matched filter from $c_1^0(t)$ to $c_1^{\alpha_1}(t)$ is accomplished by exploiting the auto-correlation peak of the code. The receiver output after tuning is

$$y = b_1 N + MAI \tag{5.3}$$

In most CDM systems, the MAI is the most important noise source. For a large number of multiplexed signals, the probability density function of the MAI is usually approximated to be Gaussian, appealing to central limit theorem arguments. To reduce the

effect of the MAI, codes with low cross-correlation are required, especially codes that remain uncorrelated even under frequency and time shift. Note that MAI depends on $\alpha_1, \alpha_2 \ldots \alpha_K$ since the cross-correlation between codes depends on the frequency shift between them, *i.e.*, the environment temperature at all the transmitters' sites.

5.4.3 Auto & cross correlation

Codes used in non-robust OFFH-CDMA systems [112] are not appropriate, as frequency shifts lead to high correlations among codes. In this system, as described in Section 5.6, we modify square ($N=q$) extended hyperbolic congruence codes, already resistant to RF Doppler shift, for this robust FFH-CDMA system. The used codes are one-coincidence sequences (see Section 3.11).

Let $c_k(i,j)$ be the frequency-hop pattern of user k when the time slot is i and the frequency slot is j. Therefore $c_k(i,j)$ is one if there is a transmission for user k in time slot $1 \le i \le N$ and frequency slot $1 \le j \le q$; otherwise it is zero. Let

$$\Omega_1 = \left| \min_k \alpha_k \right| \qquad \Omega_2 = \max_k \alpha_k$$

Each code in the code family should be selected to maximize the peak and minimize the side-lobes of the auto-correlation function over all delays t and frequency shifts s:

$$R_m(\tau, s) = \sum_{j=0}^{q} \sum_{i=0}^{N} \mathbf{c}_m(i, j)\,\mathbf{c}_m(i-\tau, j-s) \quad \begin{matrix} where -N+1 \le \tau \le N-1, \\ and\ -\Omega_1 + 1 \le s \le \Omega_2 - 1 \end{matrix} \tag{5.4}$$

Secondly, the cross-correlation should be minimized for all pairs of codes c_m and c_p in the code family for all delays t and frequency shifts s:

$$R_{m,p}(\tau, s) = \sum_{j=0}^{q} \sum_{i=0}^{N} \mathbf{c}_m(i, j)\,\mathbf{c}_p(i-\tau, j-s) \quad \begin{matrix} where -N+1 \le \tau \le N-1, \\ and\ -\Omega_1 + 1 \le s \le \Omega_2 - 1 \end{matrix} \tag{5.5}$$

5.4.4 SIR & Probability of error

To evaluate the signal to interference ratio at the receiver output we require the probability density function of the time-shift (or delay) as well as that of the frequency-shift between any users. As in an asynchronous system, the probability density function (*pdf*) of

the random time delay is well modeled as uniform over a bit duration, since no coordination exists between users. A uniform density is not however, necessarily a good model for the *pdf* of the temperature-induced frequency shift. Let $\boldsymbol{p}$ be a vector of length $(\Omega_1+\Omega_2+1)$ representing the discrete probability density function of the frequency-shift s so that

$$p(s) = P(\textit{frequency shift} = s) \textit{ and } \sum_{s=\Omega_1+1}^{\Omega_2-1} p(s) = 1 \tag{5.6}$$

In a real system, the *pdf* can be estimated using statistical analysis of the parameters influencing environmental fluctuations.

Let $\overline{R}_{m,p}$ be the cross-correlation averaged over delay and frequency-shift between codes m and p. Since the time-shift and the frequency-shift are independent variables, we arrive at

$$\overline{R}_{m,p} = \frac{1}{2N-1} \sum_{s=-\Omega_1+1}^{\Omega_2-1} p(s) \sum_{\tau=-N+1}^{N-1} R_{m,p}(\tau, s) \tag{5.7}$$

The variance of the cross-correlation between codes m and p is

$$\sigma^2_{m,p} = \frac{1}{2N-1} \sum_{s=-\Omega_1+1}^{\Omega_2-1} p(s) \sum_{\tau=-N+1}^{N-1} \left| R_{m,p}(\tau, s) - \overline{R}_{m,p} \right|^2 \tag{5.8}$$

Finally, the expressions of the signal interference ratio and the probability of error, remain the same as in Section 3.3. The parameters, however, should be calculated using equations (5.6-5.8).

5.5 Environmental effects on the FFH signal

As explained in Section 5.3.1, Bragg gratings can be modeled as having non-frequency selective drift in their reflectivity. Furthermore, fiber Bragg gratings are a key component in several optical devices, especially DFB laser sources, which are widely used in telecommunications due to their monomode output, stability and simplicity.

When the temperature of one FFH transmitter increases, all wavelengths of the transmitted FFH signal simultaneously and identically increase, *i.e.*, non-frequency selective drift. As mentioned in Section 5.3,1 the Bragg grating wavelength shift actually depends on the Bragg wavelength, but the restricted region of interest (30 nm in the 1550 nm region) makes non-frequency selective drift a reasonable assumption. For the DFB based FFH encoder, it should be assumed that no mode hopping occurs when the temperature shifts.

If the spectrum of the data modulated wideband signal is large and flat enough, the total transmitted energy does not change with the ambient temperature variation. In effect, the number of transmitted pulses and their energy do not change. An example of an FFH encoded signal is shown in Figure 5.4 a). The code is $\mathbf{w}_0=[f_{-5}\ f_{-4}\ f_1\ f_{-1}\ f_{-2}\ f_4\ f_{-3}\ f_3\ f_2\ f_0\ f_5]$ at the initial ambient transmitter temperature T_0 (which corresponds to the squares marked by 0). Let ΔT be the positive temperature change corresponding to a wavelength drift of one increment B_0, *i.e.*, the temperature causing λ_k to drift to λ_{k+1}.

When the ambient temperature changes with an amount equal to α times ΔT becoming $T_\alpha=T_0+\alpha\Delta T$ the effectively transmitted sequence will be $\mathbf{w}_\alpha=[f_{-5+\alpha}\ f_{-4+\alpha}\ f_{1+\alpha}\ f_{-1+\alpha}\ f_{-2+\alpha}\ f_{4+\alpha}\ f_{-3+\alpha}\ f_{3+\alpha}\ f_{2+\alpha}\ f_{\alpha}\ f_{5+\alpha}]$. Let $\mathbf{I}$ be a vector of N-1 components (N-1=10 in the example of Figure 5.4 a) describing the wavelength subscript increment in the code.

$$\mathbf{I}_k(i) = subscript(\mathbf{u}_k(i+1)) - subscript(\mathbf{u}_k(i)) \tag{5.9}$$

For example the first component of $\mathbf{I}$ equals the second wavelength subscript of the code minus the first wavelength subscript. For $\mathbf{w}_0$, we calculate $\mathbf{I}=[1\ 5\ -2\ -1\ 6\ -7\ 6\ -1\ -2\ 5]$. $\mathbf{w}_\alpha$ and $\mathbf{w}_0$ have identical increment vector $\mathbf{I}$ because the one is only frequency dimension shifted to the other. Note that the increment vector is a placement operator of length N-1.

In our system where transmitters are not temperature-stabilized, the increment vector of the frequency FFH code is sufficient to decode the message. The receiver starts with a decoder programmed for the desired user (that is for the correct increment vector) and tuned to a nominal set of frequencies corresponding to the nominal temperature T_0. The receiver tunes the decoder gratings in union (*i.e.* maintaining the same increment vector) and searches for an auto-correlation peak. In figure 5.4 b), we superpose two FFH hopping patterns having different increment vectors. Acceptable cross-correlation properties are maintained for any time and/or frequency shift between the codes. In Section 5.6, we show that the capacity of this multiplexing system is reduced compared to the optical FFH-CDMA with a stabilized environment.

We addressed Bragg gratings and DFB lasers as examples of encoding/decoding devices to combat the effect of the environment on the FFH-signal. However, it is important to note that the robustness property of the system is inherent to the FFH communications technique itself. Hence, any encoding device having non-frequency selective drift can be used.

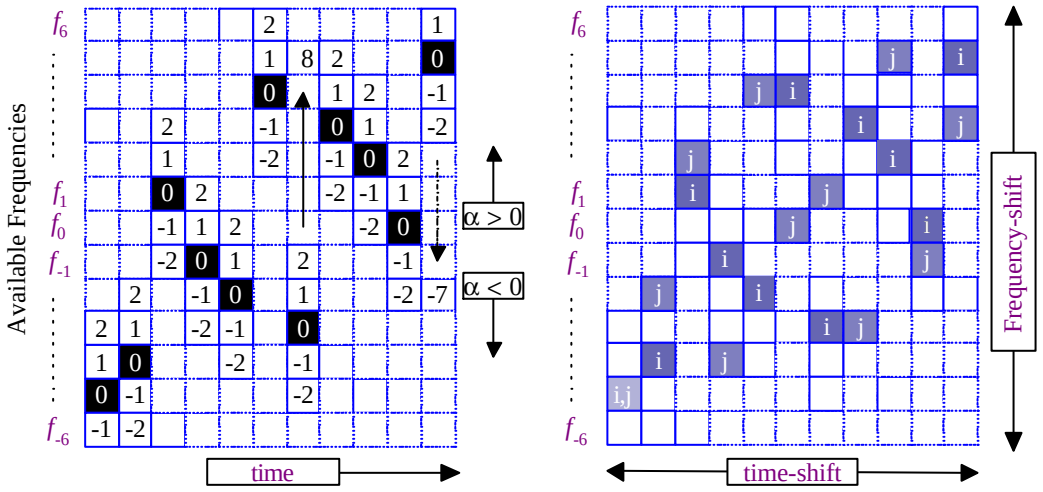

a) Temperature fluctuation effect on OFFH signal

b) Two-dimensional correlation between i^{th} and j^{th} codes.

Figure 5.4: Temperature variation effect on FFH-CDMA signal.

5.6 Performance Evaluation

In Figure 5.3, we described a robust FFH-CDM system based on multiple Bragg gratings and composed of one programmable receiver and K transmitters. A broadband source and a rapid external modulator (at the chip-rate or lower) can be shared between all the users or a sub-group of users to generate a stream of broadband short pulses (chip-duration). Each transmitter uses its own low rate (bit-rate) external modulator to insert its data sequence into the incoming short pulses, and its fixed multiple Bragg gratings to insert its own code.

5.6.1 Processing Gain

The processing gain PG is a critical integer parameter for every CDMA system, as it quantifies the resources shared between users via the codes. The higher the PG, the higher the number of available codes and the greater the ease of discriminating among users. In FFH-CDM, the PG is expressed as

$$PG = \{number\ of\ \ frequency\ slots\} \times \{number\ of\ time\ slots\} \tag{5.10}$$

where the number of available wavelengths (or frequencies) in the system is limited by 1) the bandwidth of the source and 2) grating tuning bandwidth. The combination of fiber stretching (up to 7 nm) and compression (up to 30 nm) leads to very wide range of tunability in the system, consider that the source bandwidth is the limiting factor for determining the number of available wavelengths. In temperature stabilized optical FFH-CDMA, the entire source bandwidth (*BW*) can be used for encoding, however this robust FFH-CDMA system requires upper and lower guard bands (each with bandwidth *GB*) to accommodate frequency drifts due to environmental effects. This results in a decrease in the number of frequency slots q, hence a reduction of the processing gain and the reduced capacity alluded to previously. The number of frequency slots is reduced per

$$q_0 = \frac{BW}{B_0} \quad \text{vs.} \quad q = \frac{BW - 2GB}{B_0} \tag{5.11}$$

where B_0 is the combined bandwidth of the frequency slot and spacing between slots.

5.6.2 Derivation of Codes

The encoding space is rectangular (N time slots < q frequency slots), however most RF FFH-codes assume $N=q$. In [108], the authors developed a new family of codes called extended hyperbolic codes (EHC) which have good auto and cross-correlation properties under simultaneous frequency and time shift. The EHC placement operator can be expressed as

$$y_{i,m}(k) \equiv \begin{cases} 1/(ik+m) \mod(p) & \text{if } ik \neq -m \mod(p) \\ 0 & \text{if } ik = -m \mod(p) \end{cases} \tag{5.12}$$

where, p is a prime number (for our system $p=q$), $k=1,...,p-1$ is the number of chip time slots, i is the user number and $m=0,...,p-1$ is the so called message number. For this application we can select m=0 and consequently reduce the cross-correlation between codes. While the EHC codes are not rectangular codes, they can be adapted to our needs. Since the $q \times q$ codes satisfy the required auto- and cross-correlation properties, any truncated codes of size $q \times N$ will also have the same properties.

While the EHC codes in [108] offer good performance for frequency shifts from $-q$ to q, our system has shifts constrained by the guard bands (by construction the guard bands represent maximal frequency variation). Therefore, our codes need to be efficient for shifts equal to

$$-(q_0 - q)/2 \leq s \leq (q_0 - q)/2$$

We therefore propose the following modified EHC codes

$$y_{i,0}(k) \equiv \begin{cases} 1/(ik) \mod(p) & \text{if } k \neq 0 \mod(p) \\ 0 & \text{if } k = 0 \mod(p) \end{cases} \tag{5.13}$$
$$\text{for } i = 1,\ldots,N-1;\ k = 0,1,\ldots,N-1$$

This derives p-1 different modified (or truncated) extended hyperbolic codes (TEHC). Each of them uses N frequencies among the available p. It should be noted that the TEHC have performance at least as good as the EHC codes, however they remain sub-optimal.

5.6.3 Illustrative example

A super-fluorescent source (SFS) can provide a signal of 30 nm bandwidth centered at the wavelength 1550 nm. Using the same Bragg gratings physical parameters and wavelength spacing as in [112], we achieve up to q_0=135 available disjoint frequency slices taking into account the adequate spacing between slots. In the time domain, a fiber of 20 cm length supports 12 gratings for a data rate of 500 MB/sec. To match the OC 12 standard (622 MB/sec), a shorter length of 16 cm is assumed here for 12 gratings without significant overlap between chip pulses (physical spacing between gratings being reduced from 8 mm to 4 mm). Using this parameters a temperature stabilized FFH-CDMA has PG= $q_0 \times N$= 135×12=1620.

In order to determine the guard bands required we assume T_0=0° C to be the maximal temperature and 4 nm to be the maximum wavelength increase and/or decrease expected due to temperature fluctuations. In [207], the fiber DFB lasers presented high linearity in a temperature range as wide as ~400° C in the interval (-196° to 200° C), which leads to a frequency shift of ~4 nm. This means that remaining bandwidth for encoding is (30-2×4)=22 nm corresponding to ~99 wavelengths. For ease of code generation we select the prime number q=97 as the effective available number of wavelengths to be shared among the robust FFH-CDMA system. The processing gain of the robust FFH-CDMA is consequently PG=97×12=1164.

5.6.4 Simulation results: Auto-correlation function

In this section, we simulate two 12-wavelength multiple Bragg gratings using the parameters of the previous illustrative example and we restricted *q* to 17. We derived the TEHCs and we simulated ambient temperature variation of one selected desired encoder scanning the interval −100 to +100 ºC in 5 ºC steps. This includes, for example, the range of ambient winter temperature in Québec City, where temperatures can be lower than -60ºC in open areas; and where it can exceed 30 ºC in enclosed areas. Figure 6 shows that the correlation between an encoder maintained at nominal initial temperature of 0 ºC and a decoder searching through all possible temperature and time delays. We se a high central

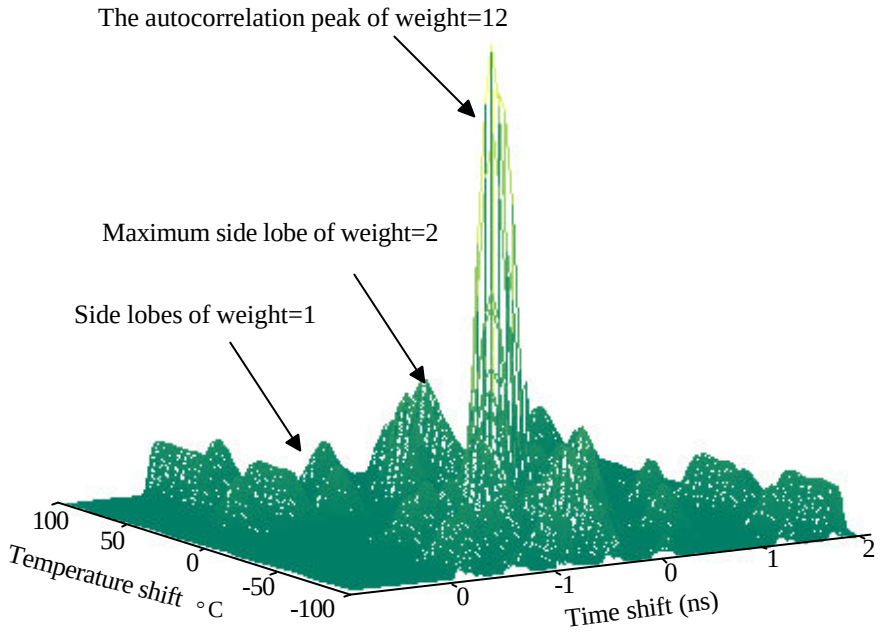

Figure 5.5: Two-dimensional (time and temperature shifts) auto-correlation function.

peak (weight 12) when the decoder temperature is 0 ºC and time synchronization is achieved. Otherwise, the correlation leads to side-lobes with maximum weight of 2.

5.6.5 Probability of Error

To evaluate the system performance in terms of probability of error we assume a Gaussian *pdf* for the temperature, with mean T_0 and standard deviation η. The temperature of each transmitter is assumed independent and identically distributed. Simulations use parameters from the previous section and TEHC codes described in Section 5.6. In the following, we evaluate the probability of error of the system averaged over all users, as well as the probability of error of a single user. We present the probability of error as a function of the number of active users, for various values of η. Recall ΔT is the temperature shift leading to frequency drift B_0.

5.6.5.1 Average Probability of Error vs. Capacity

In Figure 5.6, we present the average probability of error of the proposed robust communications system as a function of the number of users. The curves clearly show that the higher the number of active transmitters, the higher the probability or error. This is obviously due to the increased MAI.

It is important to note that the environment stabilized FFH-CDMA system gives an upper bound (curve (a)) to the probability of error in the system. Stabilization of the transmitters keeps all users' signals in the central frequency band and out of the guard bands, which leads to greater cross-correlation between users and higher MAI. On the other hand, a uniform distribution of the frequency shift gives a lower bound to the probability of error (curve (d)), as drifted codes tend to cover the entire available bandwidth. Curves (b) and (c) correspond respectively to a temperature shift *pdf* with $\eta=2.55\times\Delta T$ and $\eta=7.65\times\Delta T$.

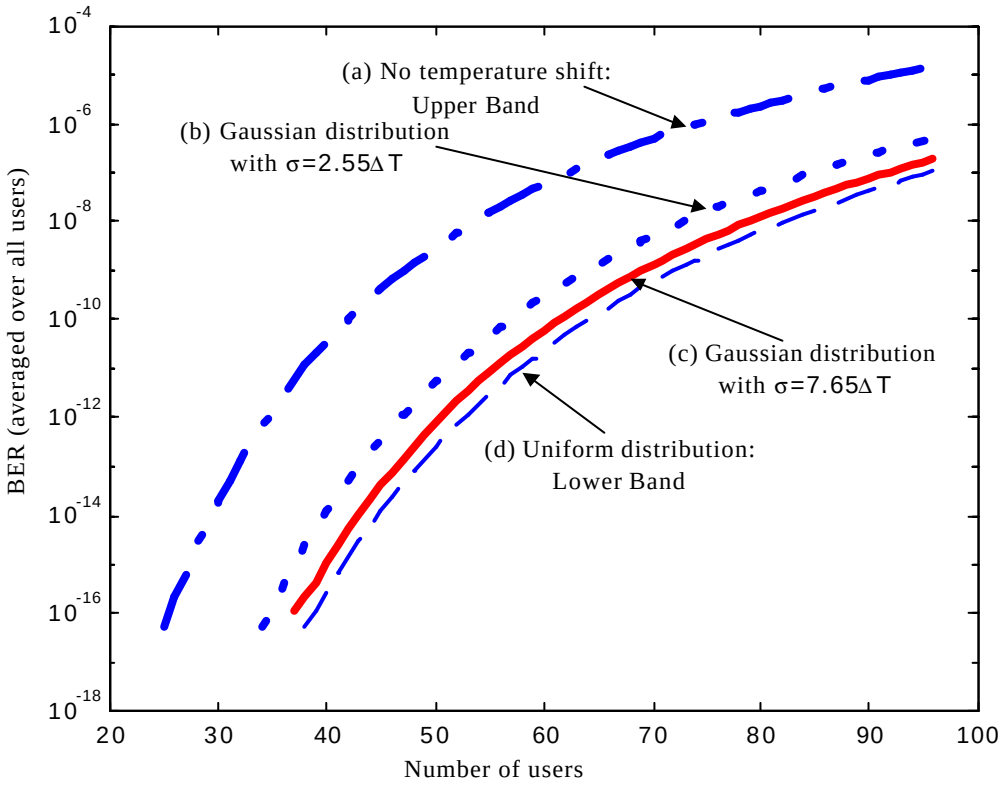

Figure 5.6: Average Probability of Error *vs*. Capacity.

As can be expected, decreasing η leads to increasing MAI and a degradation of the average probability of error. Figure 5.6 shows that for probability of error of 10^{-9} the system can accommodate $\approx$45 simultaneous users in a temperature-stable scenario and 74 simultaneous users when the temperature is uniformly distributed.

5.6.5.2 Single Probability of Error vs. Capacity

Suppose that one-transmitter exhibits a frequency shift, therefore pulses from its signal are present in a guard band. This reduces its coincidence probability with the interferers, *i.e.* reduces the MAI, and consequently improves its probability of error. Figure 5.7 shows the single user probability of error versus the number of users depending on the frequency shift of the desired user. An unchanged temperature shift gives an upper bound to the probability of error since the variance of the MAI is the highest. When the transmitter exhibits the maximum frequency shift the single probability of error achieves its lower bound since the MAI is at its lowest.

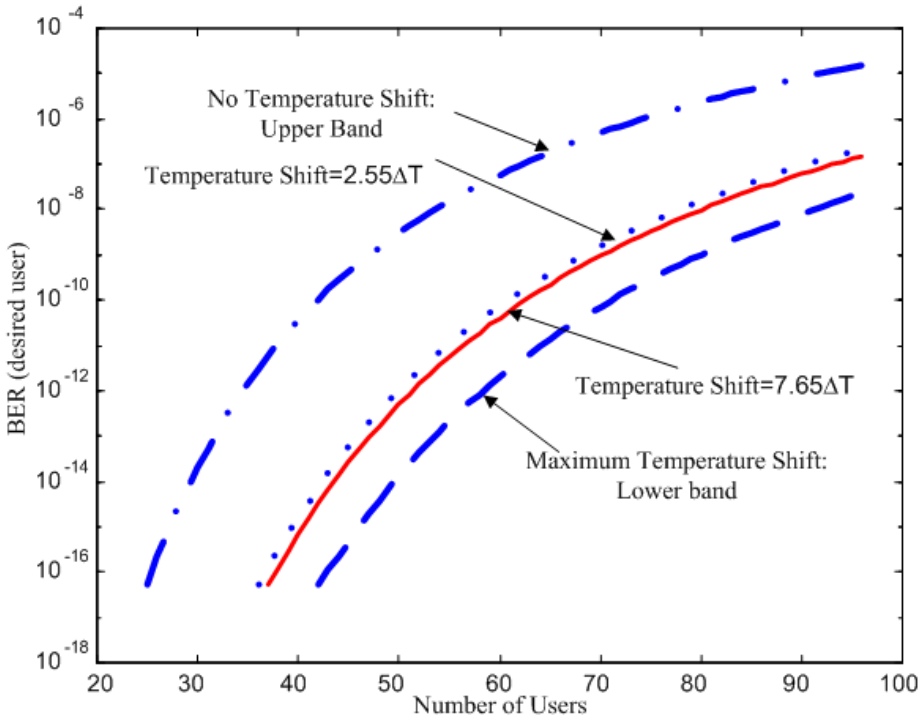

Figure 5.7: Single Probability of Error *vs*. Capacity.

Chapter

6

Experimental Demonstration

OFFH-CDMA Setup

In this chapter, we address the issues relating to a practical implementation of the OFFH-CDMA system. We describe four experimental setups; one of them is a writing system of Bragg gratings that enabled the design and manufacturing of encoders/decoders multiple Bragg gratings. The three others consist of demonstration prototypes of Optical Fast Frequency Hopping-CDMA. The prototypes represent the three generations of the same system; the first is a two channels version, demonstrated in April 1999, the second includes eight channels, demonstrated in August 1999; and the third is a 16 channels achieved in March 2000. Throughout the chapter, we present series of measurements, observations and results.

In Section 6.1, we review the principle of the experimental setup we have exploited to design our multiple Bragg gratings (MBGs). The writing system is designed by Cortès and LaRochelle in our laboratory [190]. It has played an essential role in the design of the FFH encoders/decoders. Indeed, successful OFFH-CDMA encoding/decoding operation imposes serious accuracy in the MBG parameters. We have designed an additional mechanical fiber positioning system that has enabled us to fulfill this accuracy requirement.

In Section 6.2, we present the design parameters we have selected for the experimental demonstration of the encoding/decoding principle. We characterize the designed MBGs, and then discuss the achieved results. The first version of the experimental setup, including two encoders and one decoder, is described in Section 6.3. The auto- and cross-correlation functions are measured for different transmission rates, demonstrating appreciable results.

In Section 6.4, a second version of the OFFH-CDMA setup simulating eight simultaneous transmitting encoders and one reconfigurable decoder is described. The auto- and cross-correlation functions are measured again. They clearly describe successful decoding for different encoded signals. We finally present a high capacity version of OFFH-CDMA setup including sixteen encoders and four programmable decoders with a series of measurements of encoded decoded series of bits for 800 MHz transmission rates and higher.

6.1 Bragg Grating Writing Technique

6.1.1 Setup Principle

The writing technique we have used to fabricate our MBGs consists of a Sagnac interferometer (see Figure 6.1). A UV light pulsed beam, with a repetition frequency of 80 MHz generated by a quadrupled YAG laser output, is also used. The phase mask splits the beam into two sub-beams of diffraction orders +1 and –1. The two sub-beams travel through two different optical paths (i.e., through the mirrors M1 and M2) with slightly different lengths, then interfere in a plane where the fiber should be positioned. The fiber is placed in a plane that is slightly above the phase mask. The mirrors M1 and M2 are slightly tilted with respect to the x-y plane in order to focus the interference on the fiber.

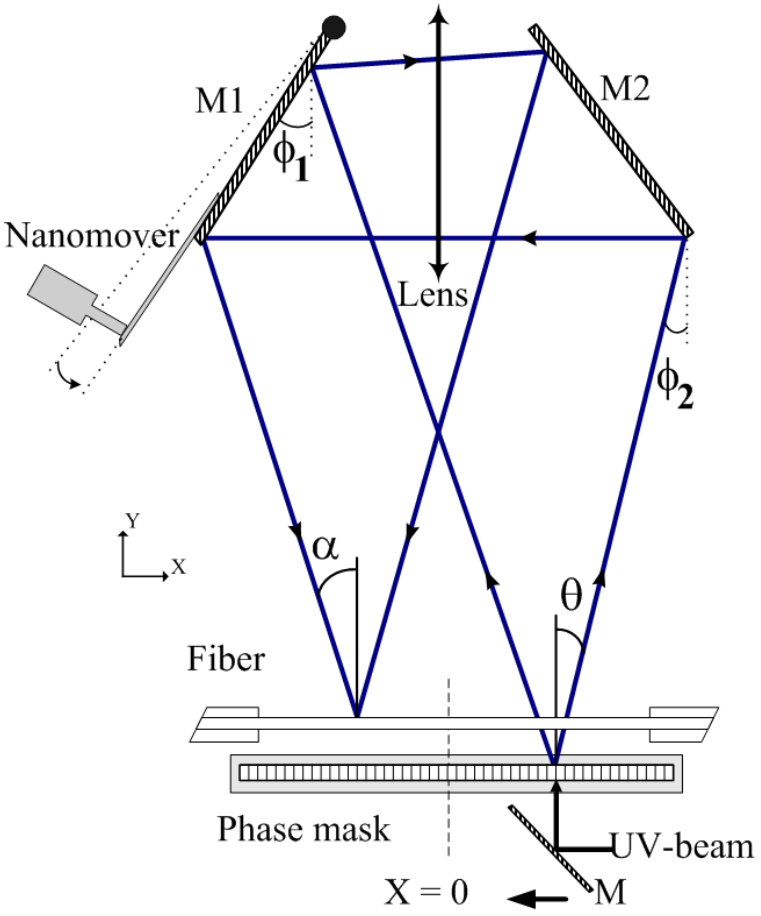

Figure 6.1: Sangnac Interferometer based Bragg gratings' writing Setup.

When we move the mirror M along the phase mask, the interference pattern scans a fiber segment with predetermined length. The angle θ is determined by the phase mask period Λ_m, and the angle α depends on the three parameters θ, ϕ_1 and ϕ_2. The angles ϕ_1 and ϕ_2 determine the mirror positions. When $\phi_1 = \phi_2 = \pi/4 - \theta/2$, the grating will be at the wavelength $\lambda_{B0} = n_{eff} \Lambda_m$, where n_{eff} is the effective refractive index of the fundamental guided mode, including the photo-induced DC component. In such a case, $\alpha = \theta$, and the interference pattern occurs exactly above the phase mask.

In order to write gratings for other wavelengths, the mirror M1 should be moved to change the angle ϕ_1. Cortès and LaRochelle [190] have reported that a wavelength range from 800 nm to more than 1700 nm is theoretically attainable. For $\lambda_B < \lambda_{B0}$, the fiber is brought closer to the mirrors to position it in the interference pattern. In the same way, for $\lambda_B > \lambda_{B0}$, the fiber is moved away from the mirrors.

Furthermore, when the UV light scans the phase mask, the time overlap between pulses coming from different sub-beams varies, hence varying the intensity of the interference over the fiber. This means that index changes in the fibers vary along the fiber, thus intrinsically introducing apodization. Gaussian apodization results for gratings of 4 cm length and a truncated Gaussian is obtained for smaller gratings. To perform linearly chirped Bragg gratings, we continuously vary the angle ϕ_1 during the scanning of the phase mask.

6.1.2 Reproducibility Problem

The writing technique, as described above, allows high flexibility in writing almost any single Bragg grating. In order to meet the OFFH-CDMA requirements, we need to extend such flexibility for a structure of multiple Bragg gratings.

In OFFH-CDMA, the contrast between the auto-correlation peak and cross-correlation peaks determines the signal to noise ratio of the system, hence determining the system bit error rate. Firstly, any frequency misalignment between the encoder and the decoder can dramatically decrease the auto-correlation peak energy and height. Secondly, inaccurate physical spacing between the gratings prevents he desired user chip-pulses to

recombine exactly in the same chip interval and thus decreases the sharpness of the auto-correlation, hence its height. Thirdly, gratings that have different reflectivity peaks (in height and width) lead to chips with different weight (or energy). This is not predicted in the design of FFH-codes, and it can change the statistics of the multiple access interference.

The OFFH-CDMA requirements can hence be met only if 1) the grating wavelengths values and spacing, 2) the physical spacing between them, and 3) their reflectivities, can be accurately produced and reproduced over different fibers. We have designed an additional mechanism within the writing system in order to allow this reproducibility. We leave further details for the Appendix A where a photograph of the mechanical system is provided Figure 6.2 gives an idea about the fiber-array positioning system that has allowed writing multiple Bragg gratings with high reproducibility.

In addition to fixing the fibers in a parallel array, the designed mechanism allows to move them together with five non-correlated degrees of freedom. This enables us to search the position in the 3D-space in which the interference pattern is best observed. Moreover, it allows us to keep the same position with respect to the pattern center during the writing, even when we change the wavelength.

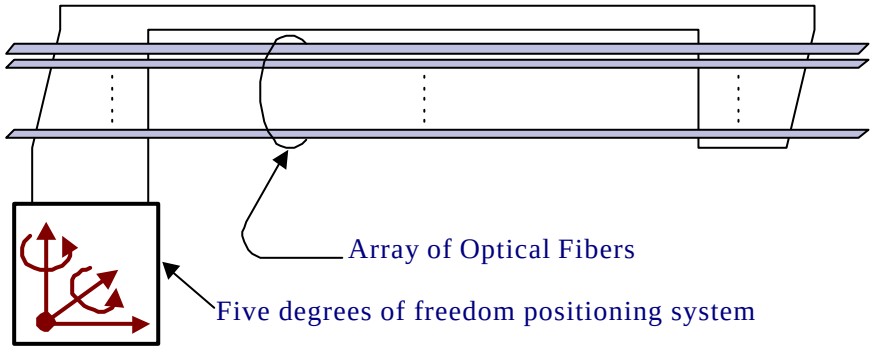

Figure 6.2: Principle of fiber array positioning system for accurate MBGs writing in different fibers.

6.2 Design of the Encoder/Decoder

In Chapter 4, we have introduced the all-tunable multiple Bragg gratings as an ideal (i.e., *all-options*) reconfigurable encoder/decoder, capable of delivering any FFH pattern. In the experiment, we have decided to demonstrate the principle using fixed encoder/decoders in order to avoid mechanical complexity; that is in no way related to the encoding/decoding principle. The MBGs should hence be written for predetermined codes.

6.2.1 MBG Specifications

Recall that the maximum length of the MBG is constrained by the maximum bit rate in the system. The physical spacing between gratings corresponds to a round trip time equal to a chip duration, hence equal to the short pulse duration. We selected an FFH-code using the algorithm of Bin [88], where the frequency hopping pattern is presented in Figure 6.3 a). This assumes eight gratings in the MBGs. We placed the gratings within 8 cm of fibre, with 1 cm of physical spacing between each adjacent pair, and each grating being 8 mm long. The parameters are shown in Figure 6.3 b).

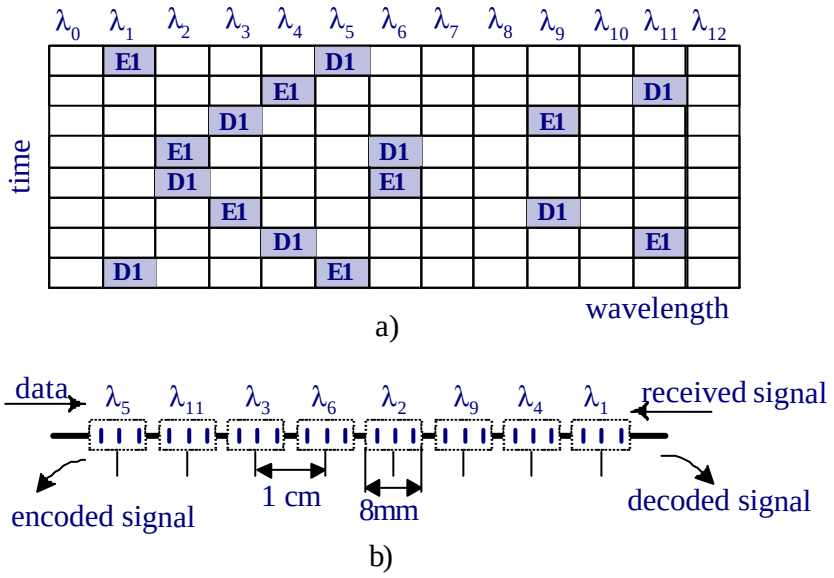

Figure 6.3 a) hop patterns, E1 (respectively D1) refers to the time/frequency slots used by the encoder 1 (respe ctively decoder 1) b) MBGs physical parameters.

We have explained, in the previous section, the three important specifications that all gratings should specify to correctly perform encoding/decoding. First, identical reflectivity peaks, in height and width. Second, identical wavelength values and pacing. The third consists of identical physical spacing between gratings. Note that the encoder pattern is symmetrical to that of the decoder with respect to the time axis, which corresponds to the physical symmetry between the encoder and the decoder. This will be experimentally measured in the following section.

6.2.2 Encoder/decoder Characterization

In Figure 6.4 a), we show the reflectivity of the encoder in solid lines, and that of the decoder -measured with wavelength steps of 0.01 nm- in dotted lines. All the MBGs

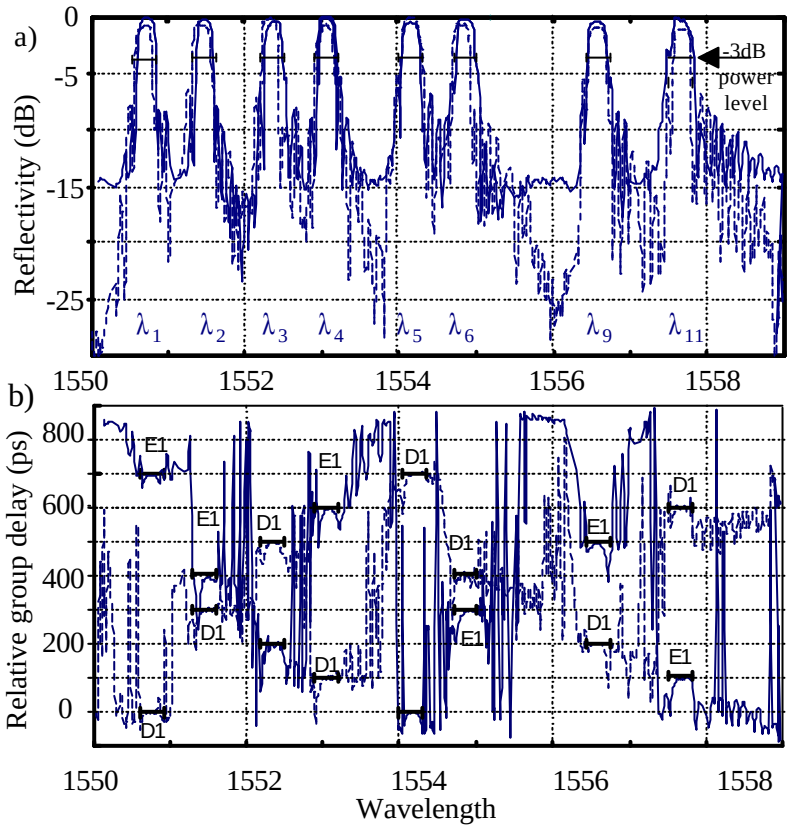

Figure 6.4: a) Reflectivity, and b) group delay of the encoder (solid line) and the decoder (dashed line).

have met the previously mentioned specifications. We measure a maximum peak variation of 1 dB; wavelength spacing in multiples of 0.8 nm, with a precision <0.15 nm in the same fiber. The maximum variation of absolute wavelength between encoder and decoder is <0.08 nm, and the physical spacing is 1 cm, fixed with a precision <10 µm. This corresponds to a 100 ps hopping time (or chip duration). The whole MBG length is 8 cm, corresponding to a bit rate of 1.25 Gb/sec; such a value is compatible with the Gigabit Ethernet standard.

The reflectivity peaks have a mean FWHM < 0.24 nm (see bars across reflectivity peaks in Figure 6.4 a) and corresponding bars in the group delay curves in Figure 6.4 b). Examining the group delay during the FWHM intervals shows that the MBGs achieve the frequency-hopping pattern of Figure 6.3 a).

6.2.3 Encoder/Decoder Back-to Back characterization

In order to verify the quality of the designed MBGs we used the setup of Figure 6.5 a). We first connected the correct encoder to the decoder back-to-back, and measured the cumulative reflectivity and group delay curves. We also performed the same experiment using an encoder written to a different code, *i.e.*, considered as an interferer. The measured results are plotted in Figures 6.5 b) and c).

Decoding is successful only when the delays introduced by the encoder for each frequency element have a complementary delay from the decoder, *i.e.*, the same code. This leads to a single cumulative delay for all frequency elements (see the 0.4 ns line in-group delay of Figure 6.5 c) for back-to-back correctly matched MBG pairs). This means that the pulses coming from the desired user will recombine at the decoder output and lead to a high auto-correlation peak. As seen in the dashed line of Figure 6.5 c), when the encoder and the decoder are mismatched (as is the case for interfering signals), delays are different for each frequency element and there is no autocorrelation peak. This contributes to low-level cross-correlation peaks only.

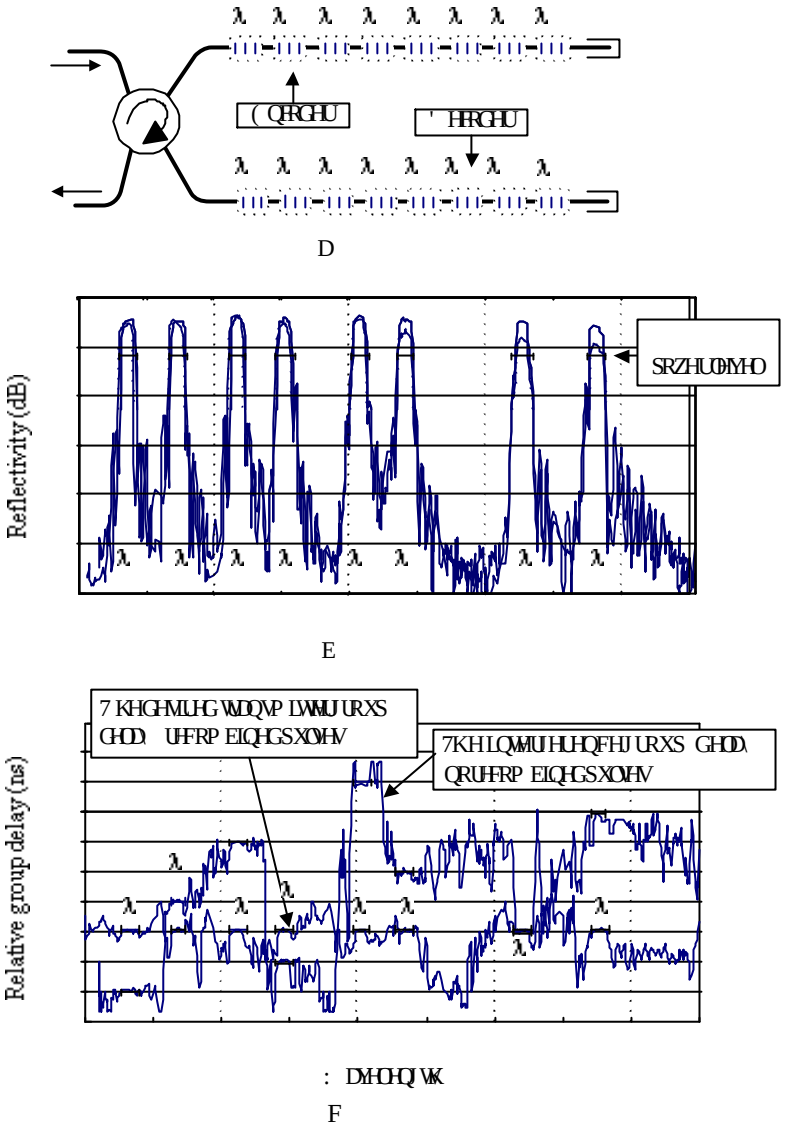

Figure 6.5 a) back to back setting for cumulative reflectivity and delay measurements; b) reflectivity and c) group delay for a back-to-back, correctly matched encoder/decoder pair (solid line) and a mismatched pair (dashed lines).

6.3 Experimental Results

In this section, we describe the OFFH-CDMA experimental setup, including one desired encoder, one interferer and one decoder.

6.3.1 The OFFH-CDMA Setup

In Figure 6.6, we illustrate the experimental setup we used for the demontration of the OFFH-CDMA principle. The amplified spontaneous emission (ASE) of an erbium-doped fiber amplifier (EDFA) is user as an incoherent broadband high-power source. A Lithium Niobate Mach-Zehnder interferometer is used as an external modulator. At the output of the latter, we obtain a train of broadband short-pulses. We use an electric short-pulse generator available in the laboratory, delivering 312-picosecond-width pulses, to drive the external modulator. Note that the system is designed and optimized for 100 ps pulses. This signal is split into the desired encoder and the interferer MBGs through distinct circulators (Figure 6.6).

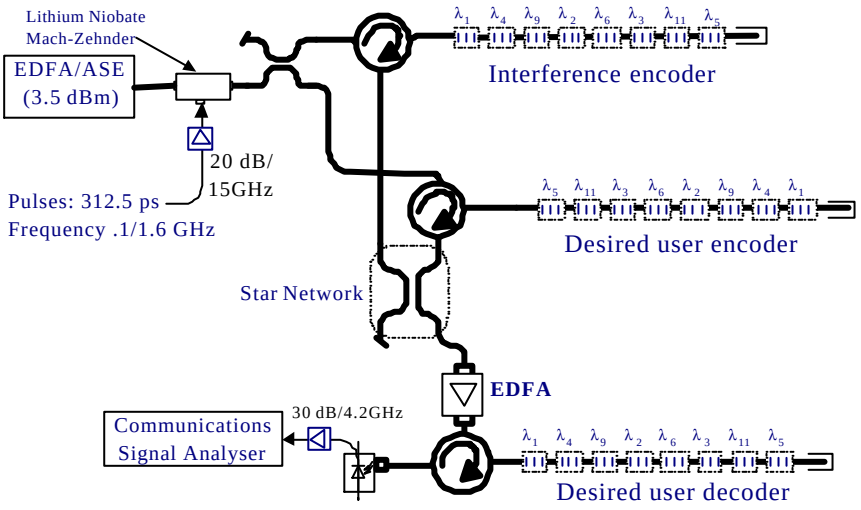

Figure 6.6 Experimental setup of an FFH-CDMA communications system including two transmitters and one receiver.

The encoded signals, reflected from the MBGs, are summed into the same fiber, and then amplified with an EDFA. At the receiver end, the EDFA output is fed into the decoder matched to the desired user signal. The decoded signal, consisting of a sum of the desired user signal plus the interference contribution, is observed in a Communications Signal Analyzer. In the following section, we analyze the received signal.

6.3.2 Measure of the Auto and Cross-correlation

Transmitted and received pulses with 100 MHz repetition rate are superposed in Figure 6.7 a) showing a strong auto-correlation peak with no appreciable distortion. The plot is zoomed in Figure 6.7 b), this theoretically consists on a time convolution between three functions, each of which is two dimensional. The first is the transmitted broadband pulse, the second is response of the encoder and the third is the response of the decoder. The auto-correlation peak is also clearly distinguishable in Figure 6.7 c) where an interferer is present. Figure 6.7 d) shows the interferer only; No desired user signal is transmitted.

Due to equipment availability the short pulses used in this experiment are three times larger than the values for which the encoder/decoder is optimized. We should also note that no electric filtering and/or smoothing is performed on the signal. The Bragg gratings are 8-mm long, however, the writing system allows complete Gaussian apodization only over 35-mm lengths. Hence our gratings correspond to a highly truncated Gaussian apodization, i.e., almost uniform. This creates high reflectivity side-lobes, introduces high in-band delay (or dispersion), and out-of-band spreading of energy (*i.e.,* the energy in the side-lobes can be highly delayed by the main-lobe energy).

The zoomed autocorrelation peak (Figure 6.7 a)) shows clear asymmetry suggesting phase (or dispersion) effects. Inherent dispersion introduced by the grating themselves is a strong factor. This issue is common to other application areas of Bragg gratings and no deep study have been done for the focused application of this thesis.

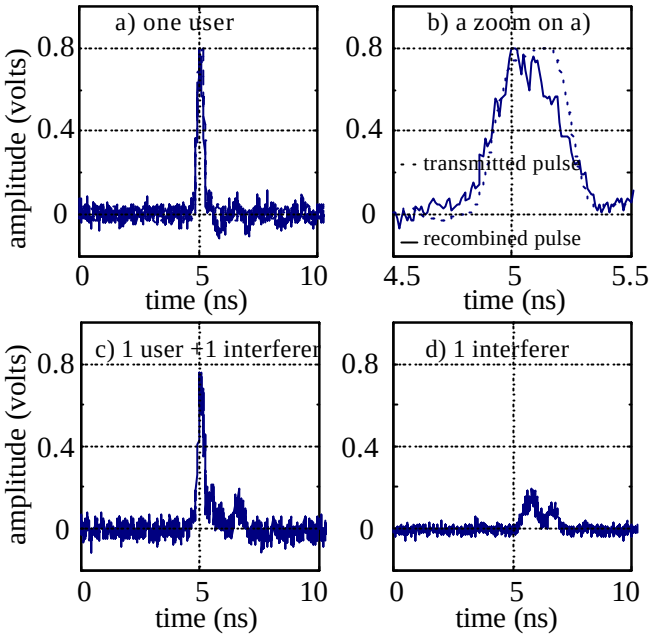

Figure 6.7 Decoder output for different scenarios.

6.3.3 Different Transmission rates:

In Figure 6.8, we plot trains of auto-correlation peaks for different repetition rates. When the repetition frequency is much lower than the bit rate, pulses are distributed in the time axis, and the auto- and cross-correlation may not occur in the same time-interval. The interference effect can be rigorously observed only when the repetition frequency is pushed to its maximum.

Figures 6.8 a), b), c) and d) report respectively the decoded signals for repetition rates of .2, .4, .8, and 1.6 GHz. The auto-correlation is clearly distinguishable in each case. Note that 1.6 GHz exceeds the design parameter of 1.25 GHz and no serious distortion was observed in the shape of the received signal. It can be expected, however, that this frequency excess will not be tolerable when a high number of interferers is present. In fact, it will enhance the interference contribution, dramatically decreasing the bit error rate of the

system. In order to measure the bit error rate, additional electronic filtering, chip integration, threshold comparison and decision should be performed.

The signal traces in Figure 6.8 show the autocorrelation pulses followed by sub-pulses (or ghosts) that are mainly due to the side-lobes of the gratings. This is also possible that an undesirable ASE reflection in the network creates this periodical ghosts. Note that manipulating ASE through the network causes multiple reflection that can be of importance in power, since this includes very wide spectrum.

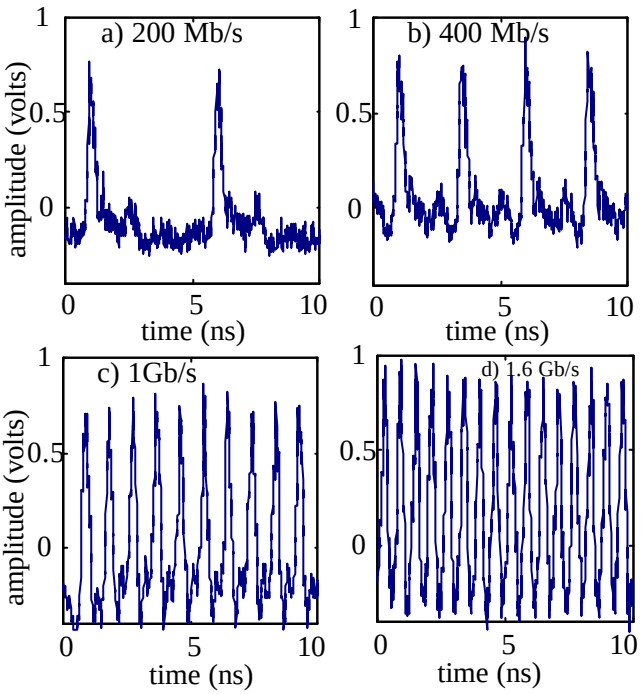

Figure 6.8: One desired transmitter and one interferer; data rates varying from 0.2 to 1.6 Gb/s.

6.4 High Capacity OFFH-CDMA

In this section, we increase the number of simultaneous encoders up to eight, and we demonstrate dynamic decoding. We select a special family of codes that can reduce the tuning complexity requirement. This allows changing the code by tuning the whole fiber in the same time instead of tuning each signal grating separately [120]. We demonstrate a decoder that allows dynamic selection of different encoder signals.

6.4.1 Encoder/Decoder Parameters

Figure 6.9 a) shows a part of the encoding space, with the hopping patterns of the eight encoders and that of the decoder at a position matched with the first encoder. The time-frequency squares corresponding to the i^{th} encoder are marked by E_i; those corresponding to the decoder are marked by D_i. Note that when the MBG of the decoder is stretched, its FFH pattern translates to the right along the frequency axis in Figure 6.9 a).

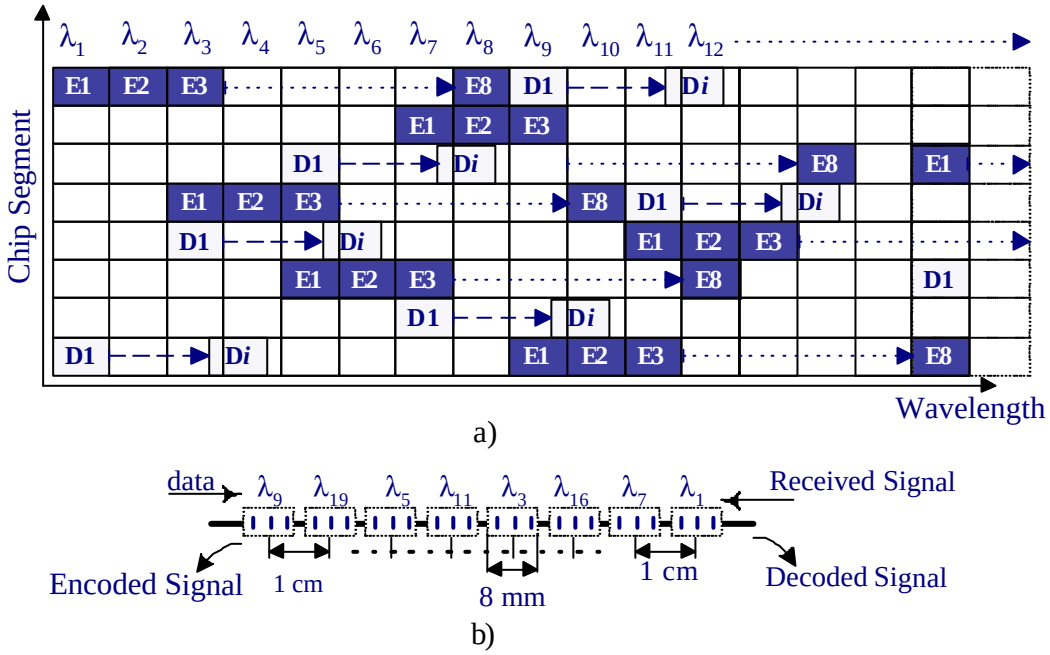

Figure 6.9: a) A part of the frequency-hopping pattern of eight encoders (E1…E8) and one reconfigurable decoder at a position matched to the first encoder (D1); b) parameters of the encoder/decoder number one.

The time-frequency squares of the decoder will change from the initial position marked by D_1 to others marked by D_i, where i is an arbitrary position. In Figure 6.9 a) we show the decoder hopping pattern where D_i represents an intermediate position between D3 and D4.

It should be noted that the codes used for this experiment are selected so that, when a code is shifted in the frequency dimension, the process creates a second code that maintains the one-coincidence criteria within it [120]. In our knowledge, only L. Bin codes [88] satisfy this property. Hence, the eight codes presented in the Figure 6.9 a) represent a family of one-coincidence FFH codes. The major advantage of this consists in the fact that the tuning operation is highly simplified, since only one tuning mechanism is required, as described by Boulianne et *al.* [120]. This, however, dramatically reduces the cardinality of the code family. The number of possible codes is lower than the number of available wavelengths in the encoding space.

6.4.2 Eight Encoders and a Programmable Decoder Setup

As illustrated in Figure 6.10, the setup is similar to that shown in Figure 6.6. A 1:8 passive splitter is connected at the second port of the transmitter's circulator. The 8 encoders are connected to the 8 ports of the splitter. Each encoder inserts its *fingerprint*

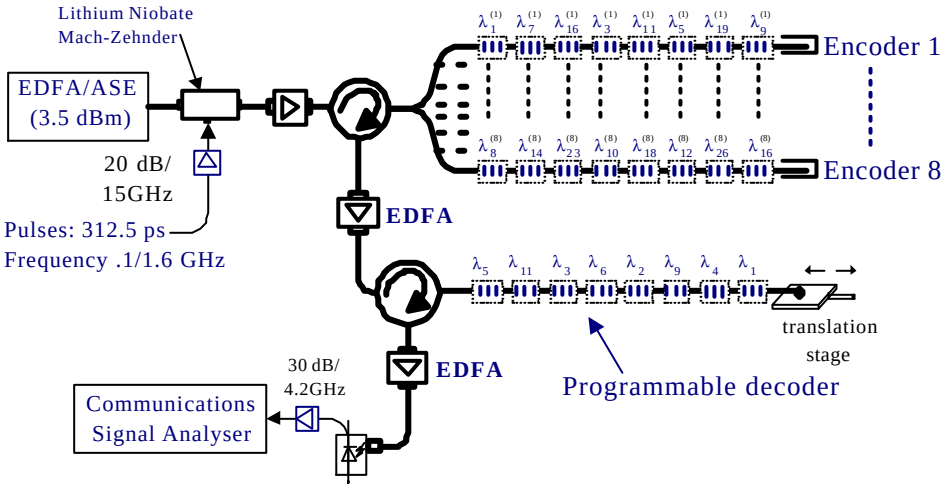

Fig. 6.10: OFFH-CDMA Setup including eight encoders and one reconfigurable decoder.

(or code) into the transmitted train of pulses. The encoder MBG designs are initially identical. In the setup, each encoder MBG is independently stretched so that it represents one different encoder among the eight. The wavelength spacing or increment is 0.4 nm (50 GHz).

Figure 6.11 shows the reflected spectra of all the encoders, E1...E8 and the decoder D before it has been tuned to a specific encoder. When the decoder fiber is stretched using the translation mechanism shown in Figure 6.10, its spectrum trans lates up and sequentially matches different encoder spectra.

Figure 6.12 depicts the decoded signal waveform, corresponding to the pulse pattern 1 1 1 1 at an 800 MHz repetition rate, for different wavelength shifts made by the decoder. Curves C1, C2, C4, C6, and C8 correspond to decoder wavelength shifts, for which no encoder signal is present, *i.e.*, only the interference is present.

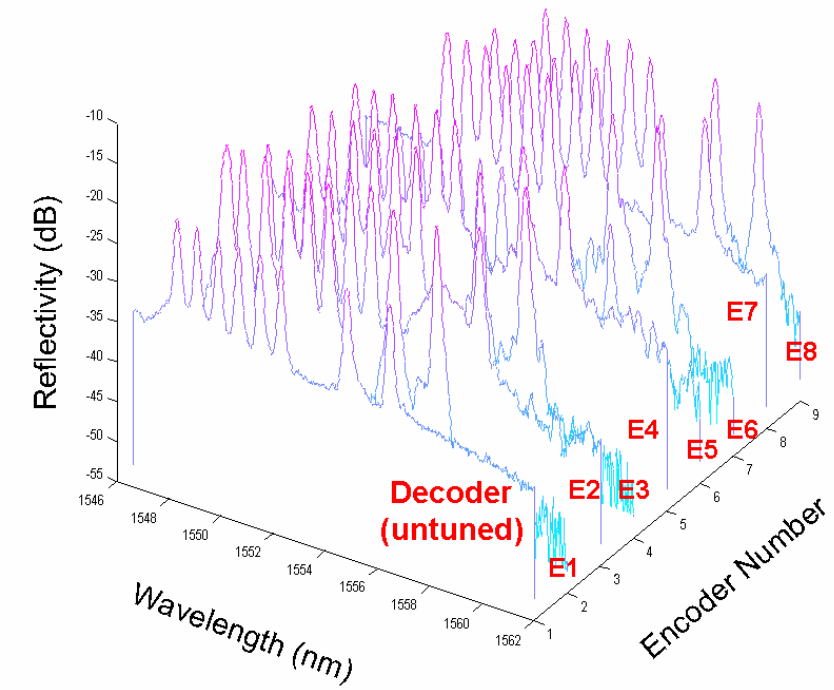

Fig. 6.11 Spectra of the untuned decoder and eight encoders (E1 - E8)

Curves C3, C5, and C7, however, correspond to the encoded signals coming from the encoders E1, E2, and E3, respectively. The difference in power level between the curves C3, C5, and C7 is due to imperfections in the encoders' reproducibility and, more importantly, different coupling losses.

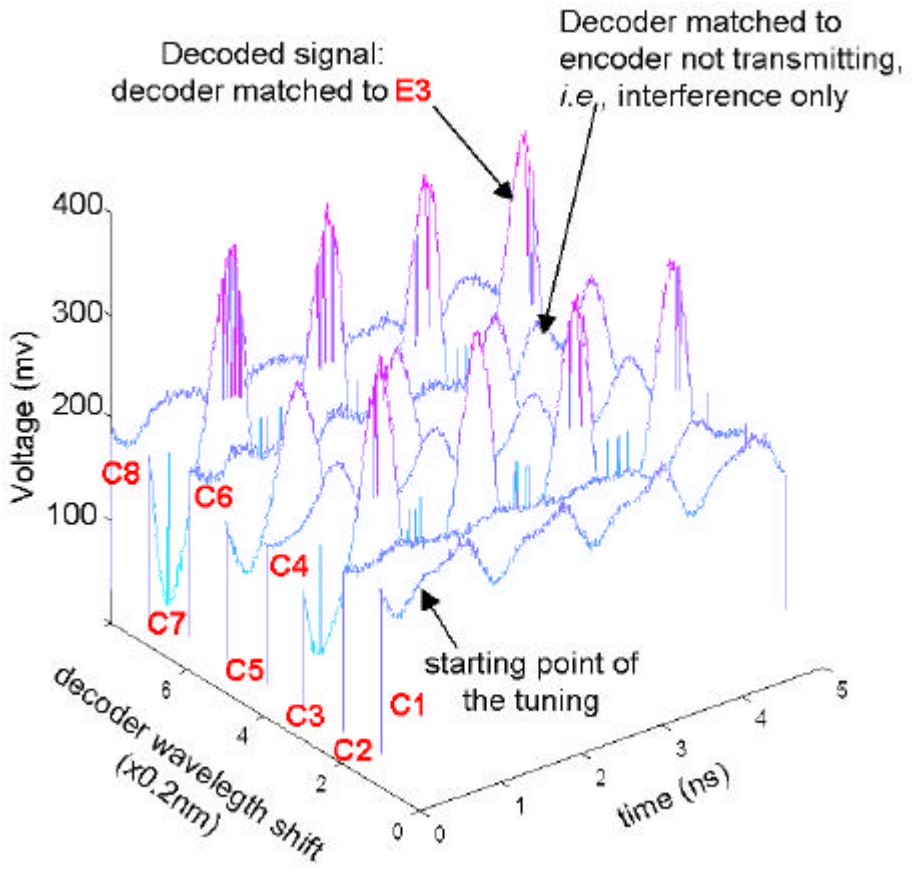

Fig. 6.12 Curves for the decoded signal for different decoder settings

6.4.3 Sixteen Encoders/4 Tunable Decoders Setup

In this setup, 16 encoders and 4 decoders are included representing in a typical 16 channels optical CDMA setup, all in a 7 nm band (Figure 6.13).

6.4.3.1 Encoders/decoders characteristics:

In order to build the setup we designed 4 sets of 5 identical MBGs. We have simultaneously written each set for the same FFH-pattern. We refer to the code *j* from the set *i*, where *j*=1,..,5 and *i*=1,..,4, by (s_i , c_j). In Figure 6.14, we show the four patterns used for the four sets. Recall that we selected FFH-patterns which have the property that each code is a frequency-shifted copy of the other. Each MBG is fixed on a separate stretching stage. Before stretching, the five MBGs of each set are identical. One MBG from set s_1 is maintained without stretching and considered having the code (s_1,c_1), a second is stretched so as its reflectivity translates by 0.4 nm and hence locked to the code (s_1, c_2), the third is stretched so as their wavelengths translate by 0.8 nm (two times the spacing), and so on until the fourth fiber. The fifth is used as a tunable decoder in order to decode any among the other four encoders of the same set. The similar procedure is applied to the remaining three sets in order to complete the architecture of 16 encoders and 4 tunable decoders.

6.4.3.2 The Setup Description

The amplified spontaneous emission (ASE) of an erbium-doped fiber amplifier (EDFA) is used as an incoherent broadband high-power source. A Lithium Niobate Mach-Zehnder interferometer is used in order to insert the data in the optical broadband signal using RZ waveforms with low duty cycle. We use an electric short-pulse generator delivering 300-picosecond-width pulses, to drive the external modulator. Note that the system is designed and optimized for 150 ps pulses. The data modulated signal is split into the 16 encoders through one 2:2 passive splitter, two circulators and two 1:8 passive splitters. An EDFA is place at the output of each circulator in order to compensate for the spitting loss of 18 dB and the coupling loss of the circulator (*i.e.,* a total of ˜20 dB).

Note that the signal power is split two times because it propagates through the coupler in the two directions before transmission. If each encoder uses its own source, the signal will be spit only one time and the system will support higher capacity before requiring amplification.

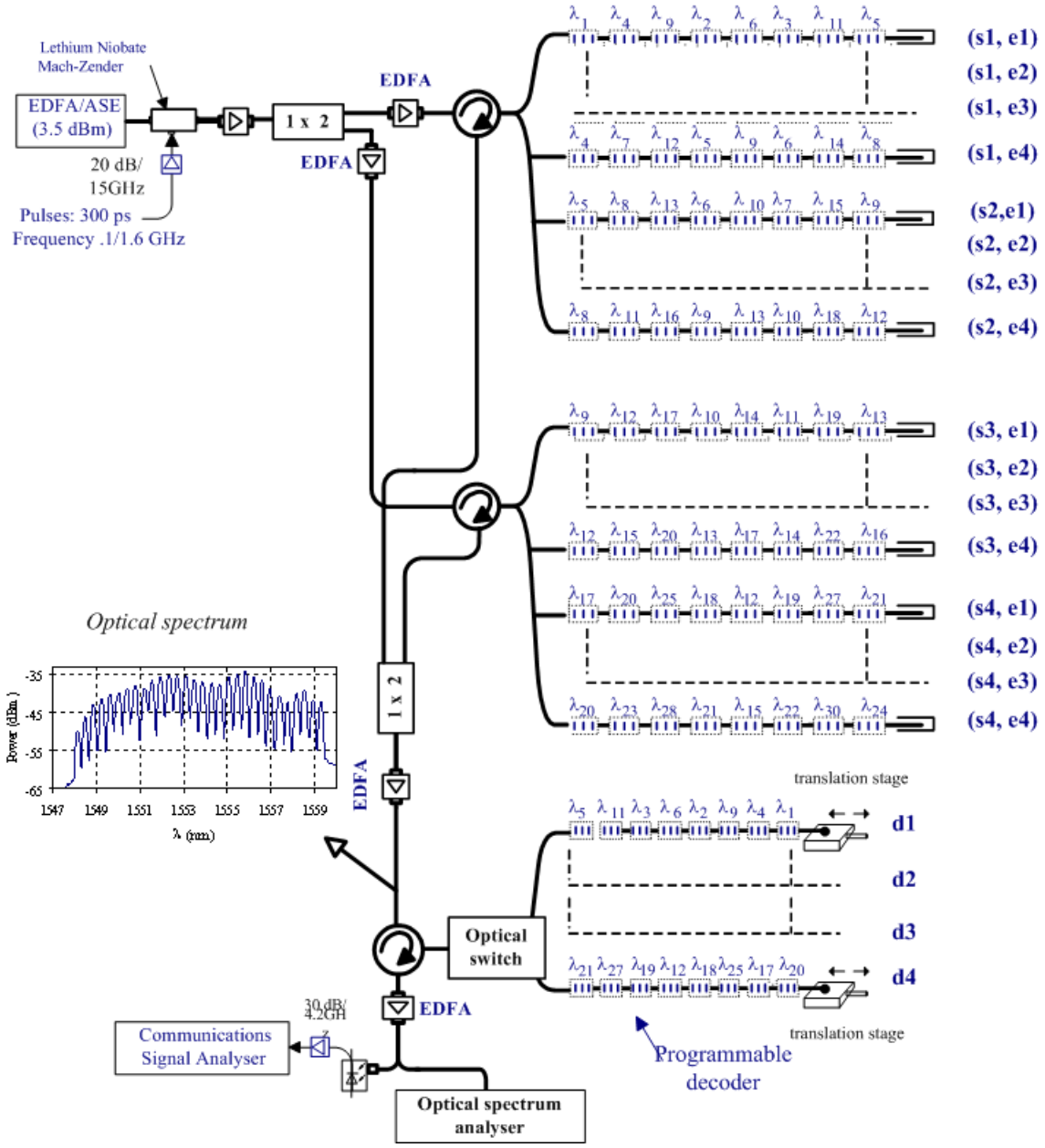

Figure 6.13: Sixteen encoders/4 tuneable decoder setup.

The encoded signals are summed into the same fiber through a passive coupler then amplified by an EDFA. At the receiver end, the EDFA output is fed into four separate tunable decoders through an opto-mechanic switch. Each decoded signal, consisting of a sum of the desired user signal plus the interference contribution, is observed simultaneously in a Communications Signal Analyzer (CSA) and optical spectrum analyzer (OSA).

6.4.3.3 Measurements

In Figure 6.15, we show the decoded signal, for four different tuning positions of the decoders, in its time (left) and frequency (right) dimensions using the CSA and the OSA (optical spectrum analyzer) respectively. In Figure 6.15 a) and c) the decoded signal presents a noise bursts and no recognizable pulses in the time dimension. In the frequency dimension, the decoder filters an arbitrary signal from the network that is a combination of relatively low power sub-bands coming from different transmitters. When compared with the spectrums of Figures 6.15 b) and d) the difference between right and wrong decoding is easily recognizable. When the decoder is well matched to a particular encoder, the decoded signal carry higher power and their wavelengths exhibit less-distortion. Moreover, Figure 6.15 b) and d), present traces with distinguishable peaks restoring the data sequence.

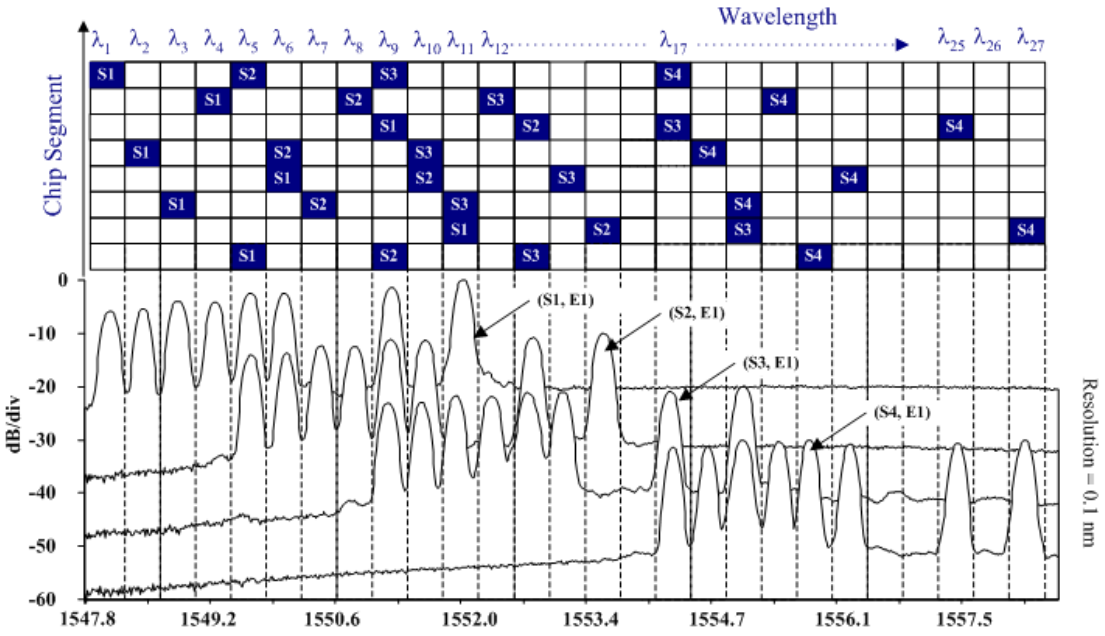

Figure 6.14: FFH patterns and optical spectrums of the four designed sets of MBGs.

The signal also presents cross-correlation pulses coming from the other 7 interferers. The contrast between the auto- and the cross-correlation functions remains appreciable. Here, we reported results for one set; the other sets present almost identical performance.

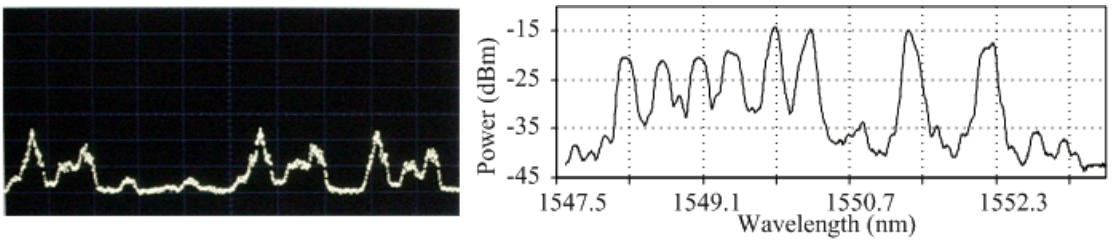

a) Noise bursts only (left) and its relative spectrum (right): the decoder is not matched to an existing encoder, this is tunde to an intermediate position between (s1, e1) and (s1, e2).

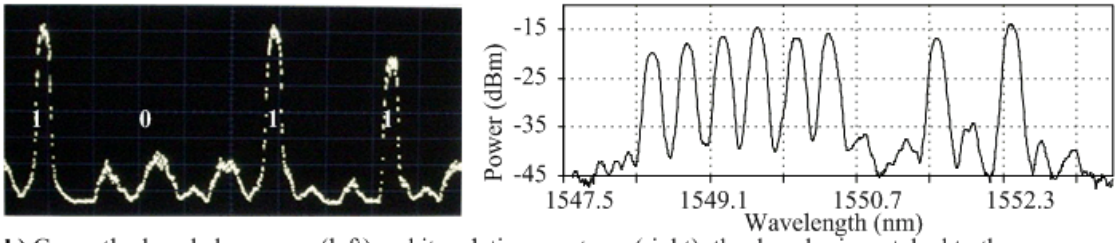

b) Correctly decoded message (left) and its relative spectrum (right): the decoder is matched to the encoder (s1, e2).

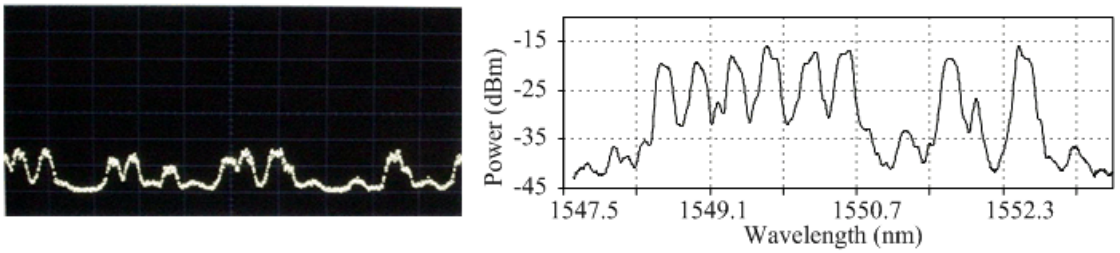

c) Noise bursts only (left) and its relative spectrum (right): the decoder is tuned to an internediate position between (s_1, e_2) and (s_1, e_3).

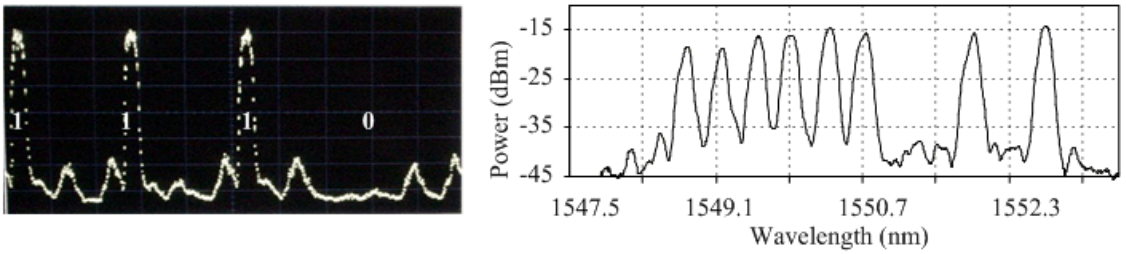

d) Correctly decoded message (left) and its relative spectrum (right): the decoder is matched to the encoder (s1, e3).

Figure 6.15: Measured decoded signal: traces (left) and spectrum (right), for different tuning positions of the decoder, corresponding to a system including eight encoders.

By examining the spectrum of the decoded signal we observe that the wavelengths have different values. This is due to the number of active transmitters simultaneously sharing each wavelength. In this family of codes, the frequencies are not equivalently used between codes, hence concentrating the power in the center frequencies in the band. The non-uniformity of the EDFA gain as well as the broadband source can also have an important effect on the disequilibria between the frequencies power. In [121], Fouli et *al.* addressed the effect of the static and dynamic gain of the EDFA on the OFFH-CDMA system. They demonstrated that the latter is inherently robust compared to the WDM (wavelength division multiplexing) system.

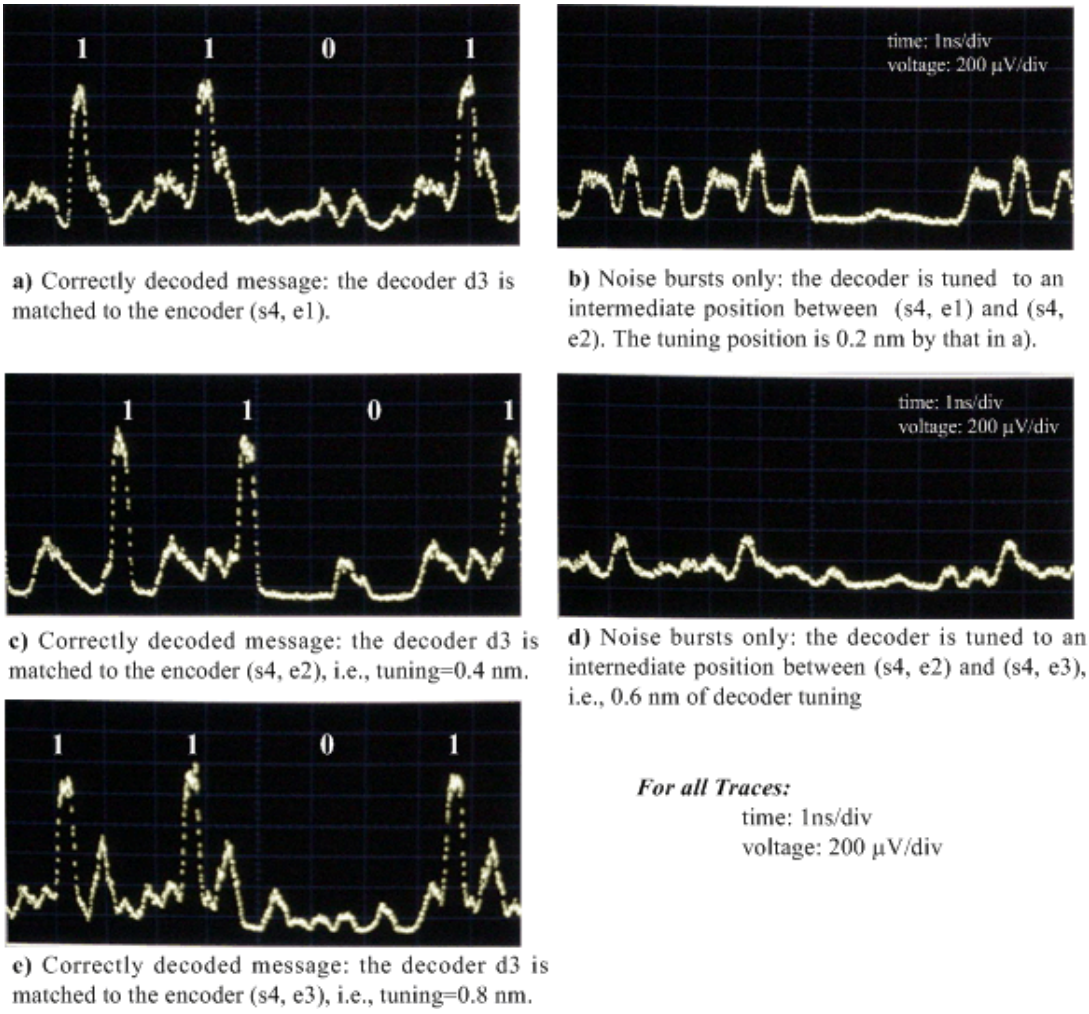

a) Correctly decoded message: the decoder d3 is matched to the encoder (s4, e1).

b) Noise bursts only: the decoder is tuned to an intermediate position between (s4, e1) and (s4, e2). The tuning position is 0.2 nm by that in a).

c) Correctly decoded message: the decoder d3 is matched to the encoder (s4, e2), i.e., tuning=0.4 nm.

d) Noise bursts only: the decoder is tuned to an internediate position between (s4, e2) and (s4, e3), i.e., 0.6 nm of decoder tuning

e) Correctly decoded message: the decoder d3 is matched to the encoder (s4, e3), i.e., tuning=0.8 nm.

Figure 6.16: Measured best case decoded signal, for different tuning positions of the decoder, corresponding to a system including sixteen encoders.

Here all the 16 encoders are connected. In Figure 6.16 (respectively 6.17) we report the best (respectively worst) decoding case. In the best case, the decoded signals show high and clearly distinguishable peaks. The height of the cross-correlation peaks sometimes approaches the half of the auto-correlation peak. In the worst case, even if the data sequence is still recognizable, the cross-correlation peaks become sometimes concurrent to those of the autocorrelation. Recall that using pulses of 300 ps rather than the 150 ps for which the system is optimized, has two effects: it decreases the autocorrelation peak and increases the cross-correlation peaks. Using shorter pulses will increase the concentration of the desired user signal and the spreading of the interference power. We expect that if a correct pulse width is used, this can lead to a four times increase in the number of codes that can be superposed in the same waveband. The family of codes adopted here allows easy tuning; however it highly limits the number of codes.

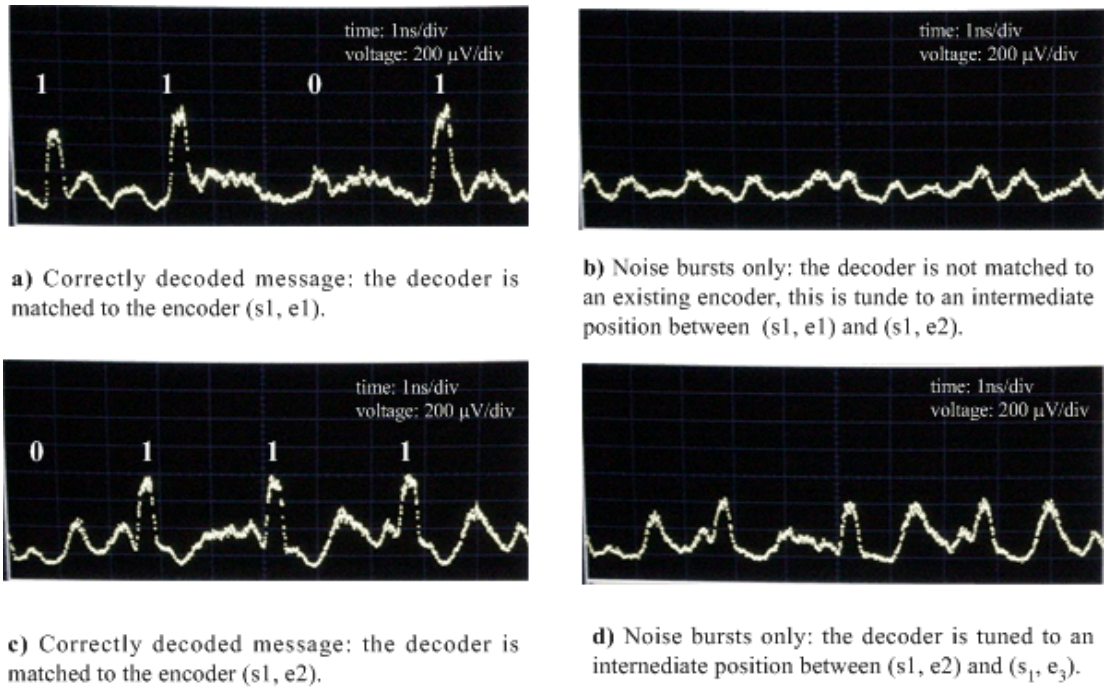

a) Correctly decoded message: the decoder is matched to the encoder (s1, e1).

b) Noise bursts only: the decoder is not matched to an existing encoder, this is tunde to an intermediate position between (s1, e1) and (s1, e2).

c) Correctly decoded message: the decoder is matched to the encoder (s1, e2).

d) Noise bursts only: the decoder is tuned to an internediate position between (s1, e2) and (s_1, e_3).

Figure 6.17: Measured worst case decoded signal, for different tuning positions of the decoder, corresponding to a system including sixteen encoders.

6.4.4 Interference Statistics and Demonstration of the Gaussian Approximation:

It is known that in CDMA the multiple access interference (MAI) is the most important noise source. Since no coordination or synchronization exists between users, each interferer contribution in a decoded signal is usually theoretically modeled as a random variable. The MAI hence is a sum of statistically independent random variables. Relating to the high number law, when the number of interferers is high, the MAI probability distribution is assumed Gaussian. Figure 6.18 a) depicts the decoded signal

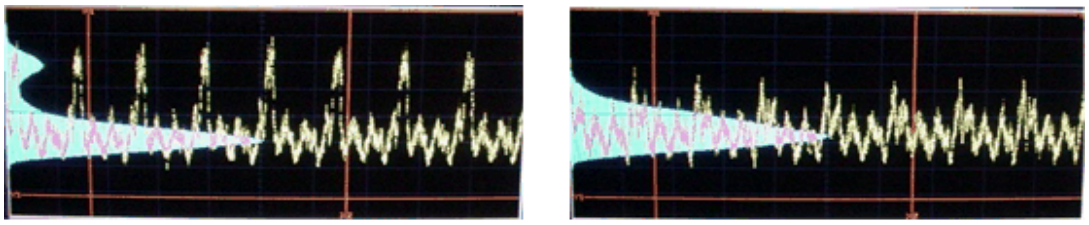

a) The decoded signal when 15 interferers are active and the desired encoder is active (left) or idle (right). The 0 level histogram is a perfectly Gaussian.

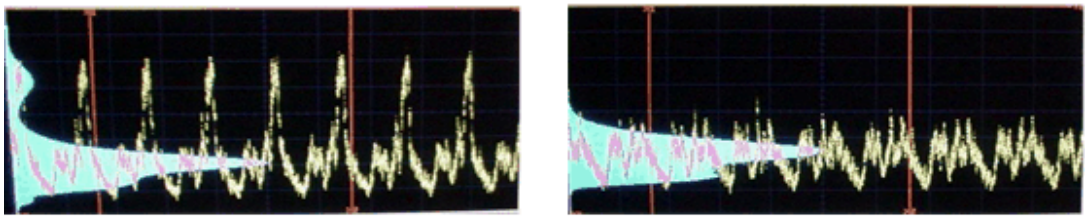

b) 7 interferers are active and the desired encoder is active (left) or idle (right). The 0 level histogram is has a distribution resembling less to a Gaussian. The gaussian approximation is less effective than in a).

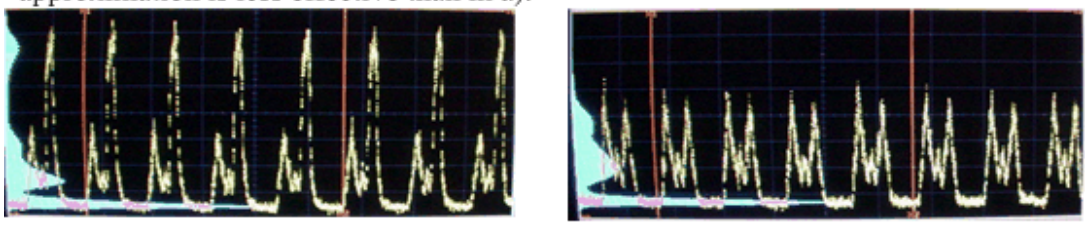

c) Only 2 interferers are active and the desired encoder is active (left) or idle (right). The 0 level histogram has a distribution composed from three distinct gaussian functions. The gaussian approximation is clearly false.

Figure 6.18: The interference statistics when the desired user is active (left) and idle (right)

when 16 encoders are active, *i.e*., 15 interferers exist. The histogram corresponding to the 0 level presents the MAI probability density, hence almost Gaussian. Figure 6.18 b) however shows the histograms where only eight users are active; the distribution is clearly not Gaussian. The approximation hence is not accurate for eight and lower number of users. Figure 6.18 c) corresponds to a case of only two interferers. We observe three distinct Gaussian functions around the zero level.

Chapter

7

OFFH-CDMA

Perspectives & Potential Applications

In this chapter, we focus on the potential of OFFH-CDMA for commercial exploitation, comparing it with previous positive optical CDMA systems. Our perspective favors systems that incorporate recent device technology, but nonetheless has the maturity to assure reasonable component cost. In particular, the use of fiber Bragg gratings is considered a key enabling technology.

7.1 Hypothetical OCDMA

We can deduce from the overview of OCDMA techniques in Chapter 1 that two elementary optical components are necessary to achieve the most flexible encoding operation. The first, the fiber-delay-line, performs pulse positioning in the time domain (in the case of coherent systems, a phase shift can also be introduced). An ideal delay line would allow dynamic tuning of its length. The second optical component is a frequency-selective (pass or reflection) filter. The ideal filter would allow dynamic tuning of its central frequency, amplitude, and phase response. A system that could provide these two ideal characteristics (tunable time delay and frequency response) would be capable of performing arbitrary encoding, in time and in frequency, using amplitude and phase modulation as well.

In Figure 7.1, we show a hypothetical setting that can fulfill those ideal requirements. This includes a number N of programmable mirrors M_i and delay lines l_i, for i=1…N, and assumes an incident broadband signal carrying the information data. Each mirror M_i is assumed capable of selecting a precise frequency component f_i with a predetermined reflectivity R_i, including the amplitude and the phase responses.

If the delay line l_i is programmable, the position of the waveform reflected by the i^{th} mirror (M_I) reflected is changeable. Varying the physical separation l_i between successive mirrors also changes the relative phases φ_i between those reflected waveforms (or pulses). In principle, the phase parameter should be taken into account only when a coherent broadband source is used and/or a coherent CDMA system is studied. Otherwise, only the mirrors' frequencies and reflections (amplitude only), in addition to the physical separation l_i between them, need to be taken into account.

In Figure 7.1, we considered the reflection rather than the transmission of the mirrors because this inherently allows a cascaded architecture in the encoder. When operated in transmission, the filters should be placed in parallel, and the input signal should be split into N paths, each path with a different physical length, and leading to a different filter. Operating in transmission mode introduces a power loss in addition to a more complicated architecture.

7.2 Potentials of MBG

The Bragg grating is usually interpreted as a cascade of low reflectivity mirrors with a periodic physical spacing, *i.e.*, inherently it operates like the architecture of Figure 7.1. The multiple Bragg gratings (MBG) can also be seen as having the structure of Figure 7.1. For OFFH-CDMA, the gratings are designed with high reflectivity, and no gratings are superposed in the same location. This results in two points: 1) no frequency can be used more than once, and 2) no more than one frequency can be used at a time.

The MBG used for OFFH-CDMA is a close approximation of the hypothetical architecture of Figure 7.1, where the gratings play the role of mirrors. However, only the frequency and the physical spacing (time) are taken into account in the design. Recent experiments demonstrated other variants of encoding/decoding systems using other parameters in the MBG structure [177-178].

An MBG with low reflectivity gratings and very precise physical separation was

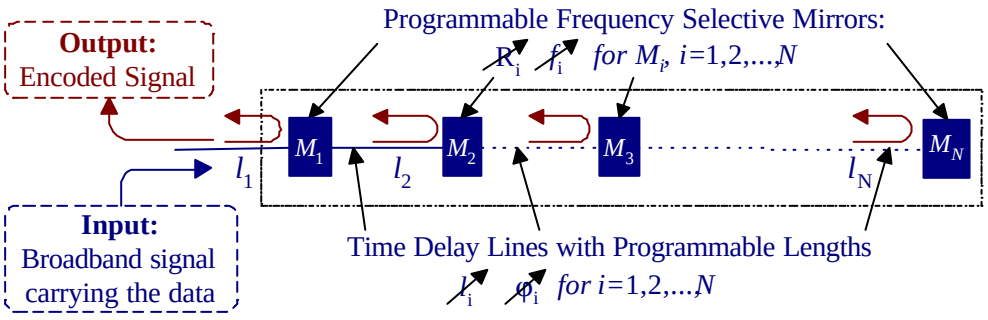

Figure 7.1 Hypothetical encoder: all the parameters are programmable

proposed in order to implement coherent FE-CDMA, *i.e.* the Salehi & Wiener scheme [55]. A low reflectivity MBG where all the gratings reflect the same frequency but with different percentage (different amplitudes) was proposed, hence implementing an incoherent DS-CDMA scheme with possible multi-level codes. Later, the spacing in the MBG was precise enough to introduce a fixed phase shift between the reflected pulses, hence allowing implementation of a coherent (bipolar) DS-CDMA system.

Although very promising, these trials do not allow, to our knowledge, a practical manner to reconfigure or program the encoder/decoder. On the other hand, FFH-CDMA can use piezo-electric devices to change the order of the center frequencies of the Bragg gratings, effectively changing the hop pattern and therefore allowing for programmable codes. This promises a high degree of programmability for the MBG, hence approaching the ideal encoder.

In the following, we propose an enhanced architecture of the OFFH-CDMA where the phase is also considered as a modulating parameter in the chip waveforms.

7.3 Coherent OFFH-CDMA Proposal

A coherent OFFH-CDMA system where the phase plays a role in the encoding scheme can also be achieved. If the line delay elements between the gratings are precise enough, this can introduce a predetermined phase shift between the chips frequencies. This assumes that a coherent source is used. The delay elements can be made tunable using heaters similar to those in Kitayama's coherent DS-CDMA and the system can also be programmable. The proposal is realistic, although it requires more stringent and expensive optical devices and packaging complexity. Figure 7.2 a) shows the architecture of the proposed coherent OFFH-CDMA encoder/decoder. Figure 7.2 b) illustrates an encoded coherent OFFH-CDMA signal. The time-spreading of the chip pulses is not shown here, this is however qualitatively described in section 3.4.

7.4 OFFH-CDMA and Other Positive Systems

In this final section, we conclude with a summary of the advantages offered by the OFFH-CDMA system.

7.4.1 Resource Accessibility

The simultaneous utilization of the time and frequency domains in OFFH-CDMA offers notable flexibility in the selection of codes, more easily satisfying required quasi-orthogonality (or transparency) between simultaneous users than incoherent DS- or FE-CDMA. OFFH-CDMA can take advantage of the huge bandwidth in a single mode fiber and available broadband sources to make a very high number of frequency slices (or wavelengths). Moreover, the possibility to make very short pulses in optics is a second advantage that increases phenomenally the accessible space for FFH encoding. It is convenient to look at that space as a huge two-dimensional matrix shared by the clients.

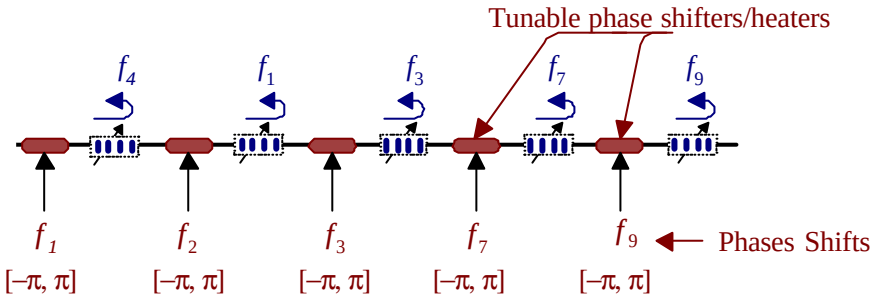

a) Coherent OFFH-CDMA encoder

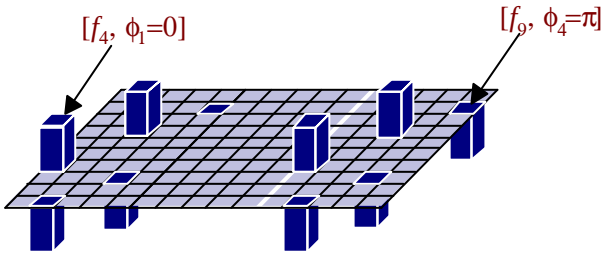

b) Coherent OFFH-CDMA encoded signal

Figure 7.2: Proposed Coherent OFFH-CDMA system.

The FFH-codes can be seen as very sparse matrices where the one-value elements represent the used time-frequency squares in the available space.

7.4.2 Receiver Electronics Requirements

FE-CDMA requires the least demanding electronics in the detection stage, as the bandwidth of the components is only equal to that of the received data. However, it requires a perfectly balanced photodetector, for which the cost rapidly increases for high bit rates. FFH-CDMA requires faster electronics, at the chip rate. However, the number of chips per code is orders of magnitude lower than that of incoherent DS-CDMA. For incoherent DS-CDMA, pulses of a few picoseconds duration are required to achieve very long codes with satisfactory performance, necessitating expensive ultra high-speed electronics, or complex all-optical non-linear time-gating and power thresholding methods that are still in research stages.

7.4.3 Interferometric Beat Noise problem

FE-CDMA, due to the use of an incoherent source, has its performance limited by interferometric noise. The signal to noise ratio is less dependent on the received power than the ratio r of the optical bandwidth to the data bandwidth. For the same capacity, OFFH-CDMA requires fewer frequencies than FE-CDMA. This reduces the effective optical bandwidth, hence minimizing r. Secondly, in OFFH-CDMA, the electrical bandwidth is determined by the chip rate and not the bit rate. Thus, it is much higher than that of FE-CDMA, further minimizing the ratio r. Finally, the OFFH-decoder inherently filters out the frequency bins that do not exist in the desired user pattern, *i.e.*, interferers' frequency bins. Hence, the photodetctor does not detect all the optical power in the network as is the case in FE-CDMA. Therefore, OFFH-CMDA is not limited by interferometric noise.

7.4.4 Power Budget

The in-fiber, in-line structure of the MBG avoids 1) the splitting/combining losses of incoherent DS-CDMA schemes, 2) the coupling losses in space-coding based

FE-CDMA, as well as other WDM demultiplexer based systems such as array waveguide gratings (AWG).

7.4.5 Dispersion Budget

OFFH-CDMA is, in principle, a dispersion-limited system. The limitation should however be less dramatic than in FE-CDMA systems. FFH-codes require fewer frequencies than their FE counterparts, for a comparable capacity. The codes can be selected so that frequencies belonging to the same code are as close as possible, hence minimizing the dispersion effect.

7.4.6 Technology cost

Bragg gratings are probably the lowest cost optical devices performing frequency selection, since their fabrication can be automated. Incoherent sources such as a LED, or the ASE of a semiconductor optical amplifier (SOA), are among the lowest cost sources, and are much less expensive than coherent MLLs. The circulator can be replaced by a 3dB coupler within an isolator making the approach more cost-effective. This introduces however an additional power loss of approximately 4 dB. FFH-CDMA promises gigabits per second connections per client [113].

7.5 OFFH-CDMA Potential Applications

In this Section, we describe satellite ideas relating to possible enhancement of the proposed OFFH-CDMA system. Only key enhancements are given here, without any in-depth development. They can be considered in future works in this research area.

7.5.1 Multirate OFFH-CDMA

The access environment is characterized by the wide variety of protocols, i.e., Ethernet, ATM, SONET, IP, etc. Multiple data rates and various frames (or cells, packets) formats coexist in the same environment hence motivating the development of multirate protocol. The simultaneous delivery of data, video and voice also motivates this issue.

In OFFH-CDMA, the physical placement in the fiber is exploited to perform in-time encoding or pulse positioning; therefore the length of the encoder is inversely proportional to the maximum bit-rate. For example, to achieve a 500 Mbits/sec data bit rate, we should place all gratings within 20 cm of fiber, taking into account the velocity of light in the fiber. To communicate at higher bit rates, the gratings must be written in a shorter fiber length.

In Figure 7.3a), we show a low-rate encoder and its grating positions (5 in this example) along the fiber, with length L_{LR}. In Figure 7.3 b), a different user has the same number of gratings in a fiber of length $L_{HR}<L_{LR}$. The two users can share the same communication medium, provided their FFH codes are well selected to minimize the interference between them. It is important to note that we can truncate the one-coincidence codes in the time dimension to create shorter one-coincidence codes. Truncated codes with different lengths are also one-coincidence codes.

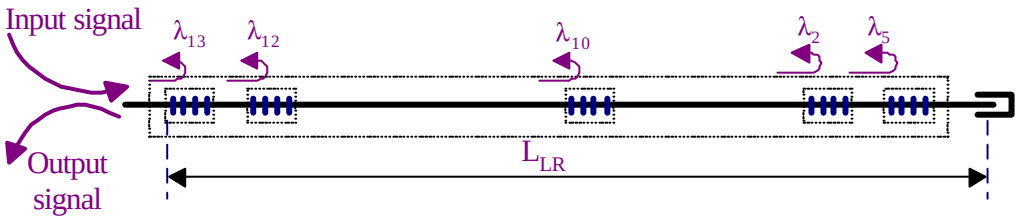

a) Low rate OFFH-CDMA user's encoder

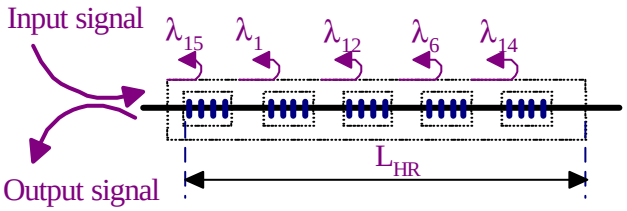

b) High rate OFFH-CDMA user's encoder

Figure 7.3: Encoders' architectures for Multirate OFFH-CDMA system.

7.5.2 Multi-performance OFFH-CDMA

Accommodating different channels to communicate with different performance levels is a desirable feature in a communication system. This can include differentiation in bit error rate, security, service guaranty etc. In addition, different transmission protocols naturally do not have identical performance levels. In this section we especially describe how the OFFH-CDMA encoding can inherently be exploited in order to modify the weight of the code hence modifying its performance level.

The number of ones in every positive optical CDMA code represents its power (or weight). The higher the number of ones in one user code, the higher its signal to noise ratio, and hence the higher its performance. High performance means low error probability and/or high security in data transmission.

Figure 7.4 a) shows an example of an encoder corresponding to a high-performance user with 7 gratings, i.e. it has 7 ones in its code. Figure 7.3 b), however, shows a low-performance user encoder that uses only 4 gratings, i.e. it has only 4 ones in its code. FFH

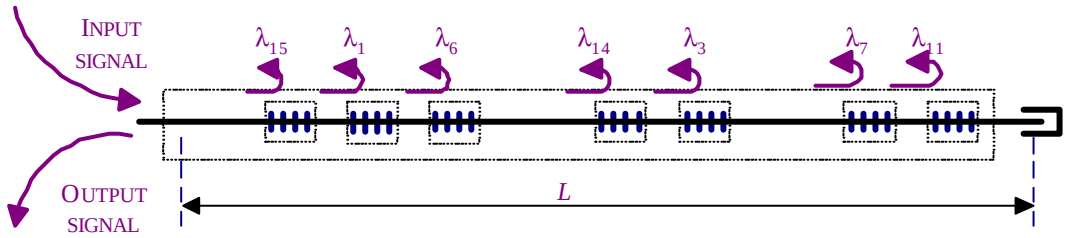

a) High weight (high performance) user's encoder

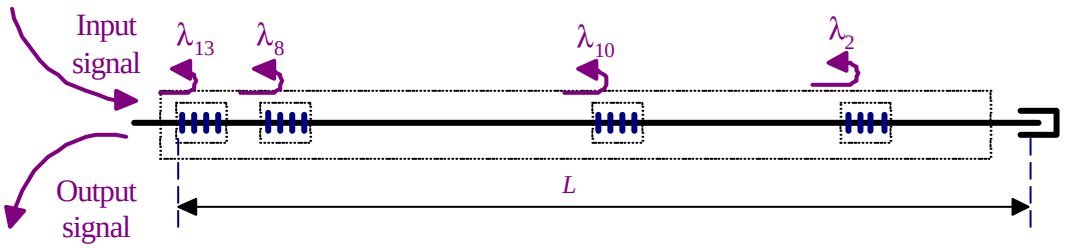

b) Low weight (low performance) user's encoder

Figure 7.4: Multi-performance encoders principle

codes should also be adequately selected to minimize interference between those codes. Nullifying some columns in one-coincidence codes in order to decrease their weight is a straightforward non-optimal method to develop such multi-performance codes.

7.5.3 Hybrid FE-/OFFH-CDMA

As explained in Section 1.6.2, incoherent FE-CDMA implies that (0,1) encoding is performed uniquely in the frequency domain, and the users share the entire time domain. To recover data, one receiver should divide the received signal into two branches: the first uses a mask identical to that of the encoder, and the second uses the complementary mask. For some suitably selected families of frequency domain codes, the redundancy of information in the two branches can serve to efficiently reject (common mode) interference signals.

The idea is to superpose or combine the FE-CDMA techniques with OFFH-CDMA using a series of Bragg gratings. This hybrid FE/FFH-CDMA system can be viewed as an

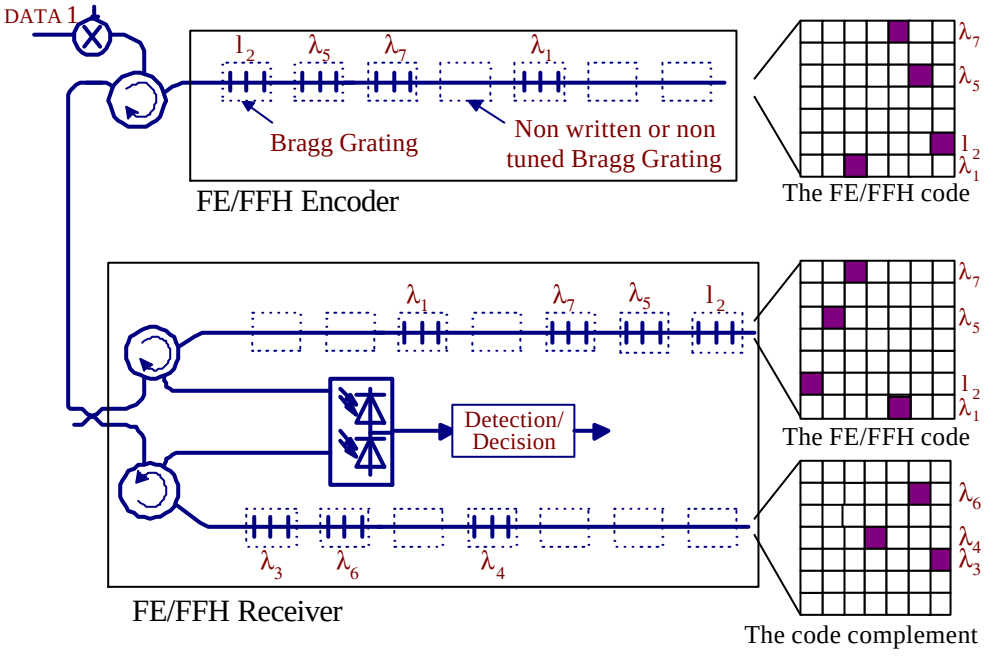

Figure 7.5: Architecture of Hybrid FE/OFFH-CDMA system

enhanced technique of OFFH system because it increases the capacity of the system in terms of the number of users. Figure 7.5 shows a possible architecture of a hybrid FE/OFFH-CDMA communication system. The wavelengths used in a given FFH code can be interpreted as the output of a multi-wavelength (or broadband) source that operates only at given chip times. The FFH code, in the example of Figure 7.5, consists of a combination of the shown FE/FFH code (e.g., [λ2, λ5, λ7, 0, λ1, 0, 0]) and its complement (e.g., [0, 0, 0, λ4, 0, λ6, λ3]), where the zero elements mean that no power is transmitted. In this example, the FFH code can hence be represented by [λ2, λ5, λ7, λ4, λ1, λ6, λ3].

This means that a second level encoding can be performed on these wavelengths, consisting of transmitting just a subset of them, and stopping the others in the same manner as in a conventional FE-CDMA system. Hence, the FE can be performed as a second encoding level over FFH encoding, leading to enhanced capacity.

Conclusion

The thesis is an investigation of a new method of optical code division multiple access (CDMA) communications we invented and referred to as optical fast frequency hopping- (OFFH-) CDMA. The investigation work consisted of a combination of theoretical, numerical and experimental aspects providing a deep and complete proof of concept of the invented communications technology.

We defined the fundamental principles of the OFFH-CDMA and proposed a set of implementation solutions. We have found, that multiple Bragg gratings (MBG) offer the most elegant method to implement the OFFH-CDMA encoding/decoding functions.

Through theoretical and computer simulation analysis, we have verified and demonstrated the effectiveness of the new principle. We have also proposed and investigated a version of the system especially appropriate for communications in hostile temperature and stability conditions. Finally, we built three generations of an OFFH-CDMA experimental setup. The last one includes sixteen encoders and four programmable decoders. The technology demonstrated successful encoding/decoding operation in various communications scenarios.

Finally, we explored and described potentials new applications and future proofs of the OFFH-CDMA technology. We proposed new encoding/decoding architectures that enable a network to accommodate subscribers with different data rates and performance levels.

References

Spread Spectrum

1. Peterson, R. L., Ziemer, R. F., Borth, D. E. "Introduction to Spread Spectrum Communications", Printice-Hall, Inc., A Simon & Schuster Company, 1995, NJ 07458.
2. Proakis, J. G. "Digital Communications", Third Edition, 1995, McGraw-Hill Series in Electrical and Computer Engineering, NY 10020.
3. Taub, H. and Schilling, D. L., "Principles of Communication Systems", Second Edition, 1986, McGraw-Hill Series in Electrical and Computer Engineering.
4. Ziemer, T. "Principles of Communications", Fourth Edition, 1995, John Wiley & Sons, Inc. 0 471 12496 6.
5. Utlaut, W., "Spread Spectrum: Principles and Possible Application to Spectrum Utilization and Allocation", *IEEE Communications Magazine*, September, 1978, pp. 21-31.
6. Viterbi, A. J., "Spread Spectrum Communications - Myths and Realities", *IEEE Communications Magazine*, May, 1979, pp. 11-18.
7. Viterbi, A. J., "CDMA-Principles of Spread Spectrum Communications", 1995, Addison-Western Publishing company Reading, MA.
8. Eng, Thomas , Milstein, Laurence B., "Comparison of Hybrid FDMA/CDMA Systems", *IEEE Journal on Selected Areas in Communications*, June, 1994, vol. 12, no. 5, pp. 938-951.
9. Schilling, D. L., Milstein, Laurence B., R. Pickholz, M. Kullback, F. Miller, "Spread Spectrum for Commercial Communications", *IEEE Communications Magazine*, April, 1991, pp. 66-79.
10. Rappaport, S. S., Grieco, D. M., "Spread Spectrum Signal Acquisition: Methods and Technology", *IEEE Communications Magazine*, June 1984, vol. 22, no. 6, pp. 4-22.
11. Spracklen, C. T. , C. Smythe, "Communication Protocols for a Spread Spectrum Local Area Network", FOC/LAN '84, pp. 70-74.
12. Green, P.E. Jr, "Fiber Optic Networks", Englewood Cliffs, Prentice Hall, 1993.
13. Takakusaki, K., "Correlator, Synchronizer Provided With the Correlator, and Fast Frequency Ho pping Spread Spectrum Receiver Provided With the Synchronizer", US Patent, 5 625 641, April, 29, 1997.

OCDMA Tutorials

14. Salehi, J. A., "Emerging Optical Code-Division Multiple Access Communications Systems", *IEEE Network Magazine*, March, 1989, pp. 31-39.
15. Iversen, K., Hampicke, D., "Comparison and classification of all-optical CDMA systems for future telecommunication networks", SPIE vol 2614, pp 110-121, December 1995.
16. Karafolas, N., Uttamchandani, D., "Optical Fiber Code Division Multiple Access Networks: A Review", *Optical Fiber Technology*, vol. 2, pp. 149-168, 1996.
17. Iversen, K., Mackenheim, J., Hampicke, D., "A basic theory of fiber-optic CDMA", *IEEE International symposium on Spread Spectrum Techniques and Application*, pp 431-437, September 1996.

DS-CDMA

18. Prucnal, P., Santoro, M. "Spread spectrum fiber optic local area network using CDMA and optical correlation," IEEE/OSA *Journal of Lightwave Technology*, May 1986, vol. 4, no. 5, pp. 307-314.

19. Prucnal, P., Santoro, M. and Sehgal S. K., "Ultrafast all-optical multiple access fiber networks," IEEE J. *Select. Areas Commun.*, Sept. 1986, vol. 4, no. 5.

20. Santoro, M., Prucnal, P., "Asynchronous fiber optic local area network using CDMA and optical correlation," IEEE Proceedings, 1986, vol. 75, no. 9, pp. 1336-1338.

21. Foschini, Gerard J., Giovanni Vannucci, "Using Spread-Spectrum in a High-Capacity Fiber-Optic Local Network", *Journal of Lightwave Technology*, March, 1988, no. 3, pp. 370-379.

22. Vannucci, Giovanni, Yang, S., "Experimental Spreading and Despreading of the Optical Spectrum", *IEEE Transactions On Communications*, July, 1989, vol. 37, pp. 777-780.

23. Sampson, D. D., Griffin, R. A., Jackson, D. A., "Photonic CDMA By Coherent Matched Filtering Using Time-Addressed Coding In Optical Ladder", *Journal of Lightwave Technology*, November 1994, vol. 12, no. 11, pp. 2001-2010.

24. Benedetto, S., Olmo, G., "Performance Evaluation of Coherent Code Division Multiple Access", *Electronics Letters*, October 24, 1991, vol. 27, no. 22, pp. 2000-2002.

25. Sampson, D. D., Jackson, D. A., "Coherent optical fiber communications system using all-optical correlation processing", *Optics Letters*, May 15, 1990, no. 15, pp. 585-587.

26. Chang, Y. L., Marhic, M. E., "Fiber-optic ladder networks for inverse decoding coherent CDMA", *IEEE/OSA Journal of Lightwave Technology*, December 1992, vol. 10, no. 2, pp. 1952-1962.

27. Marom, E., and Ramer, O.G., "Encoding-decoding optical fiber network, "*Electronic. Letters*, vol. 14, no. 3, pp. 48-49, 1978.

28. Marhic, M.E., "Coherent optical CDMA networks, " *IEEE/OSA Journal of Lightwave Technology*, vol. 11, no. 5/6, pp. 854-864, 1993.

29. Wada, N., Kitayama, K.-I. "Fundamental Properties of 10 Gbit/s Coherent Optical Code Division Multiplexing: Experiment," *Optical Review*, vol. 5, no. 1, pp. 31-38, 1998.

30. Wada, N., Kitayama, K.-I. "10 Gbit/s Optical Code Division Multiplexing using 8-chip Optical Bipolar Code and Coherent Detection," submitted to *IEEE/OSA Journal of Lightwave Technology Oct 1998*.

31. Kwong, W. C., Perrier, Philippe A., Prucnal, P. R., "Performance Comparison of Asynchronous and Synchronous Code-Division Multiple-Access", *IEEE Transactions On Communications*, November, 1991, vol. 39, no. 11, pp. 1625-1634.

32. Ruchet, B., "Réalisation Expérimental d'une détection cohérente pour un système optique CDMA/FDMA, *Mémoire de Maîtrise*, Université Laval, Québec *1998*.

33. Barry, J.R. and Lee, E.E, "Performance of Coherent Optical Receivers", *Proceedings of the IEEE*, vol. 78, no. 8, pp. 1369-1394, 1990.

34. Pendock, G. J., Sampson, D. D., "Increasing the transmission capacity of coherence multiplexed communication systems by using differential detection," *IEEE Photonics Technology Letters*, vol. 7, December 1995, pp 1504-1506.

Positive DS-CDMA & OOC

35. Salehi, J. A., Brackett, C. A., "Fundamental Principles of Fiber Optics Code Division Multiple Access (FO-CDMA)", IEEE *ICC*, 1987, pp. 1601-1609.

36. Salehi, J. A., Brackett, C. A., "Code division multiple-user techniques in optical fiber networks - Part I", *IEEE Transactions on Communications*, August 1989, vol. 37, no. 8, pp. 824-833.

37. Salehi, J. A., Brackett, C. A., "Code division multiple-user techniques in optical fiber networks - Part II", *IEEE Transactions on Communications*, August 1989, vol. 37, no. 8, pp. 834-842.

38. Yang, G. C., "Performance Analysis For Synchronization and System on CDMA Optical-Fiber Networks", *IEEE Transactions On Communications*, Oct 1994 , no. 10, pp. 1238-1248.

39. Kwon, H. M., "Optical Orthogonal Code-Division Multiple-Access System .2. Multibits Sequence-Period", *IEEE Transactions on Communications*, Aug 94, vol. 42, no. 8, pp. 2592-02599.

40. Chung, F. R., Salehi, J. A., "Optical Orthogonal Codes: Design, Analysis and Applications", *IEEE Transactions on Information Theory*, May 1989, vol. 35, no. 3, pp. 595-604.

41. Kostic, Z., Titlebaum, E. L., "The design and performance analysis for several new classes of codes for optical synchronous CDMA and for arbitrary-medium-time-hopping synchronous CDMA communications Systems", *IEEE Transactions on Communications*, Aug 1994, vol. 42, no. 8, pp. 2608-2617.

42. Chung, H., Kumar, P.V., "Optical orthogonal codes-New Bounds and an Optimal Construction", *IEEE Transactions on Information Theory*, July 1990, vol. 36, no. 4, pp. 866-873.

43. Maric, S. V., Kostic, Z., Titlebaum, E. L., "A New Family of Optical Code Sequences for Use in Spread-Spectrum Fiber-Optic Local Area Networks", *IEEE Transactions on Communications*, August 1993, vol. 41, no. 8, pp. 1217-1221.

44. Maric, S. V., Moreno, O, Corrada, C. J., "Multimedia Transmission in Fiber-Optic LAN's Using Optical CDMA", *Journal of Lightwave Technology*, October 1996, vol. 14, no. 10, pp. 2149-2153.

45. Yang, G. C., "Performance Comparsaon of Multiwavelength CDMA and WDMA + CDMA for Fiber-Optic Networks", *IEEE Transactions On Communications*, Nov 1997 , vol. 45, no. 11, pp. 1426-1434

46. Walle, H., Killat, U., "Combinatorial BER Analysis of Synchronous Optical CDMA with Prime Sequences", *IEEE Transactions on Communications*, December 1995, vol. 43, no. 12, pp. 2894-2895.

47. Lam, Alex W., Hussain, A. M., "Performance Analysis of Direct-Detection Optical CDMA Systems with Avalanche Photodiodes", *IEEE Transactions On Communications*, April 1992, vol. 40, no. 4, pp. 810-821.

48. Yang, G.-C., "variable-Weight Optical Orthogonal Codes for CDMA Networks with Multiple Performance requirements", *IEEE Transactions on Communications*, January 1996, vol. 44, no. 1, pp. 47-55.

49. Olson, T., Healy, D., Osterberg, U., Prosser, R. T., "Orthogonal Waveform Encoding for high bandwidth Fiber Optic Communications", submitted July 1997.

50. Maric, S. V., Hahm, M. D., Titlebaum, E. L., "Construction and Performance Analysis of a New Family of Optical Orthogonal Codes for CDMA Fiber-Optic Networks", *IEEE Transactions on Communications*, 1996, vol. 43, no. 2/3/4, pp. 485-489.

51. Maric, S. V., "Designed Optical Orthogonal Codes for Use in CDMA Fiber-Optic Networks", *Electronics Letters*, March 1993, vol. 29, no. 6, pp. 538-539.

52. Zhang, J.-G., Kwong, W. C., "Effective design of optical code-division multiple access networks by using the modified prime code", *Electronics Letters*, January 1997, vol. 33, no. 3, pp. 229-230.

53. Azizoglu, M., Salehi, J. A., Li, Y., "Optical CDMA via Temporal Codes", *IEEE Transactions on Communications*, July 1992, vol. 40, no. 7, pp. 1162-1170.

54. Kiasaleh, Kamran, "Spread-Spectrum Optical On-Off-Keying Communication System", ICC 1989, pp. 136-140.

FE-CDMA

55. Salehi, J. A., Weiner, A. M., Heritage, Jonathan P., "Coherent Ultrashort Light Pulse Code-Division Multiple Access Communication Systems", *Journal of Lightwave Technology*, March, 1990, vol. 8, pp. 478-491.

56. Sardasai, H.P., Chang, C.-C, and Weiner, A.M., "A Femtosecond code-Division Multiple-Access communication System Test Bed", IEEE/OSA *Journal of Lightwave Technology*, November 1998, vol. 16, no. 11, pp. 1953-1964.

57. Weiner, A. M., Heritage, J. P., Thurston, R. N., "Synthesis of phase-coherent, picosecond optical square pulses", *Optics Letters*, March, 1986, vol. 11, no. 3, pp. 153-155.

58. Weiner, A. M., Heritage, J. P., Salehi, J. A., "Encoding and Decoding of femtosecond pulses", *Optics Letters*, April, 1988, vol. 16, no. 4, pp. 300-302.

59. Weiner, A. M., Heritage, J. P., Kirschner, E. M., "High-resolution femtosecond pulse shaping", *Journal of the Optical Society of America B*, August, 1988, vol. 5, no. 8, pp. 1563-1572.

60. Thurston, R. N., Heritage, J. P., Weiner, A. M, Tomlinson, W. J., "Analysis of Picosecond Pulse Shape Synthesis by Spectral Masking in a Grating Pulse compressor", *IEEE Journal of Quantum Electronics*, May 1986, vol. 22, no. 5, pp. 682-696.

61. Hajela, D. J., Salehi, J. A., "Limits to the Encoding and Bounds on the Performance of Coherent Ultrashort Light Pulse", *IEEE Transactions on Communications*, February, 1992, Vol. 40, pp. 325-336.

62. Yao, X. S., Feinberg, J., Logan, R., Maleki, L., "Limitations on Peak Pulse Power, Pulse Width, and Coding Mask Misalignment in a Fiber-Optic", *Journal of Lightwave Technology*, May/June, 1993, vol. 11, no. 5/6, pp. 836-846.

63. Crespo, P., Honig, M. L., Salehi, J. A., "Spread-Time Code Division Multiple Access", *GLOBECOM* '91, 1991, pp. 836-840.

64. Zaccarin, Denis, Kavehrad, Mohsen, "An Optical CDMA System Based on Spectral Encoding of LED", *IEEE Photonics Technology Letters*, April, 1993, vol. 4, no. 4, pp. 479-482.

65. Zaccarin, Denis, Kavehrad, Mohsen, "Performance Evaluation of Optical CDMA Systems Using Non-Coherent Detection and Bipolar Codes", *Journal of Lightwave Technology*, January, 1994, vol. 12, no. 1, pp. 96-105.

66. Zaccarin, Denis, Kavehrad, Mohsen, "Optical CDMA with new coding strategies and new architectures to achieve bipolar capacity with unipolar codes", *OFC* '94 Technical Digest, February, 1994, pp. 168-170.

67. Zaccarin, Denis, Kavehrad, Mohsen, "Optical CDMA by Spectral Encoding of LED for Ultrafast ATM Switching", *ICC* '94.

68. Zaccarin, Denis, Kavehrad, Mohsen, "New architecture for incoherent optical CDMA to achieve bipolar capacity", *Electronics Letters*, February, 1994, vol. 30, no. 3, pp. 258-259.

69. Kavehrad, M., Zaccarin, Denis, "Optical Code-Division-Multiplexed Systems Based on Spectral Encoding of Noncoherent Sources", *Journal of Lightwave Technology*, March 1995, vol. 13, no. 3, pp. 534-545.

70. Iversen, K., Ziemann, O., "An all-optical CDMA communication network by spectral encoding of LED using acoustically tunable optical filters", *Proceedings of the International Symposium on Signals, Systems and Electronics*, 1995, pp. 529-532.

71. Iversen, K., Ziemann, O., "On optical CDMA based on spectral encoding with integrated optical devices ", *SPIE*, vol. 2614, pp. 142-152, 1995.

72. Iversen, K., Mückenheim, J, Ziemann, O., "Comparison of Optical Code Division Multiplexing and Spectral Sliced WDM based on Broadband Sources", *European Conference on Networks and Optical Communication* (NOC '96), June 1995.

73. Nguyen, L., Dennis, T, Aazhang, B., Young, J. F., "Experimental Demonstration of Bipolar Codes for Optical spectral Amplitude CDMA Communication", *Journal of Lightwave Technology*, September 1997, vol. 15, no. 9, pp. 1647-1653.

74. Lam, C. F., Dennis T, Tong, K, Wu, M. C., Yablonovitch, E., "Experimental Demonstration of Bipolar Optical System Using a Balanced Transmitter and Complementary Spectral Encoding," *IEEE Photonics Technology Letters*, vol. 10, no. 10, pp. 1504-1506,

75. Moller, L., "An optical CDMA method based on periodic spectrum encoding", in Proc. 13th EFOC-N, Brighton, U.K., 1995, pp. 178-181.

76. Pfeifer, T. "frequency-Encoded Optical CDMA transmission System and Optical Receiver Therfor", US Patent No. 5 784 506, July, 21, 1998.

77. T. Pfeiffer, M. Witte, and B. Deppisch, "High-speed transmission of broad-band thermal light pulses over dispersive fibers," *IEEE Photonics Technology Letters*, vol. 11, no. 3, pp. 385-387.

78. Pfeiffer, T., Deppisch, B., Wytte, M., and Heidemann, R. "Operational Stability of spectrally Encoded Optical CDMA System Using Inexpensive Transmitters Without Spectral Control" *IEEE Photonics Technology Letters*, vol. 11, no. 7, pp. 1284-1293, July 1999.

79. Smith, E. D. J., Blaikie, R. J., and Taylor, D. P., "Performance Enhancement of Spectral-Amplitude-Coding Optical CDMA Using Pulse-Position Modulation", *IEEE Transactions on Communications*, Sept. 1998, vol. 46, no. 9, pp. 1176-1185.

80. Lee, J. S., Chung, Y. C., DiGiovanni, D. J., "Spectrum-Sliced Fiber Amplifier Light Source for Multichannel WDM Applications", *IEEE Photonics Technology Letters*, December 1993, vol. 5, No. 12, pp. 1458-1461.

81. Smith, E. D. J., Gough, P. T., Taylor, D. P., "Noise limits of optical spectral-encoding CDMA systems", *Electronics Letters*, 17 August 1995, vol. 31, no. 17, pp. 1469-1470.

82. Eskildsen, L., Hansen, P. B., "Interferometric Noise in Lightwave Systems with Optical Preamplifiers", *IEEE Photonics Technology Letters*, November 1997, vol. 9, no. 11, pp. 1538-1540.

83. Gilfedder, T. H., Andonovic, I., Shabeer, M., "Performance of dense EDM routed passive optical networks due to interferometric noise effects", International Journal of Optoelectronics, 1997, vol. 11, no. 1, pp. 43-46.

84. Feldman, R. D., "Crosstalk and Loss in Wavelength Division Multiplexed Systems Employing Spectral Slicing", *IEEE Journal of Lightwave Technology*, November 1997, vol. 15, no. 11, pp. 1823-1831.

85. Jin, W., "Investigation of Interferometric Noise in Fiber-Optic Bragg Grating Sensors by Use of Tunable Laser Sources", *Applied Optics*, May 1998, vol. 37, no. 13, pp. 2517-2525.

86. Boulianne L.P. "SYSTÈME DE COMMUNICATION OPTIQUE À ACCÈS MULTIPLE PAR RÉPARTITION DE CODE À SAUT RAPIDE DE FRÉQUENCE, ", Mémoire de maîtrise, Université Laval. Janvier 2000.

Radio-Frequency FH-CDMA et FH-Codes

87. Shaar, A. A., Davies, P. A., "A survey of one-coincidence sequences for frequency-hopped spread spectrum systems", *IEE Proceedings*, December 1984, vol. 131, no. 7, pp. 719-724.

88. Bin, L., "One-Coincidence Sequences with Specified Distance Between Adjacent Symbols for Frequency-Hopping Multiple Access.", *IEEE Transactions on Communications*, April 1997, vol. 45, no. 4, pp. 408-410.

89. Titlebaum, E. L., "Time-Frequency Hop Signals Part I: Coding Based Upon the Theory of Linear Congruences", *IEEE Transactions on Aerospace and Electronic Systems*, July 1981, vol. 17, no. 4, pp. 490-493.

90. Titlebaum, E. L., Sibul, L. H., "Time-Frequency Hop Signals Part II: Coding Based Upon Quadratic Congruence", *IEEE Transactions on Aerospace and Electronic Systems*, July 1981, vol. 17, no. 4, pp. 494-499.

91. Shaar, A. A., Davies, P. A., "Prime Sequences: Quasi-optimal Sequences for OR Channel Code Division Multiplexing", *Electronics Letters*, October 1983, vol. 19, no. 21, pp. 888-889.

92. Golomb, S. W., Taylor, H, "Constructions and Properties of Costas Arrays", *Proceedings of the IEEE*, September 1984, vol. 72, no. 9, pp. 1143-1163.

93. Costas, J, P., "A Study of a Class of Detection Waveforms Having Nearly Ideal Range-Doppler Ambiguity Properties", *Proceedings of the IEEE*, August 1984, vol. 72, no. 8, pp. 996-1009.

94. Shaar, A. A., Woodcick, C. F., Phill, D., Davies, P. A., "Number of one-coincidence sequence sets for frequency-hopping multiple access", *IEE Proceedings*, December 1984, vol. 131, no. 7, pp. 725-728.

95. Kumar, P. V., "On the Exis tence of Square Dot-Matrix Patterns Having a Specific Three-Valued Periodic-Correlation Function", *IEEE Transactions on Information Theory*, March 1988, vol. 34, no. 2, pp. 271-277.

96. Kim, Sang W., Stark, Wayne, "Optimum Rate Reed-Solomon Codes for Frequency-Hopped Spread-Spectrum Multiple-Access", *IEEE Transactions on Communications*, February, 1989, vol. 37, no. 2, pp. 138-144.

97. Izzo, L., Paura, L., "Costas Arrays with Small Number of Cross-Coincidences", *IEEE Transactions on Aerospace and Electronic Systems*, January 1989, vol. 25, no. 1, pp. 109-113.

98. Maric, S. V., Titlebaum, E. L., "Frequency Hop Multiple Access Codes Based Upon the Theory of Cubic Congrurences", *IEEE Transactions on Aerospace and Electronic Systems*, November 1990, vol. 26, no. 6, pp. 1035-1039.

99. Bellegarda, J. R., Titlebaum, E. L., "The Hit Array: An Analysis Formalism for Multiple Access Frequency Hop Coding", *IEEE Transactions on Aerospace Electronic Systems*, January 1991, vol. 27, no. 1, pp. 30-39.

100. Mersereau, R. M., "Multiple Access Frequency Hopping Patterns with low Ambiguity", *IEEE Transactions on Aerospace and Electronic Systems*, July 1981, vol. 17, no. 4, pp. 571-578.

101. McEliece, R. J., "Finite Fields for Computer Scientists and Engineers", Boston, Kluwev, 1987.

102. Maric, S. V., Titlebaum, E. L., "A Class of Frequency Hop Codes with Nearly Ideal Characteristics for Use in Multiple-Access Spread-Spectrum Communications and Radar and Sonar Systems ", *IEEE Proceedings*, 1992, pp. 1442-1447.

103. Frank, C. D., Pursley, M. B., "On the Statistical Dependence of Hits in Frequency-Hop Multiple Access", *IEEE Transactions on Communications*, vol. 38, no. 9, pp. 1483-1494.

104. Hegde, M. V., Stark, W. E., "On the Error Probability of Coded Frequency-Hopped Spread-Spectrum Multiple-Access Systems", *IEEE Transactions on Communications*, May 1990, vol. 38, no. 5, pp. 571-573.

105. Lance, E., Kaleh, G. K., "A Diversity Scheme for a Phase-Coherent Frequency-Hopping Spread-Spectrum System", *IEEE Transactions on Communications*, vol. 45, no. 9, pp. 1123-1129.

106. Lam, A. W., Sarwate, D. V., "Time-Hopping and Frequency-Hopping Multiple-Access packet Communications", *IEEE Transactions on Communications*, June 1990, vol. 38, no. 6, pp. 875-888.

107. Jugl, E., Kuhwald, T., Iversen, K., "Algorithms of (0, 1)-matrix codes", *Electronics Letters*, January 1997, vol. 33, no. 3, pp. 227-229.

108. Wronski, L. D., Hossain, R., Albicki, A., "Extended Hyperbolic Congruential Frequency Hop code: Generation and Bounds for Cross- and Auto-Ambiguity Function", *IEEE Transactions on Communications*, March 1996, vol. 44, no. 3, pp. 301-305.

109. Bierbrauer, J., Edel, Y., "New Code parameters from Reed-Solomon Subfield Codes", *IEEE Transactions on Information Theory*, May 1997, vol. 43, no. 3, pp. 953-968.

110. Bonnecase, A., Solé, P., Bachoc, C., Mourrain, B., "Type II Codes over Z4", *IEEE Transactions on Information Theory*, May 1997, vol. 43, no. 3, pp. 969-976.

111. Geraniotis, E., "Multiple-Access Capability of Frequency-Hopped Spread_Spectrum Revisited: An Analysis of the Effect of Unequal Power Levels", *IEEE Transactions on Communications*, July 1990, vol. 38, no. 7.

OFFH-CDMA

112. H. Fathallah, L. A. Rusch and S. LaRochelle "Fast Frequency Hopping Spread Spectrum for Code Division Multiple Access Communications Networks (FFH-CDMA)," *U.S. Patent Pending*, Washington D.C., June 1998.

113. H. Fathallah and L. A. Rusch "Robust Optical FFH-CDMA Communications-Coding in Place of Frequency and Temperature Controls," *IEEE Journal of Lightwave Technology*, , vol. 17, No. 8, pp. 1284-1293, August 1999.

114. H. Fathallah, L. A. Rusch, S. LaRochelle "Passive Optical Fast Frequency-Hop CDMA Communications System," *IEEE Journal of Lightwave Technology*, vol. 17, pp. 397-405, March 1999.

115. H. Fathallah, P.-Y. Cortès, L. A. Rusch, S. LaRochelle and L. Pujol, "Experimental Demonstration of an Optical Fast Frequency Hopping-CDMA Communications System," *ECOC "99: 25th European Conference on Optical Communications*, September 99, Nice, France.

116. H. Fathallah and L. A. Rusch, "Robust Optical FFH-CDMA Communications: Coding avoids Frequency/Temperature Controls," *Eleventh Tyrrhenian Workshop on Digital Communications "The Optical Network Layer: Management, Systems and Technologies, "* Italy, Sep. 1999, pp. 312-323.

117. H. Fathallah and L. A. Rusch "Robust Optical Communications without Temperature Control via FFH-CDMA," *IEEE International Conference on Communications '99*, submitted in Sept. 1998.

118. H. Fathallah, S. LaRochelle and L. A. Rusch "Analysis of an optical frequency-hop encoder with strain-tuned Bragg gratings," *OSA Topical Meeting on Bragg Gratings, Photosensitivity and Polling in Glass Waveguide,*, pp. 200-202, Oct. 1997.

119. P.Y. Cortès, H. Fathallah, S. LaRochelle, L. A. Rusch and P. Loiselle "Writing of Bragg Gratings with Wavelength Flexibility Using Sagnac Type Interferometer and Application to FFH-CDMA," *European Conference on Optical Communications (ECOC '98)*, Madrid, paper WdA15, Sept. 1998.

120. Boulianne, L.-P., Rusch, L. A. "New Architecture & Codes for Optical Frequency-Hopping Multiple Access" *ICAPT "98.*

121.K., Fouli, H. Fathallah, M. Menif and L. A., Rusch, "Equalization Advantages of Optical FFH-CDMA over WDM in EDFAs" *ICAPT 2000*.

122. Jugl, E., Iversen, K., "New Combinatorial BER bounds for Families of (0,1)-matrix codes," *Proceeding IEEE Global Telecommunications Conference*; pp. 1543-1547; Nov. 1997.

123. Andonovic, I., Tancevski, L., "Optical network architecture utilizing wavelength hopping/time spreading codes," *International Journal of Optoelectronics*, Vol. 11, no. 1, pp.1-9, 1997.

124. Tancevski, L., Andonovic, I., "Hybrid Wavelength Hopping/Time Spreading Schemes for Use in Massive Optical Networks with Increased Security," *IEEE Journal on Lightwave Technology*, vol. 14, no. 12, pp. 2636-2647, December 1996.

125. Mendez, A.J., Gagliardi, R. M., "Varieties and characteristics of discrete spectral encoding (DSE), " *IEEE International Symposium on Spread Spectrum Techniques and Applications*; pp 432-444, September 1996

126. Kiasaleh K., "Performance of Packet-Switched Fiber-Optic Frequency-Hopping Multiple-Access Networks", *IEEE Transactions On Communications*, July 1995, vol. 43, no. 7, pp. 2241-2253.

127. Kiasaleh K., "Fiber optic frequency hopping multiple access communication system," *IEEE Photonics Technology Letters*, February 1991, vol. 3, pp. 173-175.

128. Kiasaleh K., " Network architectures for fiber optic frequency hopping multiple access networks," in *Int. Workshop Advance Commun. Applicat. High Speed Networks* (IWACA `93), Munich, Germany, March 1991.

129. Daneshgaram, F., Mondin, M., "Coherent Frequency-hopped CDMA and Orthogonal Frequency Division Multiplexing with Wavelets", *Electronics Letters*, March 1995, Vol. 31, no. 6, pp. 428-429.

130. Andonovic, I., Sotobayashi, N. Wada, and K.I. Kitayama., "Experimental Demonstration of the (De)Coding of Hybrid Phase and Frequency Codes Using a Pseudolocal Oscillator for Optical Code Division Multiplexing", *IEEE Photonics Technology Letters*, vol. 10, no. 6, June 1998, pp. 887-889.

Other Bragg Gratings-based CDMA methods:

131. Geiger, H., Fu A., Ibsen M., Richardson D.J., Laming, R.I., "Demonstration of a Simple CDMA Transmitter and Receiver Using Sampled Fiber Gratings," *ECOC* "98

132. Grunnet-Jepsen, A., Johnson A. E., Maniloff, E.S., Mossberg, T.W., Munroe, M.J., Sweetser, J.N., "Demonstration of All-Fiber Sparse Lightwave CDMA Based on Temporal Phase Encoding," *IEEE Photonics Technology Letters*, vol. 11, no. 10, pp. 1283-1285, October 1999.

133. Grunnet-Jepsen, A., Johnson A. E., Maniloff, E.S., Mossberg, T.W., Munroe, M.J., Sweetser, J.N., "Fiber Bragg gratings based spectral encoder/decoder for lightwave CDMA," *Electronics Letters 24th June 1999, vol. 35, no. 13, pp 314-316*.

134. Chen, L.R., Benjamin, S.D., Smith, P.W.E., Sipe, J. E. "Application of Ultrashort Pulse Propagation in Bragg Gratings for Wavelength Division Multiplexing and Code-Division Multiple Access," *IEEE Journal of Quantum Electronics*, Vol. 34, no. 11, November 1998.

135. Hunte, D.B., and Minasian, R.A., "Programmable high-speed optical code recognition using fibre Bragg grating arrays," Electronics Letters, vol. 35, no. 5, 4th March 1999, pp.412-413.

Space-CDMA

136. Mendez, Antonio J., Kuroda, S., Gagliardi, R. M., Garmire, E., "Generalized temporal code division multiple access (CDMA) for optical communication", SPIE *Proceedings*, 1989, vol 1125, pp. 287.

137. Gagliardi, R. M., Mendez, Antonio J., "Pulse combining and time-space coding for multiple accessing with fiber arrays", *LEOS* '90, 1990, OMth14.

138. Park, E., Mendez, A. J., Garmire, E.M., "Temporal/Spatial optical CDMA networks design, demonstration, and comparison with temporal networks, " IEEE Photonic Technology Letters, vol 4, Oct. 1992, pp. 1160-1162.

139. Mendez, A.J., Lambert, J.L., Murookian, J. –M., Gagliardi, R.M., "Synthesis and demonstration of high speed bandwidth efficient optical code division multiple access (CDMA) tested at 1 Gb/s throughput," IEEE Photonic Technology Letters, Vol. 6, September 1994, pp 1146-1149.

140. Gagliardi, R. M., "Pulse-Coded Multiple Access in Space Optical Communications", *IEEE Journal on Selected Areas in Communications*, April 1995, vol. 13, no. 3, pp. 603-608.

141. Mendez, Antonio J., Gagliardi, R. M., "Matrix Codes for Ultradense Gigabit Optical CDMA Networks", *LEOS '93 Summer Topical Meeting on Gigabit Networks*, 1993,

142. Yang, G.-C., Kwong, K.C., "Two-dimensional spatial codes for image transmission in multicore-fibre CDMA networks", *Electronics Letters, 17th August 1995, vol. 31, no. 17 pp. 1482-1483 LEOS* '90, 1990, OMth14.

143. Kitayama, K. I., "Novel Spatial Spread Spectrum Based Fiber Optic CDMA Networks for Image Transmission", *IEEE Journal on Selected Areas in Communications*, May 1994, vol. 12, no. 4, pp. 762-772.

144. Kitayama, K.-I., Nakamura, M., Igasaki, Y., "Image Fiber-Optic Two-Dimensional Parallal Links Based Upon Optical Space-CDMA: Experiment," IEEE/OSA *Journal of Lightwave Technology*, Feb. 1997, vol. 15, no. 2, pp. 202-212.

145. Nakumara, M., Kitayama, K.-I., "System Performance of Optical Space Code-Division Multiple-access-based fiber-optic two-dimensional parallel data link," Applied Optics, 10 may 1998, vol. 37, no. 14, pp. 2915-2924.

146. Nakumara, M., Kitayama, K.-I., Igasaki, Y., Kaneda, Keiji "Four-channel, 8x8 bit, two-dimensional parallel transmission by use of space-code-division multiple-access encoder and decoder modules," Applied Optics, 10 July 1998, vol. 37, no. 20, pp. 4389-4398.

147. Hassen, A. A., Hershey, J. E., Riza, N. A., "Spatial Optical CDMA", *IEEE Journal on Selected Areas in Communications*, Vol. 13, no. 3, pp. 609-613.

148. Salehi, J. A, Paek, E. G., "Holographic CDMA", *IEEE Transactions on Communications*, September 1995, vol. 43, no. 9, pp. 2434-2438.

149. Salehi, J. A, "Holographic CDMA", *US Patent* 1995.

Multiuser Detection for OCDMA

150. Verdú, Sergio, Poor, H. V., "Multiuser Detection", 1993, pp. 369-410.

151. Verdú, Sergio, "Minimum Probability of Error for Asynchronous Gaussian Multiple-Access Channels", *IEEE Transactions on Information Theory*, January, 1986, IT-32, pp. 85-96.

152. Madhow, Upamanyu, Honig, Michael L., "MMSE Interference Suppression for Direct-Sequence Spread-Spectrum CDMA", *IEEE Transactions On Communications*, December, 1994, vol. 42, pp 3178-3188.

153. Varanasi, M. K., Aazhang, B., "Multistage Detection in Asynchronous CDMA Communications", *IEEE Transactions on Communications*, April, 1990, vol. 38, no. 4, pp. 508-519.

154. Verdú, Sergio, "Multiple-Access Channels with Point-Process Observations: Optimum Demodulation", *IEEE Transactions on Information Theory*, September 1986, vol. 32, no. 5, pp. 642-651.

155. Brady, David, Verdú, Sergio, "A Semiclassical Analysis of Optical Code Division Multiple Access", *IEEE Transactions on Communications*, January, 1991, vol. 39, no. pp. 85-93.

156. Nelson, Laurie B., Poor, H. Vincent, "Performance of Multiuser Detection for Optical CDMA-Part I: Error Probabilities", *IEEE Transactions on Communications*, November 1995, vol. 43, no. 11, pp. 2803-2811.

157. Nelson, Laurie B., Poor, H. Vincent, "Performance of Multiuser Detection for Optical CDMA-Part II: Asymptotic Analysis", *IEEE Transactions on Communications*, December 1995, vol. 43, no. 12, pp. 3015-3024.

158. Nelson, Laurie B., Poor, H. Vincent, "Iterative Multiuser Receivers for CDMA Channels: An EM-Based Approach", *IEEE Transactions on Communications*, December 1996, vol. 44, no. 12, pp. 1700-1710.

159. Brandt-Pearce, Maïté, Aazhang, B., "Multiuser Detection for Optical Code Division Multiple Access Systems", *IEEE Transactions on Communications*, vol 42, February/March/April, 1994, pp 1801-1810.

160. Brandt-Pearce, Maïté, Aazhang, B., "Performance Analysis of Single-user and Multiuser Detectors for Optical Code Division Multiple Access Communication Systems", *IEEE Transactions on Communications*, 1995, vol. 43, no. 2/3/4, pp. 435-444.

161. Tang, J. T. K., Ben Letaief, K., "A New Multiuser Detector for Optical Code Division Multiple Access Communications Systems", *ICC*, June 1997.

162. Ohtsuki, T., "Channel Interference Cancellation Using Electrooptic Switch and Optical Hard-Limiters for Direct-Detection Optical CDMA Systems", *ICC*, June 1997, pp. 106-109.

163. Ohtsuki, T., "Performance Analysis of Direct-Detection Optical Asynchronous CDMA Systems with Double Optical Hard-Limiters", *ICC*, June 1997, pp. 121-125.

Bragg Gratings and their applications

164. K. O. Hill, G. Meltz, “Fiber Bragg Grating Technology Fundamentals and Overview,” *IEEE Journal of Lightwave Technology*, vol. 15, no. 8, pp. 1263-1276, July 1997.

165. Giles, C. R., "Lightwave Applications of Fiber Bragg Gratings", *Journal of Lightwave Technology*, August 1997, vol.15, no.8, pp. 1391-1404.

166. Loh, W. H., Cole, M. J., Zervas, M. N., Barcelos, S., Laming, R. I., "Complex grating structures with uniform phase masks based on the moving fiber-scanning beam technique", *Optics Letters*, October 1995, vol. 20, no. 20, pp. 2051-2053.

167. Kashayap, R., "Photosensitive Optical Fibers: Devices and Application", *Optical Fiber Technology*, 1994, Vol. 1, pp. 17-34.

168. Pasto, D., Capmany, J., Ortega, D., Tatay, V., Marti, J., "Design of Appodized Linearly Chirped Fiber Gratings for Dispersion Compensation", *Journal of Lightwave Technology*, November 1997, vol. 14, no. 11, pp. 2581-2588.

169. Peral, E., Capmany, J., "Generalized Bloch Wave Analysis for Fiber and Waveguide Gratings", *Journal of Lightwave Technology*, August 1997, vol. 15, no. 8, pp. 1295-1302.

170. Erdogan, T., "Fiber Grating Spectra", *Journal of Lightwave Technology*, August 1997, vol. 15, no. 8, pp. 1277-1294.

171. Bennion, I./Williams, J. A. R., Zhang, L., Sugden, K., Doran, N. J., "UV-written in-fiber Bragg gratings", *Optical and Quantum Electronics*, 1996, pp. 93-135.

172. Palais, J. C., Zhao, Y., "Fiber Bragg Grating Coherence Spectrum Modeling, Simulation, and Characteristics", *Journal of Lightwave Technology*, January 1997, vol. 15, no. 1, pp. 154-161

173. Matsuhara, M., Hill, K. O., Watanabe, A., "Optical-Waveguide Filters: Synthesis", *Journal of the Optical Society of America B*, July 1975, vol. 65, no. 7, pp. 804-809.

174. H. Storoy, H. E. Engan, B. Sahgren and R. Stubbe, "Position weighting of fiber Bragg gratings for bandpass filtering," *Optics Letters*, vol. 22, no. 11, 1 June 1997.

175. Weller-Brophy, L. A., Hall, G. G., "Analysis of waveguide gratings: a comparison of the results of Rouards method and coupled-mode theory", *Journal of the Optical Society of America B*, 1987, vol. 4, no. 1, pp. 60-65.

176. Matsuhara, M., Hill, K. O., "Optical-Waveguide Band-Rejection Filters Design", *Applied Optics*, December 1974, vol. 13, no. 12, pp. 2886-2888.

177. Sugden, K., Zhang, L., Williams, J. A. R., Fallon, R. W., Everall, L. A., Ghisholm, K. E., Bennion, I., "Fabrication and Characterization of Bandpass Filters Based on Concatenated Chirped Fiber Gratings", *Journal of Lightwave Technology*, August 1997, vol. 15, no. 8, pp. 1424-1432.

178. Chen, L. R., Benjamin, S. D., Smith, P. W. E, Sipe, J. E., "Ultrashort Pulse Reflection from Fiber Gratings: A Numerical Investigation", *Journal of Lightwave Technology*, August 1997, vol. 15, no. 8, pp. 1503-1512.

179. Gupta, S., Mizunami, T., Shimomura, T., "Computer Control of Fiber Bragg Grating Spectral Characteristics Using a Thermal Head", *Journal of Lightwave Technology*, October 1997, vol. 15, no. 10, pp. 1925-1928.

180. Campbell, R. J., Kashyap, R., "Spectral profile and multiplexing of Bragg gratings in photosensitive fiber", *Optics Letters*, June 1991, vol. 16, no. 12, pp. 898-900.

181. Bilodeau, F., Hill, K. O., Malo, B., Johnson, D. C., Albert, J., "High-Return-Loss Narrowband All-Fiber Bandpass Bragg Transmission Filter", *IEEE Photonics Technology Letters*, January 1994, vol. 6, no. 1, pp. 80-82.

182. Wei, L., Lit, J. E. Y., "Phase-Shifted Bragg Grating Filters with Symmetrical Structures", *Journal of Lightwave Technology*, vol. 15, no. 8, pp. 1405-1410.

183. Carballar, A., Muriel, M. A., "Phase Reconstruction From Reflectivity in Fiber Bragg Gratings", *Journal of Lightwave Technology*, August 1997, vol. 15, no. 8, pp. 1314-1322.

184. Muriel, M. A., Carballar, A., "Phase reconstruction from reflectivity in uniform fiber Bragg gratings", Optics Letters, January 1997, vol. 22, no. 2, pp.93-95.

185. Ball, G. A., Morey, W. W., "Compression-tuned single-frequency Bragg grating fiber laser", *Optics Letters*, December 1, 1994, vol. 19, no. 23, pp. 1979-1981.

186. Ibsen, M., Eggleton, B. J., Sceats, M., Ouellette, F. "Broadly tunable DBR fibre laser using sampled fiber Bragg gratings", *Electronics Letters*, vol. 31, no. 1, pp. 37-38, January 1995.

187. Limberger, H. G., Ky, N. H., Costantini, D. M., Salathé, R. P., Muller, C. A. P., Fox, G. R., "Efficient Active Bragg Grating Tunable Filters", *OSA Topical Meeting on Bragg Gratings, Photosensitivity, and Polling in Glass Fibers Waveguides: Applications and Fundamentals*, Williamsburg , Virginia, USA, vol. 17, pp. 265-267, October 1997.

188. Litchinitser, N.M., Eggleton, B. J., Agrawal, G. P., “Dispersion of Cascaded Fiber Gratings in WDM Lightwave Systems,” *IEEE/OSA Journal of Lightwave Technology*, vol. 16, no. 8, August 1998, pp 1523-1529.

189. Ohn, M. M. , Alavie, A. T. , Maaskant, R. , Xu, M. G. , Bolodeau, F. , Hill, K. O. , "Tunable fiber grating dispersion using a piezoelectric stack", *OFC*, 1997, WJ3.

190. P.-Y. Cortès, F. Ouellette, S. LaRochelle, "Intrinsic apodization of Bragg gratings written using UV pulse interferometry", Electronics Letters 34 p.396-397 (1998).

191. Su, S. F. , Olshansky, R., Joyce, G., Smith, D. A. , Baran, J. E., "Use of acousto-optic tunable filters as equalizers in WDM lightwave systems", *Technical Digest of The OFC*, February, 1992, no. 5, pp. 203-204.

192. Kersey, A. D., Davis, M. A., Patrick, H. J., LeBlanc, M., Koo, K. P., Askins, C. G., Putnam, M. A., Friebele, E. J., "Fiber Gratings Sensors", *Journal of Lightwave Technology*, August 1997, vol. 15, no. 8, pp. 1442-1463.

193. Limberger, H. G., Varelas, D., Salathé, R. P., "Mechanical Reliability of UV Irradiated Fibers: Application to Bragg Grating Fabrication" *OSA Topical Meeting on Bragg Gratings, Photosensitivity, and Polling in Glass Fibers Waveguides: Applications and Fundamentals*, Williamsburg , Virginia, USA, vol. 17, pp. 46-48, October 1997.

194. Kannan, S., Lemaire, P. J., Guo, J., LuValle, M. J., "Reliability predictions on fiber gratings through alternate methods", *OSA Topical Meeting on Bragg Gratings, Photosensitivity, and Polling in Glass Fibers Waveguides: Applications and Fundamentals*, Williamsburg , Virginia, USA, vol. 17, pp. 52-54, October 1997.

195. Ortega, B., Capmany J., Cruz, J. L. "Wavelength Division Multiplexing All-Fiber Hybrid Devices Based on Fabry-Perot`s and Gratings", *IEEE/OSA Journal of Lightwave Technology*, July 1999, vol. 17, no. 7, pp. 1241-1247.

196. A. D. Kersey, “A Review of Recent Developments in Fiber Optic Sensor Technology,” *Optical Fiber Technology*, vol. 2, pp. 291-317, 1996.

197. Kersey, A. D., Davis, M. A., "Sensing Apparatus and Method for Detecting Strain Between Fiber Bragg Gratings Sensors Inscribed into Optical fiber", US Patent 7 748 312, May 5, 1998.

198. McGarrity, C., Jackson, D., “A Network for Large Numbers of Interferometric Sensors and Fiber Bragg Gratings with High Resolution and External Range,” *IEEE/OSA Journal of Lightwave Technology*, vol. 16, no.1, pp. 54-65, January 1998.

199. Kersey, A. D., Davis, M. A., Patrick, H.J., LeBlanc, M., Koo, K.P., Askins, C. G., Putnam, M. A., Friebele, E.J., “Fiber Grating Sensors,” *IEEE/OSA Journal of Lightwave Technology*, vol. 15, no. 8, August 1997, pp 1442-1463.

Optical TDM & WDM

200. Deng, L.-L., Kang, K. I., Glask, I., Prucnal, P., "A 1024-Channel Fast Tunable Delay Line for Ultrafast All-Optical TDM Networks", *IEEE Photonics Technology Letters*, November 1997, vol. 9, no. 11, pp. 1496-1498.

201. Boivin, L., Nuss, M. C., Knox, W. H., Stark, J.B., "206-Channel Chirped-Pulse Wavelength-Division Multiplexed Transmitter", *Electronics Letters, vol 33, Issue 10, 8 May 1997, pp. 827-829*.

202. Boivin, L., Nuss, M. C., Knox, W. H., Stark, J.B., "", CLEO 1999, *vol 11, p 280*.

203. Saleh, A.A.M., Simmons, J.M., "Architectural Principle of Optical Regional and Metropolitan Access Networks", *IEEE/OSA Journal of Lightwave Technology*, December 1999, vol. 17, no. 12, pp. 2431-2448.

204. Minardi, M.J., Ingram, M. A., "Adaptive Crosstalk Cancellation and Laser frequency Drift Compensation in dense WDM Networks", *IEEE/OSA Journal of Lightwave Technology*, August 1995, vol. 13, no. 8, pp. 1624-1635.

205. Hill, A. M., Payne, D. B. "Linear crosstalk in wavelength-division-multiplexed optical fiber transmission systems,", *IEEE/OSA Journal of Lightwave Technology*, June 1985, vol. 3, no. 3, pp. 643-651.

206. International Telecommunication Union, Telecommunication Standardization Sector, Study Group 15, Question 25, Recommendation G.mcs, 1996.

207. P. Varming, J. Hübner, M. Kristensen, "Five wavelength DFB fiber laser source," *Technical Digest of Optical Fiber Communications*, pp. 31-32, 1997.

208. T. Ikegami, S. Sudo and Y. Sakai, *Frequency Stabilization of Semiconductor Laser Diodes*. Boston, MA: Artech House, 1995.

209. M. Guy, B. Villeneuve, C. Latrasse and M. Têtu, "Simultaneous Absolute Frequency Control of Laser Transmitters in Both 1.3 and 1.55 μm Bands for Multiwavelength Communication Systems," *IEEE Journal of Lightwave Technology*, vol. 14, no. 6, pp. 1136-1143, June 1996

210. Zirngibl, M., Joyner, C. H., Doevr, C. R., Stalty, L. W., Presby, H. M., "An 18-channels mulitifrequency laser," IEEE Photonic Technology Letters, vol. 8, pp 870-872, July 1999.

211. Saleh, B. E. A . and M. C. Teich, B. E. A . Fundamentals of Photonics, Wiley, New York, 1991.Senior , J.M., "Optical Fiber Communications: Principles and Practice," Hall, Hemel Hempstead, Second edition, 1992

212. Rajiv Ramaswami, Kumar Sivarajan, "Optical Fiber Optical Networks: A Practical Perspective," Morgan Kaufmann Publishers, Second Edition, 2001.

213. Stern E. Thomas, and Krishna bala, "Multiwavelength Optical Networks: A Layered Approach, " Thomas E. Stern and Krishna Bala, Addison Wesley, 1999.